UNIVERSITY OF
LIVERPOOL

Investigation of Terahertz Photoconductive Antennas

Thesis submitted in accordance with
the requirements of the University of Liverpool
for the degree of Doctor of Philosophy

by

Di Li

January 2010

Department of Electrical Engineering and Electronics

Investigation of Terahertz Photoconductive Antennas

Di Li

Abstract

Terahertz (THz) frequency range usually refers to the electromagnetic spectrum between 100 GHz and 10 THz, which is between the millimetre and infrared regions. THz research has received a lot of attention because of its wide potential applications for such as high-speed wireless communications, medical imaging, remote sensing and security scanning.

Photoconductive antenna is the most popular device used to generate and detect THz waves. However, there are still many challenges in this area, for example, how to improve its radiation efficiency and how to increase its directivity to the desired direction.

In this dissertation, firstly four methods are proposed to improve the generation efficiency of photoconductive antennas. The first method is to adjust the gap of the photoconductive antenna to an optimum value which is dependent on the input laser power and the material properties of the substrate. The second method is to focus the laser beam on a very small

area rather than the whole gap and the generated power can be increased by more than 5 times. The third method is to increase the bias voltage, which can strengthen the photo-induced current. The final method discussed is to use the indentation configuration instead of the conventional dipole shape to enhance the electric field in the gap which can result in about two times stronger power radiation.

Secondly a THz horn structure is introduced to improve the directivity and the radiation efficiency of the photoconductive antenna. The conventional photoconductive antenna cannot provide high directivity, but this horn antenna can if it is designed and constructed properly. It consists of two main parts: a photoconductive emitter and a THz conical horn. A computer aided design approach has been adopted, and the simulation results show that the THz conical horn antenna with the proposed feeding structure can radiate more THz power in desired directions than conventional antenna. The directivity of this structure is proved to be 10 dB greater than the conventional photoconductive antennas. It should be pointed out that the THz horn antennas are not the same as the conventional microwave horn antennas. The major difference is on the feeding structure.

In addition, the effects of the substrate on THz photoconductive antennas are also investigated theoretically and numerically, some very interesting results are obtained.

Acknowledgement

This thesis could not be finished without the help and support of many people who are gratefully acknowledged here. At the very first, I would like to express my deepest gratitude to my supervisors, Dr. Yi Huang and Dr. Yao-Chun Shen. They have offered me valuable ideas, suggestions and criticisms with their profound knowledge and rich research experience. Their patience and kindness are greatly appreciated. Besides, they are always willing to discuss with me anytime. I have learnt from them a lot not only about dissertation writing, but also the professional ethics. I am very much obliged to their efforts of helping me complete the dissertation.

I also wish to extend my thanks to the Department of Electrical and Electronics, for their support of this study. I owe special thanks to Mr. Gordon Cook, Mr. Richard Wratten, Mr. Graham Bunting and Miss Jennifer Carus for their help when I studied in our department.

Thanks are also due to my postgraduate friends, who never failed to give me great encouragement and suggestions. Special thanks should go to Mr. Yang Lu, Mr. Hassan Chattha, Mr. Nan Zhou, and Dr. Chunhua Yang for their brainstorming with me when I failed coming up with ideas. I am also indebted to Mr. Ping Cao, Miss Jingwei Zhang, and Mr. Stephen Boyer for their encouraging me when I had problem writing this dissertation.

At last but not least, I would like to thank my family for their support all the way from the very beginning of my study. I am thankful to all my family members especially my father and mother for their thoughtfulness and encouragement.

Contents

List of Figures

List of Tables

List of Publications

[1] D. Li and Y. Huang, "Comparison of terahertz antennas", In: eds. *Proceedings of The 1st European Conference on Antennas and Propagation: EuCAP 2006*. The 1st European Conference on Antennas and Propagation, Nice, France. Nice: EuRAAP, pp. 1-5, November, 2006.

[2] D. Li and Y. Huang, "Optimisation of photoconductive antennas gap", In: eds. *Proceedings of The 2nd European Conference on Antennas and Propagation: EuCAP 2007*. The 2nd European Conference on Antennas and Propagation, Edinburgh, UK. Edinburgh: EuRAAP, pp. 248-251, November, 2007.

[3] D. Li, Y. Huang and Y. Shen, "Terahertz conical horn antenna", In: eds. *Proceedings of 3rd European Conference on Antennas and Propagation, EuCAP 2009*. The 3rd European Conference on Antennas and Propagation, Berlin, Germany. Berlin: EuRAAP, March, 2009.

[4] D. Li, Y. Huang and Y. Shen, "Development of a photoconductive horn antenna", In: eds. *Proceedings of 4th European Conference on Antennas and Propagation, EuCAP 2010*. The 4th European Conference on Antennas and Propagation, Barcelona, Spain. Barcelona: EuRAAP, April, 2010.

[5] D. Li and Y. Huang, "A theory of how to improve the excitation of the photoconductive antennas", In: eds. *2007 IEEE International Workshop on Antenna Technology Small and Smart Antennas Metamaterials and Applications, iWAT2007*. 2007 IEEE International Workshop on Antenna Technology Small and Smart Antennas Metamaterials and Applications, Cambridge, UK. Cambridge: IEEE, pp. 499-502, March , 2007.

[6] D. Li, Y. Huang and Y. Shen, "Investigation on bias electric fields produced by improved photoconductive antenna structures", In: eds. *2008*

IEEE International Workshop on Antenna Technology: Small Antennas and Novel Metamaterials, iWAT2008. 2008 IEEE International Workshop on Antenna Technology Small Antennas and Novel Metamaterials, Chiba, Japan. Chiba: IEEE, pp. 306-309, March, 2008.

[7] D. Li, Y. Huang and Y. Shen, "Effects of substrate on the performance of photoconductive antennas", In: eds. *2010 IEEE International Workshop on Antenna Technology: Small Antennas, Innovative Structures and Materials, iWAT2010*. 2010 IEEE International Workshop on Antenna Technology: Small Antennas, Innovative Structures and Materials, Lisbon, Portugal. Lisbon: IEEE, March, 2010.

[8] D. Li and Y. Huang, "An quantitative comparison of terahertz antennas", In: eds. *The 12th* Annual conference of Chinese Automation and Computing Society in the United Kingdom, *CACSUK06*.The 12th Annual conference of Chinese Automation and Computing Society in the United Kingdom,Loughborough, UK. Loughborough: CACSUK, September, 2006.

[9] D. Li, Y. Huang and Y. Shen, "Analytical modelling of electric field in biased photoconductive antenna with advanced structure", In: eds. *Loughborough Antennas and Propagation Conference*. Loughborough Antennas and Propagation Conference, Loughborough, UK. Loughborough: IET, pp. 241-244, March, 2008.

[10] D. Li, Y. Huang and Y. Shen, "Increasing the directivity of photoconductive antennas", In: eds. *2nd UK/Europe-China Workshop on Millimetre Waves and Terahertz Technologies*. The 2nd UK/Europe-China Workshop on Millimetre Waves and Terahertz Technologies, Oxford, UK. Oxford: IET, October, 2009.

[11] Y. Huang and D. Li, "Invited paper on THz antennas", In: eds. *China-UK/Europe Workshop on Millimetre Waves and Terahertz Technologies*. China-UK/Europe Workshop on Millimetre Waves and Terahertz Technologies, Chengdu, China. Chengdu: IET, October, 2008.

[12] X. Tian, Y. Wang, Y. Huang , D. Li and C. Yang, "Highly accurate

SLC image coregistration in InSAR processing technique", In: eds. *Proceedings of The 2nd European Conference on Antennas and Propagation: EuCAP 2007*. The 2nd European Conference on Antennas and Propagation, Edinburgh, UK. Edinburgh: EuRAAP, November, 2007.

[13] C. Yang, Y. Huang, D. Li and X. Tian, "UWB propagation characteristics analysis and improvement on ranging accuracy", In: eds. *Proceedings of The 2nd European Conference on Antennas and Propagation: EuCAP 2007*. The 2nd European Conference on Antennas and Propagation, Edinburgh, UK. Edinburgh: EuRAAP, November, 2007.

[14] D. Li and Y. Huang, "Optimization of photoconductive dipole antennas", International Journal of infrared and Millimeter Waves (submitted), 2010.

[15] D. Li, Y. Huang and Y. Shen, "Investigation on substrate effects of photoconductive antennas", IEEE Transactions on Antennas and Propagation (submitted), 2010.

List of Acronyms

3WFDA	Three-wire folded half-wavelength antenna
5WFDA	Five-wire folded half-wavelength antenna
CNTs	Carbon nanotubes
CPW	Coplanar waveguide
FIR	Far-infrared
FS-EOS	Free-space-electro-optic sampling
FWDA	Full wavelength dipole antenna
FWHM	Full-width half-maximum
IR	Infrared
ITO	Indium Tin Oxides
LCVD	Laser chemical vapour deposition
LT-GaAs	Low temperature GaAs
MBE	Molecular-beam-epitaxy
MDMA	3, 4-methylenedioxymethamphetamine
NLTL	Nonlinear transmission lines
PC sampling	Photoconductive sampling
QCL	Quantum cascade laser
RD-SOS	Radiation-damaged Si-on-sapphire
SI-GaAs	Semi-insulating GaAs
SRAM	Static random access memory
THz	Terahertz
THz-TDS	Time-domain terahertz spectroscopy

CHAPTER 1

INTRODUCTION

1.1 Introduction to THz Wave

Terahertz (THz) frequency band is generally referred to the spectrum between 0.1 and 10 THz. 1 THz means 1 ps in period and 300 μm in free space wavelength. Thus THz band is between the millimetre and the infrared regions and can also be called submillimetre-waves [1]. The THz region is considered as the last spectrum which is not well researched by people. It locates in the transition area from macrophysics to microcosmic quantum theory and covers the spectrum of protein molecular surge, so this region has high academic value [2]. Because of its attractive features such as chemical specificity, penetration capability, non-ionisation, and wide bandwidth, this least explored frequency band has become the focus of many researchers.

The electromagnetic spectrum is shown in Fig. 1.1. It is apparent that the THz spectrum is uniquely located between the electronic and photonic domains. Thus, optical, electronic, and a mixture of optical and electronic techniques may be used for the THz field generation, detection and processing [1]. For example, THz fields can be generated with the help of a down conversion optical process or a photoconductive process, and THz fields propagate into free space using an antenna or are guided

through a microwave-type waveguide such as the coplanar waveguide (CPW). However, there are also all-optical or all-electronic means to produce or receive THz fields, such as lasers, electronic oscillators and multipliers.

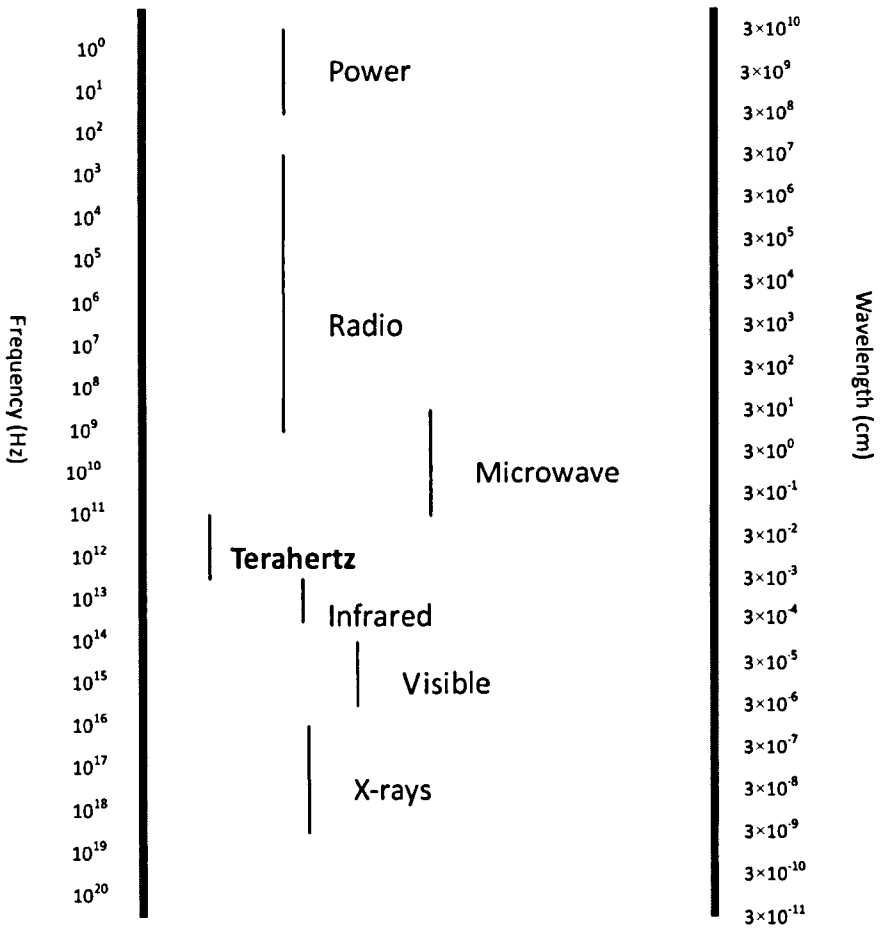

Fig. 1.1 The electromagnetic spectrum

THz radiation has some special properties. First, THz waves can pass through most clothing materials and the attenuation is low. Second, THz wave is non-ionizing and because of the high sensitivity detection

schemes it can be used at a very low power level [4]. Third, compared with visible light, THz waves have lower scattering due to their longer wavelength. Fourth, THz waves are easier to collimate than radio waves. Fifth, THz waves can provide high-resolution imaging because they have shorter wavelength than microwaves [5]. Sixth, because many solids exhibit characteristic spectral features in 0.5 to 3 THz region, THz waves can identify different chemical substances even if they are sealed inside a packet [4]. In addition, the property of THz waves in different atmospheric condition should also be considered. Fig. 1.2 shows the attenuation of THz region in different weather conditions [6]. Many factors, such as temperature, humidity and dust, are considered in this figure. According to these results, it can be found that the best condition is met in hot tropical climates.

THz region is one of the least explored regions of the spectrum. Because THz field has multidisciplinary characters, investigation of the technique requires a deep knowledge of optics and photonics, microwave engineering and semiconductor physics. The multidisciplinary characteristic of the research in THz fields does not only cover the disciplines that constitute its foundation, but also contains the areas of applications, which include astrophysics, plasma physics, spectroscopy, medical imaging, biology, and communications [1]. In addition, since THz wavelengths are between optical wavelength and microwave wavelength, the traditional analysis and design techniques from these

fields can be carried over to the terahertz region, but there are some issues that are unique to the terahertz region, which also do not make this region well developed. For example, the THz sources available now are not effective and the measurement is difficult to be operated because both the size of the devices and the radiated power are tiny [7].

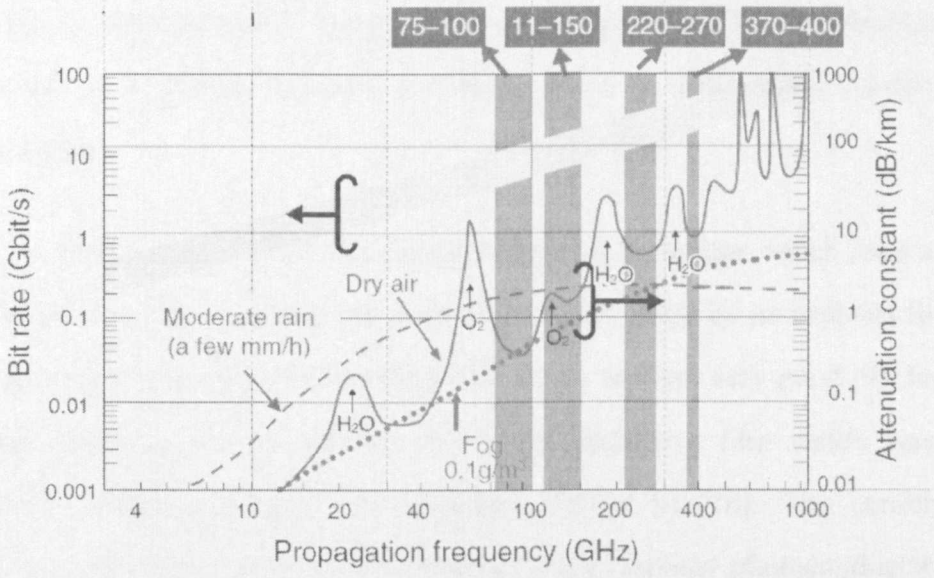

Fig. 1.2 Attenuation features of electromagnetic waves for different weather conditions [6]

1.2 Development of THz Technology

Compared with the microwave or photonics, THz band, which locates between them, is not well explored, so there are very few commercial devices for the THz frequency region and they lack the precision which is required for performing accurate measurements

although there have been some novel techniques to generate THz radiation [7]. This section will present a brief historical review of THz technology.

The first THz technology can be traced back to mid 1970s. During that period, Auston used a mode-locked Nd:glass laser to generate optical pulses to illuminate on SI-GaAs (semi-insulating GaAs) [8]. This method is used as a photoconductive switching which is now called Auston switching.

In 1980, Auston *et al.* developed a sampling technique which used a transmission line structure and a photoconductor made by amorphous Si film on fused Si substrate, but the performance was not very good [9]. In 1981, Smith *et al.* presented a new photoconductive film which was called radiation-damaged Si-on-sapphire (RD-SOS) [10]. The carrier lifetime of this new material was short, so a fast response photoconductor can be made.

In 1981, Mourou *et al.* used photoconductive switching to drive dipole antennas and electromagnetic waves of picosecond were radiated into the space [11]. In 1983, Heidemann *et al.* used photoconductive switching to drive a slot-line antenna and it also worked [12]. Both experiments proved that photoconductive switching can work well with the antenna structure for wave generation.

In 1984, Auston *et al.* used 100 fs optical pulses from colliding-pulse

passively mode-locked ring dye laser and RD-SOS to generate and detect electromagnetic pulses [13]. The configuration of this experiment was the photoconductive switch fabricated on a dielectric substrate. The ultrafast transient current in the photoconductive switch was the source and the detection part was based on the method of sampling the incident EM pulses repetitively. The pulse was only 1.6 ps which was very short and this experiment was considered as the origin of the THz optoelectronics.

In 1988, Smith *et al.* introduced a new antenna structure which can be used as both an emitter and a detector [14]. They used a photoconductive dipole structure on RD-SOS and pumped it with 120 fs optical pulses from a passively mode-locked dye laser, as shown in Fig. 1.3. This structure can generate frequency range from 100 GHz to over 1 THz and this paper was the first paper that demonstrated the photoconductive dipole structure can emit electromagnetic waves with THz frequency components.

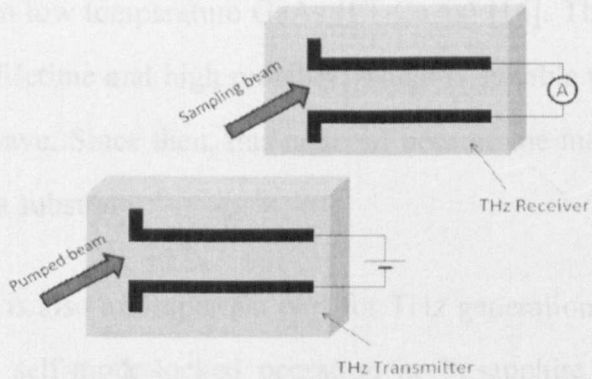

Fig. 1.3 THz transmission system by centre-feed dipole antenna

In 1989, Exter *et al.* improved the dipole structure by moving the coplanar transmission line to the end of the dipole, as shown in Fig.1.4 [15]. Because all the photo-induced current can be directed to the antenna structure, this new structure had better performs than the old structure. This new structure is widely used after this experiment and it is considered as a typical photoconductive dipole antenna structure.

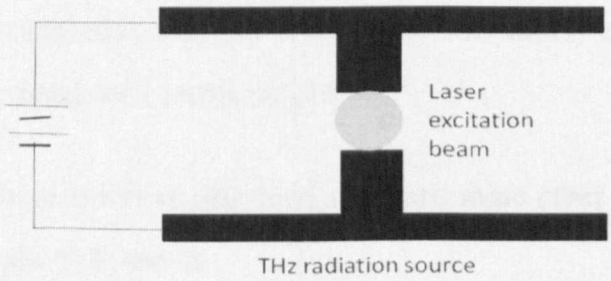

Fig.1.4 Structure of end-feed dipole antenna [15]

Because the substrate also affects the performance of the photoconductive antenna, the material of the substrate should also be investigated. In 1988, Smith *et al.* first developed the molecular-beam-epitaxy grown low temperature GaAs (LT-GaAs) [16]. This material has short carrier lifetime and high mobility, which is suitable to generate and detect THz wave. Since then, this material became the most popular one as the antenna substrate.

The laser is also an important part for THz generation and detection. In 1991, the self-mode-locked operation in Ti:sapphire oscillator was found and lead to the generation of sub-100 fs optical pulses [17]. This technique was more stable than dye laser which was the traditional way

to excite the antenna. Therefore, after the Ti:sapphire femtosecond lasers was commercially available in early 1990s, it became the most popular laser source in THz generation and detection system.

With the efforts of the researchers mentioned above, AT & T Bell Laboratory and IBM's T. J. Watson Research Centre began to be engaged in ultrafast optoelectronics in 1990s, and then THz optoelectronics was considered as an attractive area and "THz pulse" was widely used to refer to ultrafast electromagnetic transients [18].

Besides photoconductive antennas, there are some other methods to generate and detect THz waves.

In 1990, Zhang *et al.* used the semiconductor surface to generate electromagnetic pulses with picoseconds [19]. Then, Green *et al.* observed the THz wave generation dependence on crystal orientation [20]. In 1992, Hu *et al.* tested the performances of the semiconductor materials with different temperature [21]. Furthermore, some semiconductor quantum structures were also studied in early 1990s. Leo *et al.* first investigated the THz generation from double-quantum-wells by using time-resolved degenerate four-wave-mixing in 1991 [22]. Then, Planken *et al.* observed THz emission from single-quantum-wells [23] and Waschke observed THz emission from Bloch oscillations in a superlattice [24].

THz wave generation from a high-Tc superconducting thin-film

bridge with bias voltage was first observed by Hangyo in 1995 [25]. Then, Tonouchi *et al.* added an external magnetic field to improve the performance of the system in 1996 [26].

After 1990, as the most popular THz generation and detection devices, photoconductive antennas have also been developed considerably. In 1991, the structure of corner reflector array antennas was tested and proved to work in the THz band [27]. A centrally fed bow-tie antenna structure, which was very wideband, was introduced by Rebeiz in 1992 [28]. Pedersen *et al.* studied carrier transport and the screen effect of the dipole antenna on a semiconductor substrate in 1993 [29]. Jepsen *et al.* investigated the lens-coupled THz antennas which can enhance the brightness of the source in 1995 [30] and then they examined the characteristics of photoconductive dipole antennas for THz generation and detection in 1996 [31]. Cai *et al.* did some experiments to compare the performances of various photoconductive antennas in 1997 [32]. Goldsmith presented a log-periodic spirals planar antenna which was easy to be fabricated with the mixing device on the same substrate in 1998 [33]. Rudd *et al.* then tested the radiation from the lens-coupled photoconductive antenna with improved structure in 2000 [34].

As the advancement of the manufacture technologies such as Laser chemical vapour deposition (LCVD) and nanotechnologies, some new types of photoconductive antennas were investigated. Robert *et al.* introduced a helical THz antenna which can work up to 2.7 THz in 2000

[35]. In 2004, Burke first predicted nanotube transistor can work in THz band [36] and the simulation results were reported by Lan *et al.* [44]. Mendis *et al.* used a Bow-tie log-periodic antenna structure (as shown in Fig.1.5) to enhance the broadband performance in 2005 [37]. A photoconductive antenna with radial symmetry was also reported by Deibel *et al.* in that year [38]. Tani *et al.* presented a Schottky photoconductive antenna and a four-contact photoconductive antenna [39]. In 2006, Moon *et al.* changed the conventional dipole antenna structure into folded dipole structure to improve the impedance matching [40]. In 2008, Peytavit *et al.* chose a TEM horn antenna structure to fabricate on a semi-insulating GaAs substrate [41] and this type of antenna can radiate electromagnetic wave into certain locations without the help of lens.

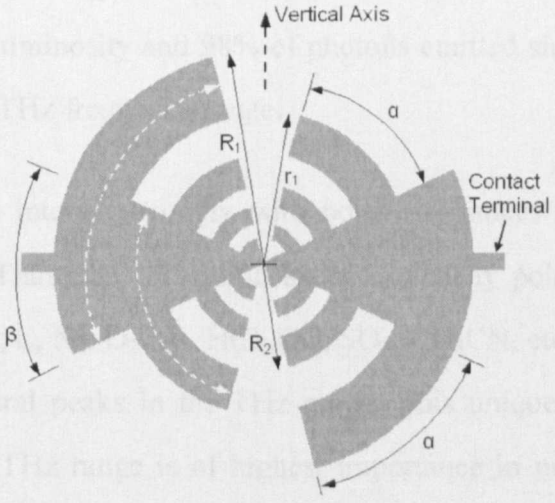

Fig. 1.5 Structure of log-periodic antenna [37]

All the techniques mentioned above are based on hybrid optical-electronic approach. Rodwell *et al.* introduced an all-electronic system which can be applied in THz area in 1987 [42]. They used monolithic nonlinear transmission lines (NLTL) to generate and detect picoseconds pulses. This technique is simple compare with optical-electronic approach but its limitation is the frequency range, which cannot reach as high as 1THz.

1.3 Main Applications of THz Technology

The THz frequency range is attractive because this is the region where unique physical phenomena with characteristic features are produced. Some of these features are listed below [43].

1) The spectral energy distribution in observable galaxies shows that 50% of the total luminosity and 98% of photons emitted since Big-Bang are located in the THz frequency range.

2) THz fields interact strongly with polar substances but penetrate those non-polar. Thus, the absorption spectra of many polar molecules, for example, H_2O, C, N_2, O_2, O_3, HCl, CO, SO_2, CH_3CN, etc., have many and distinct spectral peaks in the THz range. This unique signature of molecules in the THz range is of highest importance in monitoring the surrounding medium, air pollution detection, or gas sensing.

3) Biological tissues or other biological constituents have distinct

signatures in the THz range. For example, DNA signature, DNA manipulation and gene diagnostics were demonstrated experimentally using THz techniques.

4) Very small/miniaturized antenna arrays and circuits can be used in the THz range since the corresponding wavelengths, which impose the dimensions of antenna and circuits are much smaller than those encountered in the microwave and millimetre-wave spectral intervals. This advantage is of great importance in medical imaging and imaging devices such as THz cameras. Moreover, despite their reduced size, THz devices are able to send or receive a huge quantity of information that can be encoded in the ultra wideband of THz signals.

5) THz signals are the information carriers in the 1 to 10 Tb/s optical communications systems, which are developed now and are expected to become a commercial reality in the next decade. THz modulators able to modulate ultrafast laser diodes will use quantum devices such as ballistic diodes or transistors with a cut-off frequency well beyond 10 THz.

6) The 1 picosecond switching performance of the THz transistor is studied now by leading companies using the latest discoveries in nanotechnology. For example, the dimension of the gate of this transistor is 90 nm thick (about 5 atomic layers) and a static random access memory (SRAM) cell based on it is smaller than 1 mm^2. If the power consumption problems occurring at such a high speed will be solved, a

computer will run at a speed that is unimaginable today making possible, for example, real-time speech recognition and translation [47].

In summary, THz radiation does not damage the chemical bonds in living tissue, and thus, THz radiation is not a safety hazard to human beings. This has practical implications for terahertz radiation can be used in medical diagnostics much more safely than the highly ionising X-rays. From a more basic perspective, the vibrated and rotational energy levels of large polar molecules fall in the terahertz region, as do the energy gaps of superconductors. It is interesting to note that the world around us is immersed in an "ocean of terahertz radiation" [45].

THz radiation is presently finding impressive use in the laboratory for fundamental research [45]. These applications include:

- Spectroscopy of semiconductors, superconductors and bio-molecules
- Clinical application, *e.g.* early detection of skin cancer
- Imaging and tomography
- Quality control in industry
- Security screening
- Communications, etc.

THz spectroscopy is currently realised mainly in two approaches: continuous-wave spectroscopy, and time-domain terahertz spectroscopy (THz-TDS), which is a pulsed system. The fundamental principle of

terahertz spectroscopy is that different materials have various optical transmission characteristics in the terahertz region. Two parameters, the refractive index, and the absorption coefficient, are related to the characteristics. Therefore, different materials could be easily and quickly identified by their terahertz "signature": a particular material is passed through by a beam of terahertz radiation, and the difference between the transmitted beam and a reference beam will designate the material.

In the prospect of spectroscopy, it is a disadvantage for THz radiation to be strongly absorbed by water. However, in the field of medical diagnostics, this characteristic becomes an outstanding advantage. There is an obvious difference in the water content of cancerous tumours and healthy tissue. The difference can be detected by the absorption of terahertz radiation and therefore the cancerous tumours could be noticed. Another superior advantage of THz radiation in medical application, as previously mentioned, is its non-ionising property, which ensures no harm to those healthy tissues.

Communication system with THz frequency could offer a tremendous high data rate, which will satisfy the expanding demand for wireless communication systems. However, until present time, THz communications, with many issues largely unexplored, still remain a challenging field for scientists and researchers.

There are an increasing number of papers dealing with THz

applications. It has been revealed that THz waves possess at least the following features and potential applications [46]:

- **Energy**: objects at room temperature (300 K) emit thermal energy in this range (6 THz). Half of the cosmic background radiation from the Big Bang is in the THz part of the spectrum.

- **Signature**: from GHz to THz frequencies, numerous organic molecules exhibit strong absorption and dispersion due to rotational and vibrational transitions. These transitions are specific to the targets and enable THz-ray fingerprinting.

- **Health and safety**: THz-rays have low photon energies (4 meV at 1 THz, one millions times weaker than an x-ray photon) and will not cause harmful photo-ionization in biological tissues.

- **Defence applications:** homeland security, chemical and biological agent detection, explosives detection, see-through-the-wall applications, imaging and remote sensing.

- **Commercial applications**: high data rate communications, non-contact and non-destructive detecting and imaging, such as skin imaging for cancer detection, forgery, mail inspection, luggage inspection, gas spectroscopy.

- **Research:** physics, astronomy, sensing, plasma fusion diagnostics, THz wave microscope, and spectroscopy.

There have been some commercial devices for THz applications. Fig. 1.6 is a 3D THz imaging system for tablet coatings and cores produced by TeraView [48]. Fig. 1.7 is the T-Ray 2000 Reaserch Application Development System which was produced by Picometrix Inc [49]. Fig. 1.8 to Fig. 1.10 are some examples of THz applications which have been used in practice. Fig. 1.8 is a THz application for dental imaging. The left figure is the optical image of a tooth, the middle figure is the spectroscopic image showing the cavity and right figure is the time of flight image showing enamel and dentine structure. Fig. 1.9 is a THz application for security purpose which can detect hidden weapons. Fig. 1.10 shows the THz application for drug identification, and it can identify different drugs with different components. The polyethylene bags which contain (left to right) 3,4-Methylenedioxymethamphetamine (MDMA), aspirin and methamphetamine were put into an envelope and responded different absorption intensities by THz illumination [48, 49].

It can be predicted that THz technology will become more and more attractive, since the THz features mentioned above imply many applications in various areas as discussed.

Fig. 1.6 3D THz imaging system produced by TeraView [48]

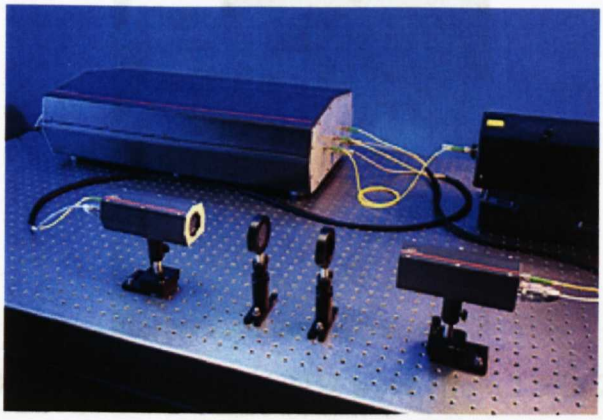

Fig. 1.7 T-Ray 2000 reaserch application development system [49]

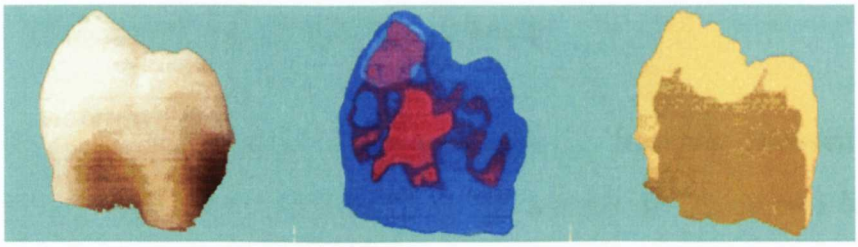

Fig. 1.8 THz imaging for human teeth (from 0.2 to 1.5 THz) [48]

Fig. 1.9 Hidden weapon detection by THz wave (94GHz) [48]

Fig. 1.10 Drug identification by THz wave (from 1.3 to 2 THz) [49]

1.4 Motivations of the Research

Although THz frequency band locates in the gap between the microwave band and infrared bands, the sources for these two bands cannot be used directly for THz range. The main problem for THz technology is how to obtain an efficient THz source with a high power level.

The solid state sources are difficult to be used in THz range because the size becomes very small leading to very small power available [50]. Fig.1.11 shows output power variation of conventional solid state sources. It can be seen that the efficiency of the sources falls drastically for higher THz range. The carrier transit time also becomes very short compared to microwave frequency signals. On the other side, conventional laser sources are not available at the THz band because suitable semiconductors are not available.

Therefore, how to obtain a cheap and simple THz source which can generate THz waves becomes an interesting research topic.

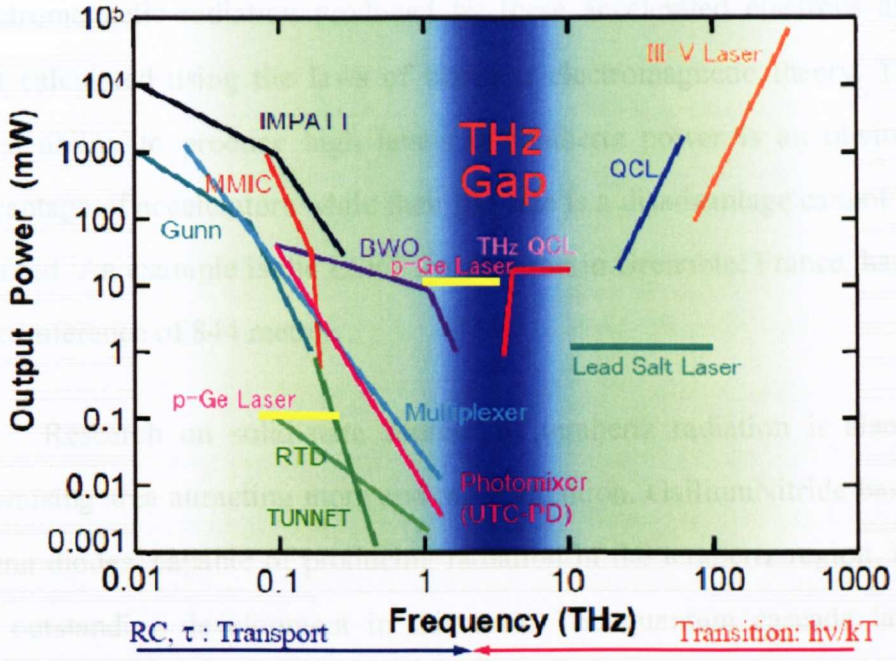

Fig.1.11 Radiated power from different THz sources [50]

The available methods to generate the terahertz wave can be divided into four different categories [45]:

1) Accelerators

2) Solid-state sources

3) Gas lasers

4) Optically-excited sources

Accelerators are able to accelerate electrons to relativistic speeds. Reasonably good agreement could be obtained between the

electromagnetic radiation produced by these accelerated electrons and that calculated using the laws of classical electromagnetic theory. The great ability to produce high levels of terahertz power is an obvious advantage of accelerators while their big size is a disadvantage cannot be ignored. An example is the ESRF synchrotron in Grenoble, France, has a circumference of 844 metres.

Research on solid-state sources of terahertz radiation is also a promising area attracting more and more attention. GalliumNitride-based Gunn diodes, capable of producing radiation in the terahertz region, are an outstanding development in this area. The quantum cascade laser (QCL), in which electrons "cascade" down a series of energy steps and emit a photon at each step, is another promising candidate.

Another source of terahertz radiation is far infrared gas lasers, such as carbon dioxide lasers and pumped methanol or ammonia lasers, which emit terahertz radiation using the energy transitions between vibrated and rotational states of the gas molecules. However, they also have the disadvantage of being heavy and bulky.

Currently the most popular sources of terahertz radiation are optically excited sources. Their principle of operation is that electromagnetic radiation is produced in different way in a semiconductor substrate or a non-linear crystal. When a semiconductor substrate is focused on by a laser beam, pairs of electrons and holes, which are

accelerated by a voltage bias applied across the semiconductor, are produced by the laser beam. Electromagnetic radiation is produced by the acceleration of these electrons and holes. In the case of nonlinear crystals, electromagnetic radiation is produced by optical rectification which is a non-linear optical effect. At present, two main types of optically-excited sources, pulsed and continuous-wave, are widely used. Pulsed systems are based on THz-TDS systems. In pulsed systems, the semiconductor is excited by extremely short, femtosecond laser pulses. Pulses of electromagnetic radiation with terahertz frequencies are produced by the formation of electron-hole pairs, and their subsequent acceleration under the applied bias produces. Continuous wave sources are based on the principle of photomixing. A semiconductor substrate is focussed on by two laser beams which are slightly different in frequency. A "beating" effect will occur because of the difference in frequency. Difference in frequency lies in the THz region will excites the semiconductor and the resulting electromagnetic energy could be radiated by using suitable antennas [45].

Therefore, it is obvious that the THz technology has not yet reached maturity and a lot of work remains to be done to improve the performances of the existing devices in the THz range.

This research work aims to find some simple ways to improve the THz source performances. The most popular THz source, photo-conductive antenna, is chosen to be analysed and some practical methods

are provided to increase the radiation power level. Since most of the previous publications have focused on the physics part only, this thesis first introduces some antenna theories to analyse this typical THz source and thus some problems such as impedance matching and the radiation pattern which are very important in the antenna area are taken into account. These works can help the researchers obtain more information about THz radiation from the THz source and make the designing work more practical.

CHAPTER 2

BASIC THEORIES OF THZ TECHNOLOGY

2.1 THz Generation and Detection using Photoconductive Antennas

Based on the introduction in last chapter, some basic theories about how to generate and detect THz waves will be discussed in this chapter. The first section will introduce the most popular method: photo-conductive effect approach and the second section will present some other THz generation and detection technologies.

2.1.1 THz Generation with Photoconductive Antennas

THz generation and detection with photoconductive effects is the most popular method in recent years. The mechanism of photoconductive effects can be described as follows. When the energy which is input into a semiconductor is larger than the bandgap, it will separate the electrons and holes. They are usually called electron-hole pairs. If a DC bias voltage is applied on the semiconductor, the electrons and holes will flow in a certain direction and a current is produced. Furthermore, if the input energy changes rapidly such as a short period pulse laser, the number of the electron-holes will change rapidly, the current intensity will also change rapidly, therefore, a time-varying electric field is produced and electromagnetic waves are generated [51]. The schematic illustration of

this process is shown in Fig. 2.1.

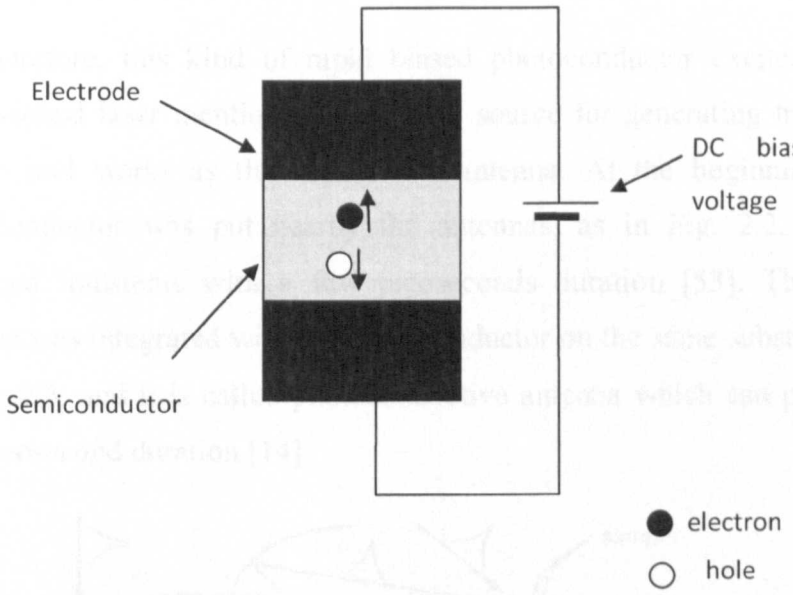

Fig. 2.1 The schematic of electron-hole pairs production

The production of ultrashort currents with a full-width half-maximum (FWHM) less than 1 picosecond depends on a number of things, such as the incoming laser pulse and the carrier lifetime in the semiconductor. Although intrinsic semiconductors have a carrier lifetime exceeding hundreds of picoseconds, some processing techniques such as annealing, ion implantation, and radiation exposure, can reduce the carrier lifetimes to sub-picosecond duration [52]. This category of semiconductors is referred to as semi-insulating semiconductors. More details about the semiconductor materials will be discussed in Section 3.2. Nowadays, the most popular semiconductor with a very short carrier

lifetime is the LT-GaAs that has a photocarrier's lifetime of 0.25 ps, where the lifetimes of electrons and holes are 0.1 ps and 0.4 ps, respectively and LT-GaAs also has a high mobility and a high breakdown field (the characteristics of LT-GaAs can be found in Section 3.2).

Therefore, this kind of rapid biased photoconductor excited by a femtosecond laser mentioned above is a source for generating transient current and works as the feed of an antenna. At the beginning, the photoconductor was put nearby the antennas, as in Fig. 2.2, and it produced transients with a few picoseconds duration [53]. Then the antenna was integrated with the photoconductor on the same substrate, as in Fig. 2.3, and it is called photoconductive antenna which can produce sub-picosecond duration [14].

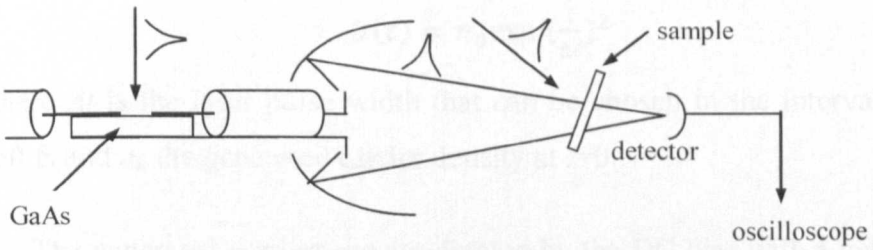

Fig. 2.2 Photoconductor separated from the antenna structure [53]

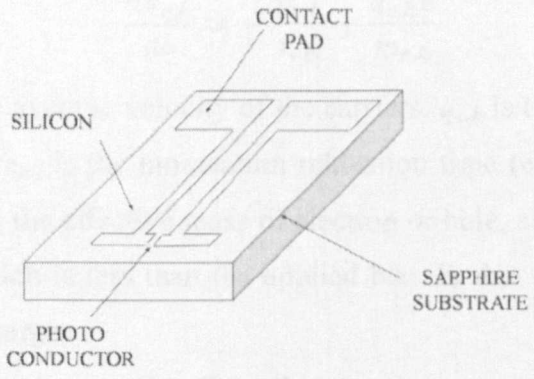

Fig. 2.3 Photoconductor integrated with the antenna structure [14]

The carrier dynamics in the photoconductors can be analysed as the following. The carrier lifetime in photoconductive antenna on a LT-GaAs semiconductor substrate is considered approximated as equal to the carrier trapping time because the trapping time in mid-gap states is much slower than the recombination time between electrons and holes. Therefore, the carrier density can be described by Drude-Lorentz theory [54]:

$$dn/dt = -n/\tau_t + G(t) \tag{2.1}$$

where n is the carrier density and $G(t)$ is the generation rate of carriers due to laser pulse excitation. The carrier lifetime τ_t can be engineered to take values in the interval 0.1–5 ps by modifying the annealing temperature for LT-GaAs containing different excess arsenic concentrations.

$$G(t) = n_0 \exp\left(\frac{t}{\Delta t}\right)^2 \tag{2.2}$$

where Δt is the laser pulse width that can be chosen in the interval 30–150 fs and n_0 the generated carrier density at t=0.

The generated carriers are accelerated by the DC bias with a velocity rate given by

$$\frac{dv_{e,h}}{dt} = -\frac{v_{e,h}}{\tau_{rel}} + \frac{q_{e,h}E}{m_{e,h}} \tag{2.3}$$

where $v_{e,h}$ are the average velocity of the carriers, $q_{e,h}$ is the charge of the electron or hole, τ_{rel} is the momentum relaxation time (equal to 30 fs in LT-GaAs), $m_{e,h}$ is the effective mass of electron or hole, and E is the local electric field, which is less than the applied bias E_b due to the screening effect of space charges.

$$E = E_b - P/\alpha\varepsilon_r \tag{2.4}$$

where ε_r is the dielectric constant, α is the geometric factor of the

semiconductor (equal to 3 for LT-GaAs) and P the polarization induced by the separation of electrons and holes.

The polarization depends on time according to the expression

$$\frac{dP}{dt} = -\frac{P}{\tau_{rec}} + J \tag{2.5}$$

where τ_{rec} is the recombination time between electrons and holes (τ_{rec}=10 ps for LT-GaAs) and J is the current density which defined as

$$J = env_h + (-e)nv_e \tag{2.6}$$

Based on the Maxwell's Equations, the THz radiation field in the far-fields can be expressed

$$E_r(z,t) = -\frac{A}{4\pi\varepsilon_0 c^2 z} \cdot \frac{\partial J}{\partial t} \tag{2.7}$$

The far-field radiation is given by

$$E_{THz} \propto \frac{\partial J}{\partial t} \propto ev\frac{\partial n}{\partial t} + en\frac{\partial v}{\partial t} \tag{2.8}$$

where v=v_e -v_h. The transient electromagnetic field E_{THz} consists of two terms: the first term describes the carrier density charge effect while the second term describes the effect of charge acceleration due to the electric field bias [55, 56].

The main results can be summarized as follows:

(1) The generated THz field E_{THz} is inversely proportional to the effective mass of the carriers. Since in LT-GaAs the effective mass of the hole is five times larger than that of the electron, the effect of holes in the THz radiation is significantly reduced compared to that of electrons but cannot be ignored due to the screening effect.

(2) In Equation (2.8), the first term is much greater than the second so that the THz radiation is produced mainly due to the ultrafast change of the carrier density $v\partial n/\partial t$, while the effect of carrier acceleration has a smaller effect.

(3) The pulse width of E_{THz} becomes larger when the width of the excitation laser pulse is increased.

(4) E_{THz} is a dynamic bias when the photoconductive antenna works as a detector. The detector acts like a filter, filtering only the shortest wavelength components of the transient electric field. The radiated THz field is thus considerably distorted.

Therefore, the performance of photoconductive antenna depends on the incident optical beam, the materials of semiconductor (carrier lifetime and mobility) substrates and the antenna geometry.

Some types of antenna structures have been investigated such as dipole antenna, slot antenna, bow-tie antenna and log periodic antenna [57, 58, and 59]. The surface impedance of the metal from the photoconductive antenna is

$$Z_s = \sqrt{\frac{i\omega\mu_0(1+i\omega\tau)}{\sigma_0}} = \frac{1}{2}\cdot\frac{\mu_0}{\tau\sigma_0} + i\omega\frac{\tau\mu_0}{\sigma_0} = R_s + iX_s \qquad (2.9)$$

where ω is the frequency, τ is the relaxation time of the electrons in the metal, and σ_0 is the conductivity.

Here a difference between the microwave antenna and the THz antenna can be found. In the microwave range, $\omega\tau \ll 1$, so the imaginary part can be negligible, which is a well-known skin effect. However, in

far-infrared (FIR) or infrared (IR) range, the imaginary part cannot be negligible and plays an important role for the antenna performance because the real part can be considered as a constant while the imaginary part increases linearly with the frequency. For example, for wavelength from 1 to 70 μm, the real part R_s is only a few ohms but the imaginary part X_s is about 10 to 60 Ω.

The thickness of the substrate also affects the performance of photoconductive antennas. In microwave range, the thickness of substrate is much smaller than wavelength, and it can cancel the substrate mode which leads to the reduction of radiation and dielectric losses. In FIR and IR ranges, the thickness is usually greater than the wavelength, so the energy above the critical angle is trapped in the substrate. Sometimes, more than 90% power is wasted in the substrate. Therefore, to obtain low-level losses, the thickness of the substrate should be very small, for example, 0.04 λ for slot antenna and 0.01 λ for dipole antenna, which means the thickness is only about several micrometers for 1 THz [60]. This problem makes it difficult to produce the antenna. To reduce the effect of this problem, a lens-coupled photoconductive antenna is used in recent years [61].

2.1.2 THz Detection with Photoconductive Antennas

THz detection is difficult because the power of THz signal is usually weak. Ultrashort electrical pulses are widely used to make the THz detection practical.

Ultrashort electrical pulses with a spectral content within the THz frequency range, produced using various physical principles are detected

using mainly two methods. The first method uses a gated photoconductive antenna and is called photoconductive sampling (PC sampling). The second method is based on the detection of the polarization change of an optical probe beam produced by the THz field when both fields are applied on an electro-optic crystal; this method is called free-space-electro-optic sampling (FS-EOS).

The configuration of PC sampling is shown in Fig. 2.4. With this method, the charge generated at the antenna terminals is [62]

$$q(\tau) = \int v(t)g(t-\tau)dt \tag{2.10}$$

where $v(t)$ is the voltage across the photoconductive gap, given by

$$v(t) = \int H(\omega)E(\omega)\,exp(i\omega t)\,d\omega \tag{2.11}$$

where $E(\omega)$ is the Fourier transform of the incident electric field pulse $E_{THz}(t)$ and $H(\omega)$ is the transfer function of the antenna, *i.e.* the ratio between the voltage induced at the antenna terminals and the incident electric field, both represented in the frequency domain, and $g(t)$ is the conductance which is given by

$$g(t) = \int I(t')\left\{1 - exp\left[1 - \frac{exp(t-t')}{\tau_{rel}}\right]\right\} exp\left[\frac{t-t'}{\tau}\right] dt' \tag{2.12}$$

From Equation (2.12) it follows that the PC sampling output signal is dependent on the incident field $E_{THz}(t)$, but also depends on the momentum relaxation time τ_{rel} and the carrier lifetime τ of the PC substrate. It was experimentally found that when THz detection is performed with a short dipole without a substrate lens [63], $H(i\omega) = 1$, and so $v(t)$ becomes directly proportional to the incident THz signal $E_{THz}(t)$. When the THz detector consists of a short dipole with a substrate lens, $H(i\omega) = i\omega$.

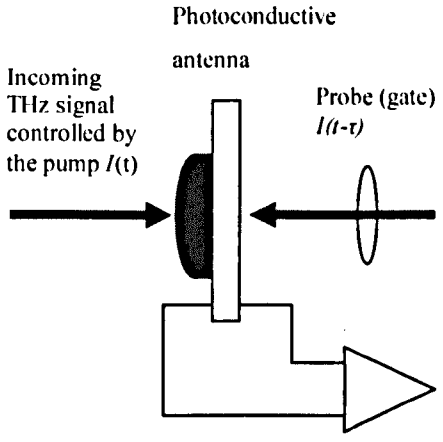

Fig. 2.4 Configuration of PC sampling [62]

The FS-EOS uses the linear electro-optic effect in an EO crystal excited by an optical probe field and the THz field. The configuration of FS-EOS is shown in Fig. 2.5. Both fields propagate in the same direction but have different polarizations. For example, if z is the propagation direction, the optical probe is polarized at 45° in the (x, y) plane perpendicular on z due to birefringence of the EO crystal, while the THz field is perpendicular on the y axis. Since the electro-optic effect is practically instantaneous at the THz scale, the output of a FS-EOS detector is directly proportional to $E_{THz}(t)$ [62]. Due to the presence of the THz field a phase retardation $\Delta\varphi$ of the optical field is produced over the distance *dz*, which is strongly dependent on the electro-optic crystal type and orientation. FS-EOS uses different types of electro-optic crystals: i) uni-axial crystals like $LaTiO_3$ or $LiNbO_3$, or ii) isotropic crystals like ZnTe with a zinc-blend structure. ZnTe is a material for which a high signal-to-noise ratio was obtained. For ZnTe the phase retardation is

given by

$$\Delta\varphi(t) = \left(\frac{\omega}{c}\right) n_0^3 r_{41} E_{THz}(\tau) dz = const_{ZnTe} \times E_{THz}(\tau) dz \quad (2.13)$$

where ω is the optical frequency of the probe and r_{41} is the electro-optic coefficient. From the above relation it follows that the THz field obtained after propagating over a length L in a ZnTe crystal, material with small absorption and a refractive index difference of $\Delta n = n_{THz} - n_{opt} = 0.22$, is

$$E_{THz}(\tau) = \Delta\varphi(\tau)/(L \times const_{ZnTe}) \quad (2.14)$$

Thus, measuring the phase change we are able to determine the time variation of the THz signal $E_{THz}(\tau)$.

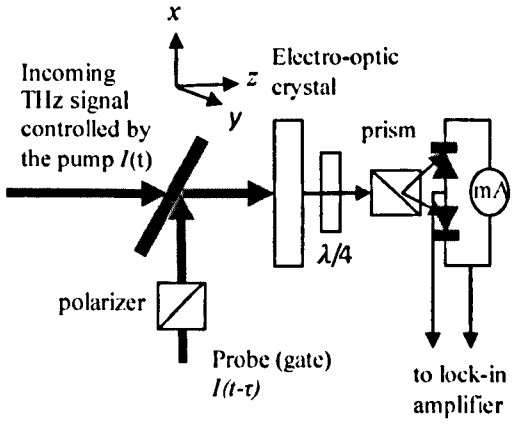

Fig. 2.5 Configuration of FS-EOS [63]

Both detection methods, which are coherent methods, were compared using the same laser power modulated by an acousto-optic modulator. At low-frequency modulation the PC sampling method shows a better signal-to-noise ratio and sensitivity, for an identical received THz average power. Increasing the modulation frequency over 1 MHz; the

performances of the FS-EOS method become comparable, *i.e.* the signal-to-noise ratio of FS-EOS becomes greater than 10^4 [64].

2.2 Other Technologies of THz Generation and Detection

Besides photoconductive effect, there are some other methods to generate and detect THz waves, such as optical rectification in nonlinear media and surge current on semiconductor surfaces. This section will introduce two methods which are also commonly used to generate and detect THz waves: NLTL and nano-devices.

2.2.1 NLTL

NLTL stands for nonlinear transmission lines [65]. As mentioned in the history review (Section 1.2), NLTL is an all-electrical THz system. It consists of a high impedance transmission line and nonlinear elements which are periodically loaded on the transmission line. The typical structure is shown in Fig. 2.6. The transmission line is usually CPW and the nonlinear elements are usually Schottky varactor diodes which are reverse-biased.

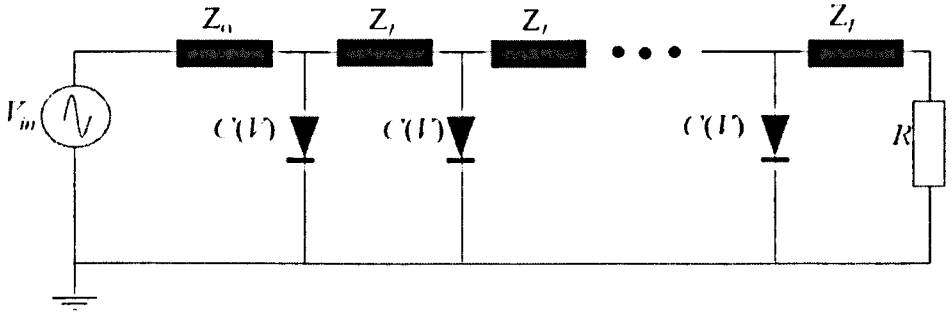

Fig. 2.6 Schematic of NLTL

The Schottky diodes work as voltage-variable capacitors which can cause a wave travelling along the transmission line, and the velocity of the wave is voltage-dependant. Therefore, the shock wave produced along the line likes a step function and it can be used as the ultrafast signal source and a strobe generator for sampling. When the input is sinusoidal wave, the negative-going transitions are changed into shock waves and the output is a saw-tooth wave. For a transmitter, the output from NLTL is usually coupled to a bow-tie antenna due to its broadband feature, and for a receiver, a sampling circuit is added between NLTL and the bow-tie antenna as shown in Fig. 2.7.

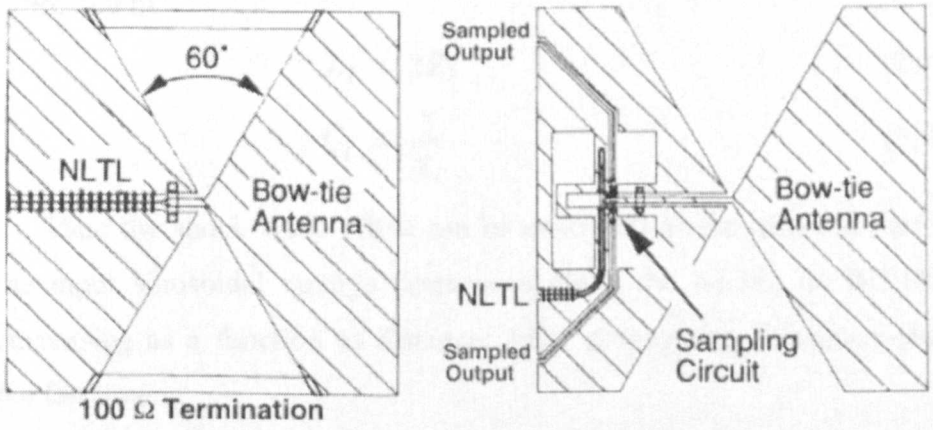

Fig. 2.7 NLTL works as transmitter (left) and receiver (right) [65]

Shock waves in NLTL are occurred because of the balance between the nonlinearity and the inherent dispersion, and the waves are compressed versions of the input excitation usually a sinusoidal wave. It can be considered that the impedance of a CPW line is formed by a series inductance L_l and a shunt capacitance C_l, and the Schottky diode is a resistance R_d in series with a variable capacitor C_d. The cut-off frequency

of the diode f_d and NLTL circuit f_n can be expressed as following:

$$f_d = \frac{1}{2\pi R_d C_d(V)} \tag{2.15}$$

$$f_n = \frac{1}{\sqrt{\pi L_l [C_l + C_d(V)]}} \tag{2.16}$$

The shock waves are generated when $f_d = f_n$. The delay between two consecutive cells is

$$\tau = \frac{d}{v_{cpw}} \tag{2.17}$$

where d is the distance between two consecutive diodes and v_{cpw} is the velocity in CPW. In addition, the inductance and the capacitance can be expressed by:

$$L_l = \tau Z_l \tag{2.18}$$

$$C_l = \frac{\tau}{Z_l} \tag{2.19}$$

Then the shock wave effect can be described as the negative part of the input sinusoidal voltage propagates along the NLTL, its fall time decreasing as a function of distance. After propagating through n-cells, the fall time is

$$t_n = t_{in} - n\tau\sqrt{1 + \frac{C_d(0)}{C_l}} - n\tau\sqrt{1 + \frac{C_d(0)}{C_l}} \tag{2.20}$$

When the fall time decreases, the dispersion that broadens the fall time is balanced by the nonlinearity, which compresses the fall time due the voltage-dependent propagation velocity. A stable fall time of the input voltage (the shock wave) is attained when the fall time compression/cell is equal to the fall time broadening/cell. After this, the shock wave propagates unchanged in shape along the NLTL.

This section has given a brief introduction to an all-electrical THz system: NLTL system. More details can be found in ref [65]. It is simple compared with the photoconductive effect approach, but it cannot be used for the frequency above 1THz.

2.2.2 Nano-Devices

From the last decade of the 20th century, nanotechnology is becoming increasingly popular in various research fields and industries. This innovative technology can also find applications in THz generation and detection. THz antenna can be made of array of Carbon nanotubes (CNTs) [66]. CNTs can be used to form finite length dipole antennas. Hallen's-type integral equation is a useful implement to investigate those antennas. The antenna effect of carbon nanotubes has already been validated [67].

Maximum antenna effect is achieved when the antenna length is multiple of half-wavelength. Transmission line model [68] could be applied to carbon nanotube antenna analysis. In transmission line model, in addition to the familiar magnetic inductance and electrostatic capacitance, the equivalent circuit also includes quantum capacitance and kinetic inductance in order to consider several additional effects. With these two components taken into account, the wave velocity in a CNT is then modified to

$$V_p = (L_k C_{total})^{1/2} \tag{2.21}$$

where $\frac{1}{C_{totla}} = \frac{1}{C_q} + \frac{1}{C_{ES}}$, C_q is the quantum capacitance, C_{ES} is the electrostatic capacitance and L_k is the kinetic inductance.

As shown in Fig. 2.8 (b), the gain becomes evidently greater when the length of the antenna increases. The gain also becomes greater with increasing number of elements in the array. In addition, suitably choosing the inter element distance d could help increasing the gain. Another advantage of this antenna is its good directivity, as can be seen from Fig. 2.8(c). Therefore, sufficient power could be radiated or absorbed from properly designed carbon nanotube antenna.

For THz detection, a bolometer is usually used. Ling *et al.* [69] proved that the bolometer can work up to 3 THz by using MEMS techniques. The bolometer is a square sheet of bismuth with a length greater than 1.5 wavelengths evaporated on a thin dielectric membrane which consists of $SiO_2/Si_3N_4/SiO_2$ and the thickness is 700nm, 350nm, 450nm for each layer, as in Fig. 2.9.

However, bolometer can only measure power. To obtain the information about both power and frequency simultaneously, an array of micromachined nanosized Fabry-Perot-like cantilevers was introduced in 2001 [70]. Fabry-Perot-like cantilever is a combination of a cantilever and a Fabry-Perot resonator as shown in Fig. 2. 10.

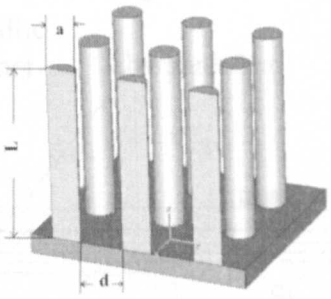

(a)

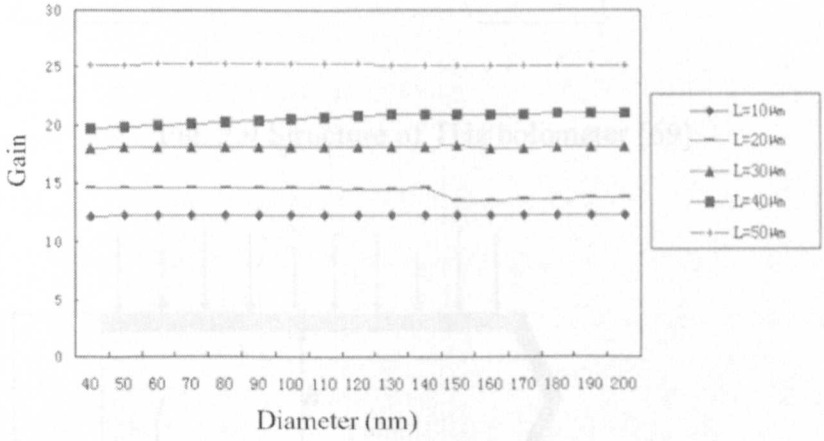

(b)

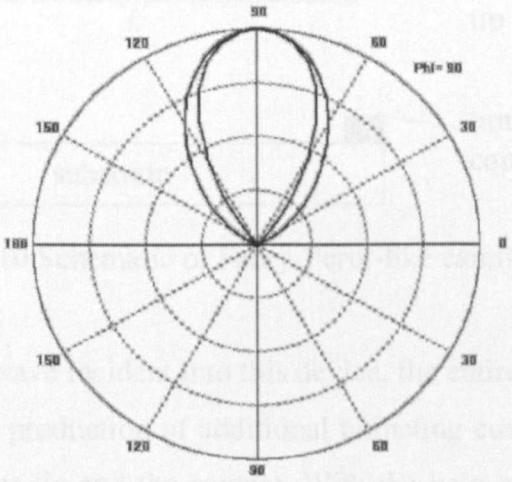

(c)

Fig. 2.8 Carbon nanotube antennas and its performances [66]

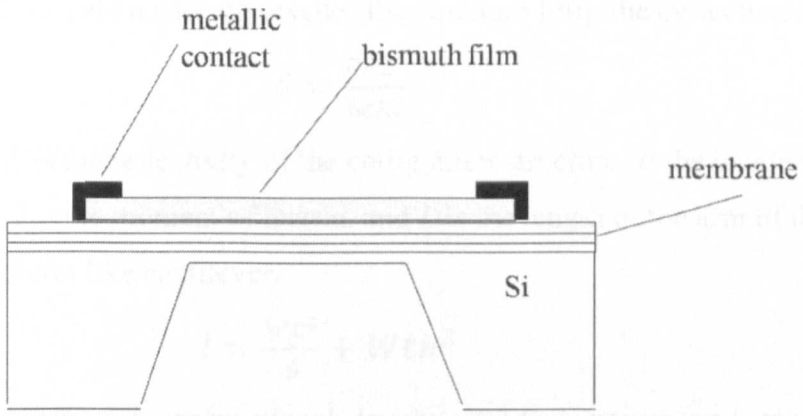

Fig. 2.9 Structure of THz bolometer [69]

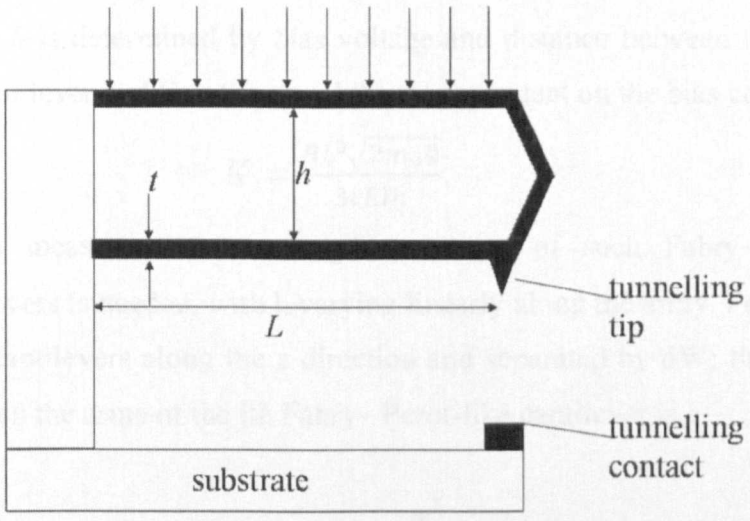

Fig. 2.10 Schematic of Fabry-Perot-like cantilevers [70]

When THz wave incident into this device, the entire structure is bend which leads to a production of additional tunneling current. This current flows between the tip and the contact. With the help of this technology, even small deflection of about 1 Å can produce large changes in current because of the exponential dependence of the tunneling current.

If THz field uniformly excites the structure [70], the deflection is:

$$\delta = \frac{RPL^3}{6cEI} \tag{2.22}$$

where R is the reflectivity of the entire microstructure, P the incident power, I is the moment of inertia, and L is the length of the arm of the Fabry–Perot like cantilever.

$$I = \frac{Wt^3}{6} + Wth^2 \tag{2.23}$$

Because δ is proportional to the incident power and measured tunneling current is exponential to the deflection, I can be calculated as following

$$I = I_0 \exp(KP) \tag{2.24}$$

where I_0 is determined by bias voltage and distance between the tip and the cantilever and K is the sensibility independent on the bias conditions

$$K = \frac{RL^3\sqrt{2m_0\emptyset}}{3cEIh} \tag{2.25}$$

To measure the wavelength an array of such Fabry–Perot-like cantilevers is needed, with h varying linearly along the array. For an array of N cantilevers along the z direction and separated by dW; the distance between the arms of the jth Fabry– Perot-like cantilever is

$$h_j = h_0 + A[(j-1)(W + dW) + \frac{W}{2}] \quad (j=1,2,3,\ldots,N) \tag{2.26}$$

Since the total reflection coefficient is periodic with h, taking maximum values at

$$h_j = (2m + 1)c/4f \tag{2.27}$$

and minimum values at

$$h_j = mc/2f \tag{2.28}$$

the frequency of the THz source can be determined monitoring the position in the array for which the reflection coefficient is minimum and/or maximum (in simple metallic cantilevers the reflectivity does not depend on its thickness.). The resolution in the bandwidth of 1.2–58 THz is $\Delta f/f \approx 10^{-3}$ in the example considered here.

2.3 Scope of the Research

Besides the technologies discussed in this chapter, there are some other methods which can generate and detect THz wave such as optical rectification in nonlinear media and THz generation using bare semiconductors. Among all of them, the technology of photoconductive antenna is the most popular one because it can generate reasonable power level even when the frequency is very high. Therefore, this thesis will analyse this technology and find some methods to improve its performance.

CHAPTER 3
THZ GENERATION AND DETECTION SYSTEM BY PHOTOCONDUCTIVE ANTENNAS

3.1 Overview of THz Generation and Detection Systems

From the discussion above, we understand that the photoconductive antenna can be used at both generation and detection system of terahertz transmission.

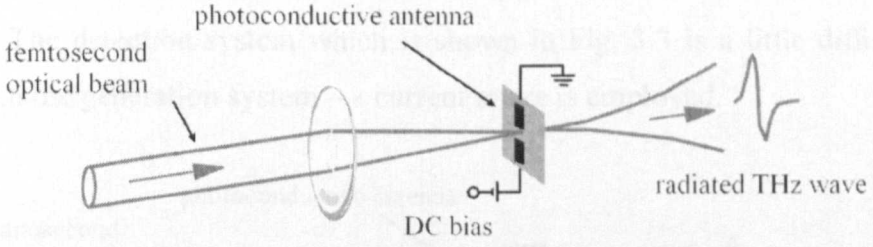

Fig. 3.1 THz generation system

The generation system is shown in Fig. 3.1. A short period laser beam (femtosecond optical beam) is focused on the substrate of the photoconductive antenna, and with the acceleration of the bias voltage, the terahertz wave is generated. The relationship between the femtosecond laser and the generated terahertz wave can be roughly

expressed by Fig. 3.2. The details will be discussed in Section 3.2.

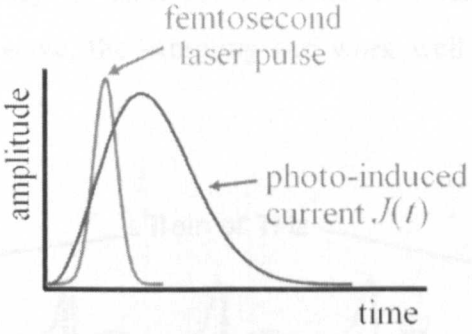

Fig. 3.2 Relationship between the laser source and the photo-current

It is obvious from Fig. 3.2 that to generate a THz wave, a very short period laser source, which is much higher than THz in frequency, must be used. It is one of the problems which limit the development of the THz technology.

The detection system which is shown in Fig. 3.3 is a little different from the generation system – a current metre is employed.

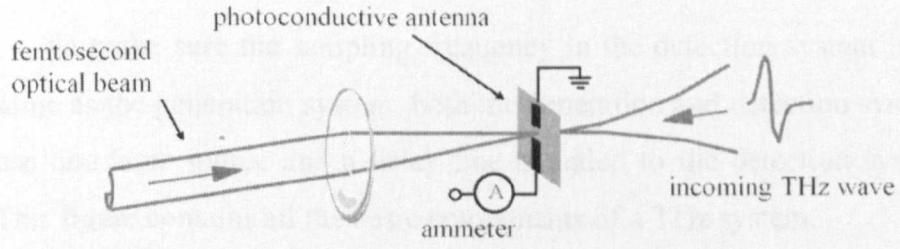

Fig. 3.3 THz detection system

The incoming THz wave works as the bias voltage, the femtosecond laser is used to sample the THz wave from the generation system, and the

ammeter replaces the DC bias voltage to detect the output current. Because the frequency of femtosecond laser is much higher than the incoming terahertz wave, the sampling can work well as shown in Fig. 3.4.

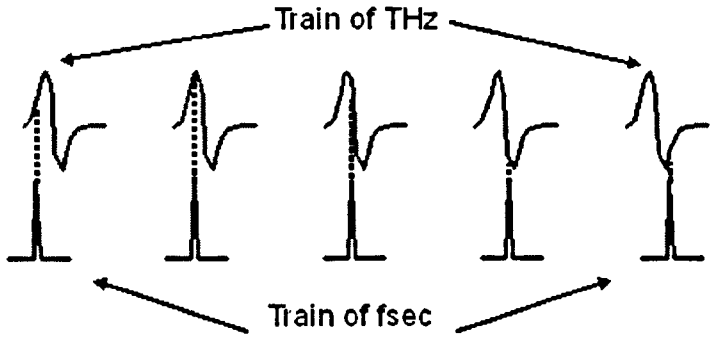

Fig. 3.4 THz sampling

Therefore, by combining the generation system and detection system, a whole terahertz transmission system can be set up.

Fig. 3.5 shows the basic structure of the THz transmission system.

To make sure the sampling frequency in the detection system is the same as the generation system, both the generation and detection systems use one laser source and a delay line is added to the detection system. This figure contains all the basic components of a THz system.

The details of the THz transmission system using photoconductive antennas will be discussed and some examples of typical photoconductive antennas will be introduced.

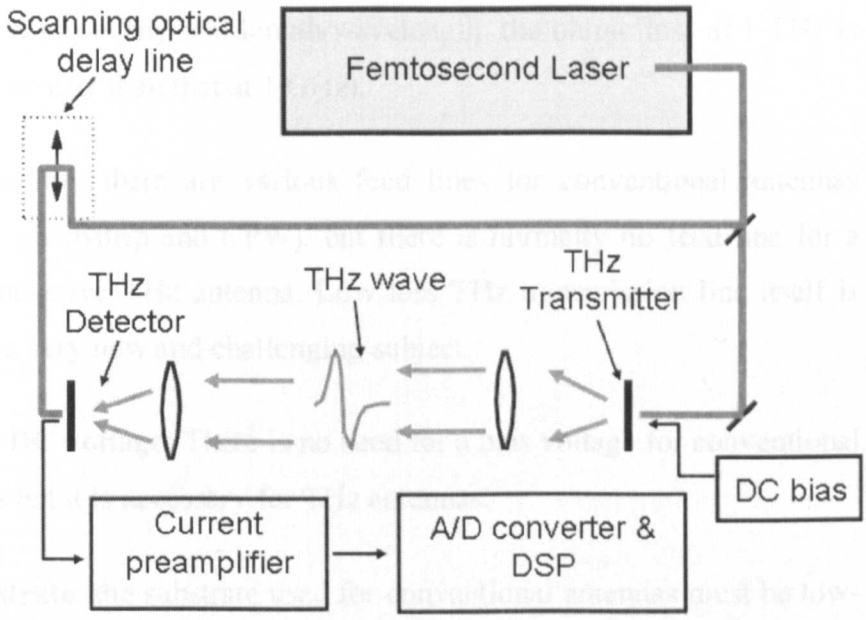

Fig. 3.5 Representative setup of THz system

3.2 Mechanism of THz Generation and Detection with Photoconductive Antennas

As it is well known, an antenna is a structure which will radiate and receive electromagnetic power in an efficient and desired manner. The antenna theory is well established. However, THz antennas are a new type of antennas developed for THz applications. Compared with conventional RF/microwave antennas, we can identify the following main differences [46]:

(1) Skin depth: the skin depth is inversely proportional to the square root of the frequency. For example, the skin depth of a gold track is 2.49 μm at 1 GHz while it is 0.0787 μm at 1 THz. For the same length, the ohmic

loss is about 32 times larger at 1 THz than that at 1 GHz (but for the same electric length = physical length/wavelength, the ohmic loss at 1 THz is actually smaller than that at 1 GHz).

(2) Feed-line: there are various feed lines for conventional antennas (such as microstrip and CPW), but there is normally no feed-line for a photoconductive THz antenna. Low loss THz transmission line itself is actually a very new and challenging subject.

(3) Bias DC voltage: There is no need for a bias voltage for conventional antennas but it is necessary for THz antennas.

(4) Substrate: the substrate used for conventional antennas must be low-loss dielectric material whilst the substrate used for THz antennas should contain a layer of a semiconductor.

(5) Manufacture: it is much harder to make a THz antenna which is normally fabricated by conventional lithography on low temperature GaAs grown at about 250°C and post annealed at 250°C for 1 minute. The metal patterns are deposited using one of the usual schemes for ohmic contact on n-type GaAs.

(6) Impedance matching and **radiation pattern** are other two important differences to be discussed in detail in this chapter.

As discussed in Section 2.1, when the biased semiconductor is excited by a femtosecond laser with photon energies greater than its bandgap, the electrons and the holes are produced in the conduction and valence band. The photocarriers density changes rapidly with the help of

a biased voltage, and it produces a time-varying current which can radiate THz wave into free-space with an antenna [51].

According to the principle of photoconductive effects discussed in Chapter 2, to generate a THz wave by photoconductive antennas, the material of the substrate should have some suitable properties such as short carrier lifetime, high mobility and high breakdown voltage.

Researchers have tried a lot of photoconductive materials and Table 1 summarises the characteristics of some typical materials. Nowadays, the most popular material is LT-GaAs, because it has the shortest carrier lifetime among all the materials and the mobility and the breakdown voltage are high enough. The physical properties of LT-GaAs depend on the manufacture process, *i.e.* the growth conditions during the molecular-beam-epitaxy (MBE) process and the post-growth annealing [71]. Fig. 3.6 shows the growth-temperature dependence of the carrier lifetime.

The antenna structure which is fabricated on the dielectric substrate should also be considered. The typical structure of the antenna is the Hertzian dipole made of Au or Ni. When a femtosecond laser pulse with the energy is larger than 1.43 eV which is the bandgap of GaAs at a room temperature, the electron-hole pairs are produced in the semiconductor substrate and accelerated by the electric field formed by DC bias voltage. Then a pulsed photocurrent is generated and the electromagnetic wave in THz region can be radiated by the antenna.

Table 1. Properties of different photoconductive materials [1]

Photoconductive materials	Carrier lifetime (ps)	Mobility ($cm^2/(V•s)$)	Resistivity (Ω•cm) (Breakdown field (V/cm))	Band gap (eV at R.T.)
Cr. Doped SI-GaAs	50~100.0	1000	10^7	1.43
LT-GaAs	0.3	150~200	10^6 (5×10^5)	1.43
SI-InP	50~100.0	1000	4×10^7	1.34
Ino-Implemanted InP	2~4	200	$>10^6$	1.34
RD-SOS	0.6	30		1.10
Amorphous Si	0.8~20	1	10^7	1.10
MOCVD CdTe	0.5	180		1.46
Ion-implanted Ge	0.6	100		0.66

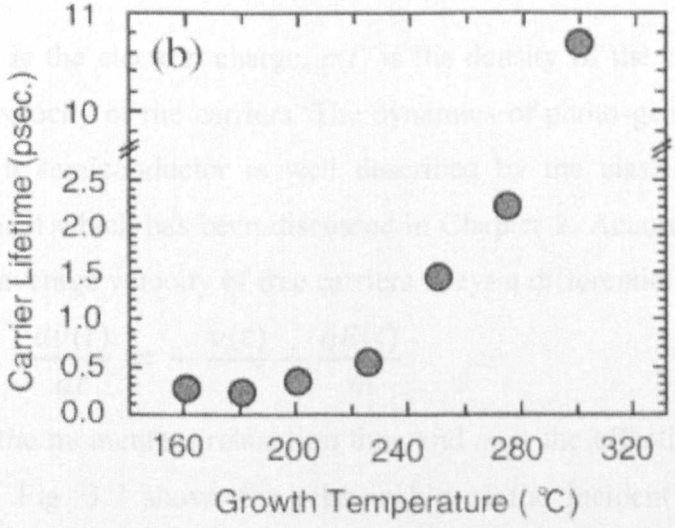

Fig. 3.6 Growth-temperature dependence of the carrier lifetime [72]

According to conventional antenna theories, in free space, the radiated electric field $E(r, t)$ from a Hertzian dipole at a distance r (which

is much greater than the wavelength of the radiation) and time t have the following relationship [73, 74, and 79].

$$E(r,t) = \frac{l_e}{4\pi\varepsilon_0 c^2 r} \cdot \frac{\partial J(t)}{\partial t} \cdot sin\theta \propto \frac{\partial J(t)}{\partial t} \tag{3.1}$$

where $J(t)$ is the current in the dipole, l_e the effective length of the dipole, ε_0 the dielectric constant of a vacuum, c the velocity of light in a vacuum, and θ the angle from the direction of the dipole.

Equation (3.1) indicates a well-known theory in THz generation that the radiation amplitude is proportional to the time derivative of the transient photocurrent $\partial J(t)/\partial t$ when the effective antenna length l_e is fixed. The photocurrent density is described as [75]

$$J(t) \propto I(t) \otimes [qn(t)v(t)] \tag{3.2}$$

where $\otimes$ means the convolutional product, $I(t)$ is the incident optical intensity, q is the electron charge, $n(t)$ is the density of the carriers and $v(t)$ is the velocity of the carriers. The dynamics of photo-generated free carriers in a semiconductor is well described by the classical Drude-Lorentz model which has been discussed in Chapter 2. According to this model, the average velocity of free carriers obeys a differential equation:

$$\frac{dv(t)}{dt} = -\frac{v(t)}{\tau} + \frac{qE(t)}{m} \tag{3.3}$$

where τ is the momentum relaxation time and m is the effective mass of the carrier. Fig. 3.7 shows the relationship of the incident pulse, the produced photocurrent and the radiated electric field [76].

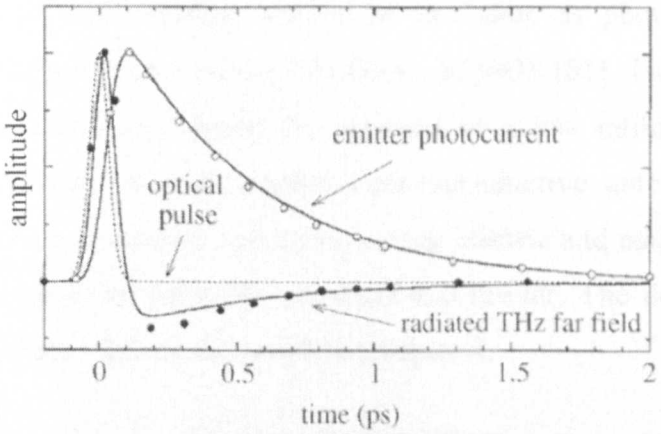

Fig. 3.7 Relationship of the incident pulse, the produced photocurrent and the radiated electric field [76]

Another phenomenon of the THz generation from a photoconductive antenna with small gap should be noticed: the generated THz pulse emitted to the substrate is larger than that to the air when the substrate is comparable with the wavelength or larger. This is based on the antenna theory that shows that a dipole antenna on the surface of dielectric material emits roughly $\varepsilon^{3/2}/2$ times more power to the dielectric material than to the air, where ε is the relative dielectric constant of the substrate [77]. Some simulation results to prove this will be presented in Chapter 5.

Large-aperture photoconductors biased with a high DC voltage are used to generate high-power THz pulse in recent years [78, 80]. Fig. 3.8 shows the typical structure of this kind of THz source which is also based on the photoconductive effect. The structure is the same as the photoconductive antenna with a small gap and the difference is that the illumination area of large-aperture PC antenna is larger than the wavelength of radiated THz wave. This feature indicates the antenna can have more bias voltage than the small Hertzian dipole structure. The

requirement of the substrate should be the same as photoconductive antenna with small gaps such as InP, GaAs, RDSOS [81]. The separation between the electrodes should be enlarged to a few millimetres. The calculation model of large aperture photoconductive antenna can be derived from the boundary conditions on the electric and magnetic fields at the interface of between the substrate and the air. The details of the calculation model will be discussed in Chapter 4.

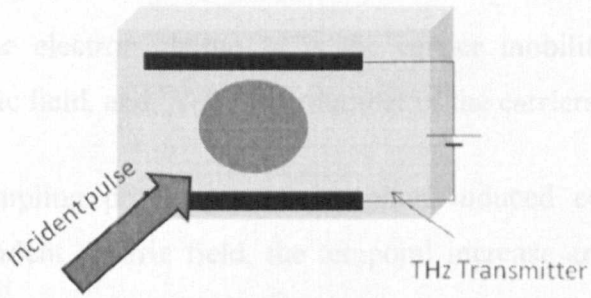

Fig. 3.8 Structure of large-aperture photoconductive antennas

In contrast to the photoconductive antenna with a small gap, the electric fields radiated into the substrate and into the air are comparable. The analysis [82] shows the relationship between them is

$$E_{air}: E_{sub} = \sqrt{\varepsilon}: 1 \tag{3.4}$$

Based on this property, Shen *et al.* did an experiment to collect the power from the air side instead of the substrate side and the absorption and dispersion of THz pulses in the substrate are minimized [83].

The principle of THz detection by photoconductive antennas is an inverse process of THz generation by photoconductive antennas [84, 85]. When the photoconductive antennas are used for detection, the bias

voltage source should be replaced by a current meter. After a laser pulse excites the substrate, the carriers are accelerated by the incident THz wave, while in THz generation process the carriers are accelerated by the bias voltage. The current produced by the accelerated carriers is proportional to the product of the incident THz field and existing photo-created carriers. Therefore, the photocurrent by the incident radiation at a time delay t can be calculated by [62]

$$J(t) = e\mu \int E(t')N(t'-t)dt' \tag{3.5}$$

where e is the electron charge, μ is the carrier mobility, $E(t)$ is the incident electric field, and $N(t)$ is the number of the carriers.

In the sampling process, to make photo-induced current exactly reflect the incident electric field, the temporal increase and decrease of $N(t)$ should be very short [86]. This is one reason why the substrate material should has short carrier lifetime. Therefore, LT-GaAs is also suitable for THz detection.

3.3 Problems of Photoconductive Antennas

There are two main problems of photoconductive antennas.

First, from the antenna theory, it is well known that, for the maximum power transfer between the feed-line and the antenna, the antenna input impedance should be the characteristic impedance of the line (50 Ω for most cases). However, for a photoconductive antenna, there is no such a feed line: the THz source is directly connected to the antenna which is different from that in the conventional antenna as shown in Fig. 3.9. The source impedance is normally not 50 Ω for the THz case. The actual

value depends on the substrate. Therefore, the impedance matching is an issue.

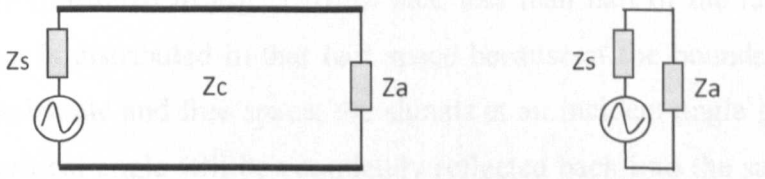

(a) Conventional antenna (b) THz antenna

Fig. 3.9 Equivalent circuits of the conventional antenna and THz antenna

As mentioned early that most photoconductive antennas use LT-GaAs substrate, which has a high relative permittivity ε_r = 12.9. The thickness of the used wafers is normally large compared to the wavelength at THz frequencies resulting in a dielectric half-space which renders the effective relative permittivity to be $\varepsilon_{re} \approx 7$. Thus a broadband self-complementary antenna has an antenna input impedance of approximately 188.5 Ω in free space and 71.5 Ω on electrically thick GaAs substrate. However, the impedance of the photomixer under illumination typically is above 10 kΩ [40] and therefore leads to a significant impedance mismatch. If P is the power accepted by the antenna, R is the impedance of the antenna and I is the AC-part of the photocurrent, the accepted power: $P = RI^2$. Obviously it is desirable to make the antenna input impedance large enough to match with the source impedance (above 10 kΩ). In reality it is hard to achieve this. Thus impedance mismatch seems to be a major contributor to the problem of the low radiated THz power [46].

Second, due to the system setup as shown in Fig. 3.1, the desired THz radiation is just in half of the space - opposite the laser source. However, the radiation from the THz antenna does not just go to the desired half space illustrated in Fig. 3.10. In fact, less than half of the radiated THz power is distributed in that half space because at the boundary between the substrate and free space, the signals at an incident angle greater than the critical angle will be completely reflected back into the substrate and it will act as a waveguide and gives rise to substrate waves, which reduce the overall radiation performance.

For GaAs substrate, because it has high refractive index n which is about 3.4, the critical angle on the surface between the substrate and the air can be calculate as

$$\theta_0 = arc\sin\left(\frac{1}{n}\right) \tag{3.6}$$

So the critical angle is about 17.1°, which means only little power can be transmitted into the air.

To overcome this problem, these substrate waves can be suppressed by the use of a Si-lens at the antenna backside to a large extend as shown in Fig. 3.11, but this requires additional mechanical adjustment. The focal point of the lens must be at the centre of the dipole antenna. The introduction of the Si hemispherical lens can direct the radiated THz waves to the desired direction and improve the radiation pattern and radiation efficiency.

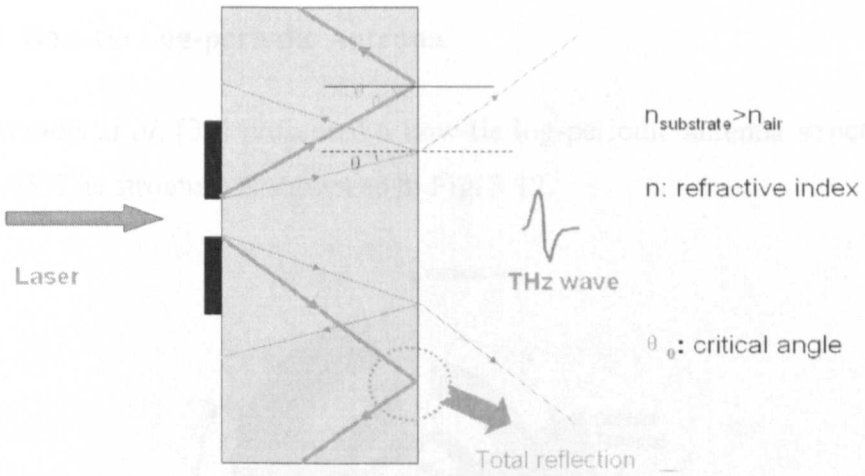

Fig. 3.10 Total reflection in photoconductive antennas

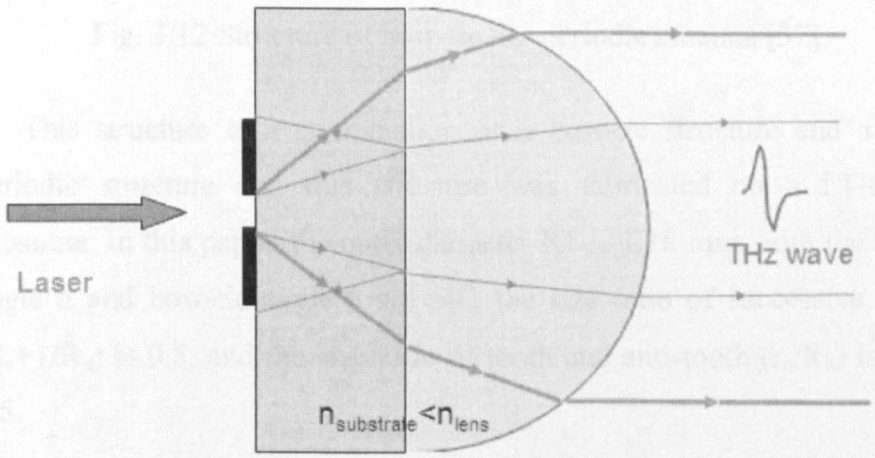

Fig. 3.11 Lens-coupled photoconductive antennas

3.4 Some New Types of Photoconductive Antennas

3.4.1 Bow-tie Log-periodic Antenna

Mendis *et al.* [37] presented a bow-tie log-periodic antenna structure in 2005. The structure is shown as in Fig. 3.12.

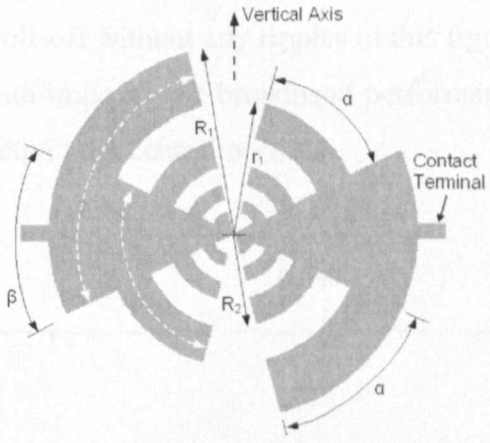

Fig. 3.12 Structure of bow-tie log-periodic antenna [37]

This structure is a combination of a bow-tie structure and a log-periodic structure and this structure was fabricated on a LT-GaAs substrate. In this paper, the outer diameter R1 is 1.28 mm, both the tooth angle α and bow-tie angle β are 50°, the size ratio of successive teeth (R_n+1/R_n) is 0.5, and the size ratio of tooth and anti-tooth (r_n/R_n) is also 0.5.

The authors used this kind of structure for both emission and detection and Fig. 3.13 shows the relationship between the amplitude of the current and the frequencies. From the measurement results, it can be seen that when the frequency is low, the antenna behaviour is similar as

log-periodic antenna, *i.e.* the antenna is resonant when the arc lengths (white dashed lines in Fig. 3.12) are equal to $\lambda_g/2$, or $\lambda_g/4$, where

$$\lambda_g = \frac{\lambda_0}{\sqrt{(\varepsilon_r + 1)/2}} \tag{3.7}$$

and λ_0 is the free-space wavelength, ε_r is the relative permittivity. When the frequency is high, this structure behaves like a bow-tie antenna, *i.e.* there is a smooth roll-off without any ripples in this figure. Therefore, this kind of structure can improve the broadband performance of the antenna by adding more teeth in the central portion.

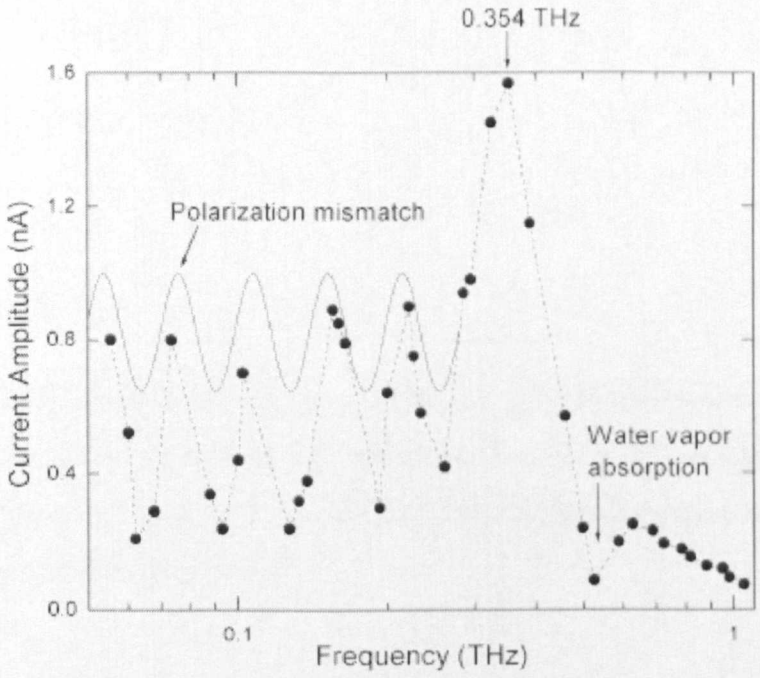

Fig. 3.13 Relationship between the current amplitude and the frequency [37]

3.4.2 Helical THz Antennas

Robert *et al.* [35] used a technique called LCVD to produce a helical antenna working in THz range. Fig. 3.14 is a photo of this kind of antenna. It is very small and difficult to be produced by traditional fabrication method. Fig. 3.15 shows the key parameters of helical antenna. From the conventional antenna theories, the parameters of helical antenna working with axial mode can be calculated. And for 1 THz, these parameters are:

$C = 341.307\ \mu m$,

$S = 81.3\ \mu m$,

$D = 15\ \mu m$,

$N = 5$,

$\alpha = 13^{o}$

Because the diameter can decide the operation frequencies of helical antennas, this paper produced different antennas with the diameters from 40 μm to 1.1 mm and demonstrated the operation frequency range was from 100 GHz to 2.7 THz.

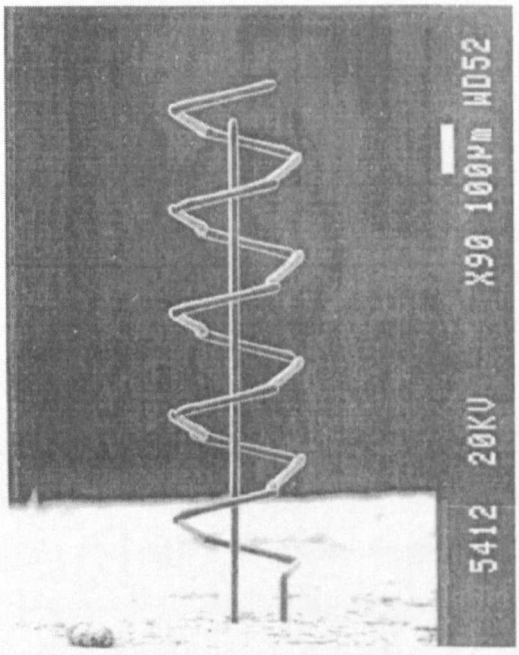

Fig. 3.14 Photo of THz helical antenna [35]

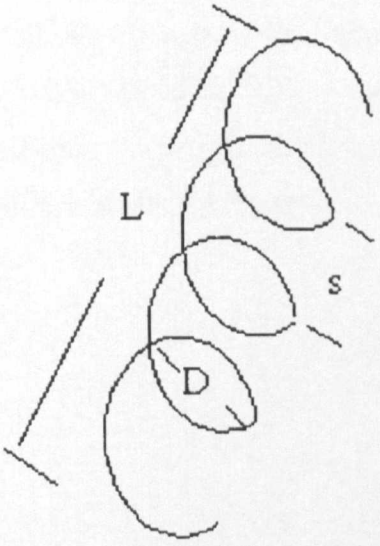

D= diameter of helix
C=circumference of helix= π D
tan α = s/C = s/ π D

$L = \sqrt{S^2 + C^2}$ length of turn

α = pitch angle
N= number of turns
d=diameter of helix wire

Fig. 3.15 Key parameters of THz helical antenna [35]

3.4.3 THz Folded Half-wavelength Dipole Antenna

To solve the impedance matching problem of photoconductive antennas, Moon *et al.* [40] introduced a folded dipole antenna structure.

Because the photomixer which works as the source of the antenna has a very high impedance (about 10 kΩ as discussed in last section), to obtain better impedance matching, the antenna impedance should be increased. Fig. 3.16 is the structure of three-wire folded half-wavelength antenna (3WFDA) and five-wire folded half-wavelength antenna (5WFDA), and Fig. 3.17 shows the input resistances of 3WFDA and 5WFDA compared with full wavelength dipole antenna (FWDA). It indicates 3WFDA and 5WFDA have higher resistances than FWDA. And then the radiation power can be predicted as shown in Fig. 3.18 and it proves that the peak values of the radiated power of 3WFDA and 5WFDA are greater than that of FWDA. However, the peak values of 3WFDA and 5WFDA are not occurred at 1THz which is the expecting frequency, but this problem can be solved by changing the physical dimensions of the antennas.

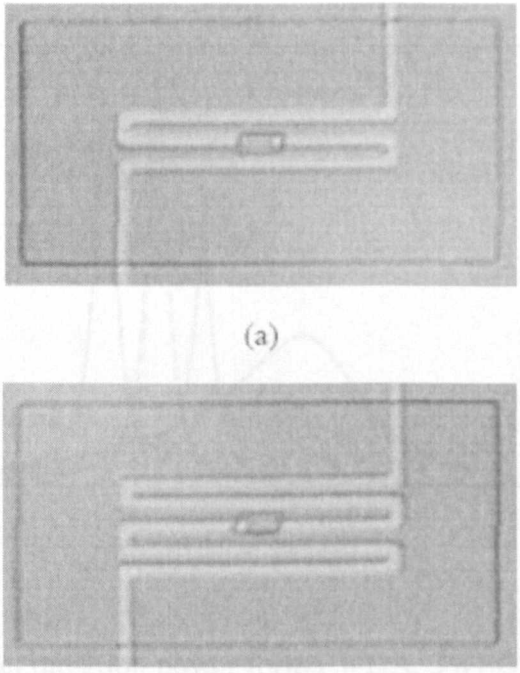

Fig. 3.16 Structure of (a) 3WFDA and (b) 5WFDA [40]

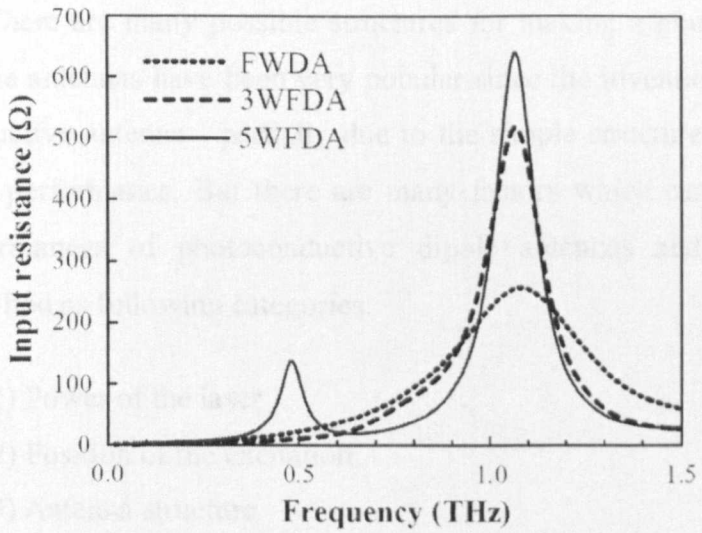

Fig. 3.17 Input resistances for FWDA, 3WFDA and 5WFDA [40]

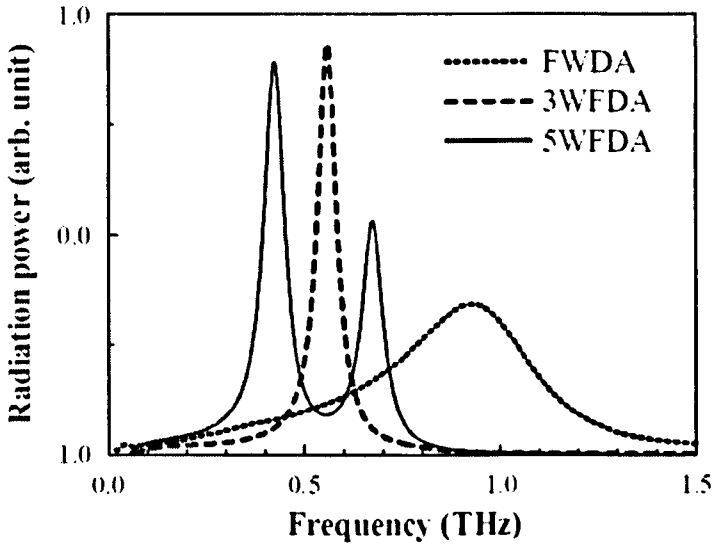

Fig. 3.18 Predict radiation power form FWDA, 3WFDA and 5WFDA [40]

3.5 Key Parameters of Photoconductive Antennas

There are many possible structures for making a good PC antenna. Dipole antennas have been very popular since the invention of the photo conductive antenna - partially due to the simple structure and relatively good performance. But there are many factors which can influence the performances of photoconductive dipole antennas and they can be classified as following categories:

(1) Power of the laser

(2) Position of the excitation

(3) Antenna structure

(4) Shape of dipole

(5) Gap of the antenna

(6) Material of the antenna

(7) Bias voltage

(8) Length of dipole

The first two categories are related to the exciting laser source and the last six are related to the antenna itself. Some brief introductions and some experiment results will be given in this section.

3.5.1. Power of the Laser

It is easy to understand that increasing the incident laser power can increase the number of carriers, and more THz power can be generated. The following is an example which can get good performance within THz range. Fig. 3.19 is its configuration [73].

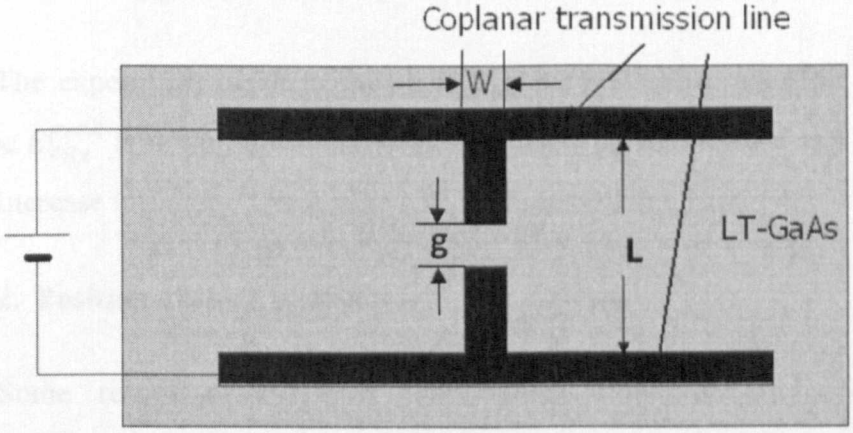

Fig. 3.19 The experimental configuration of the photoconductive antenna in [73]

The typical size of the gap g in Fig. 3.19 is 5–10 μm, and those of the antenna width W and length L are 10–20 μm and 30–50 μm, respectively. The peak value of the THz field is given by

$$E_{THz}^{peak} \propto \partial J / \partial t \approx \bar{J} T_{int} / \tau_c = \bar{G} V_b T_{int} / \tau = \bar{\sigma} \frac{W\delta}{g} V_b \frac{T_{int}}{\tau_c}$$
$$= e\mu \bar{n}_e \frac{W\delta}{g} V_b \frac{T_{int}}{\tau_c} = e\mu T_{int} \frac{(1-R)P_{in}V_b}{h\nu g^2} \quad (3.8)$$

where G is the time-averaged photo-conductance of the PC gap, σ is the time-averaged conductivity, δ is the absorption depth of the pump light, n_e is the averaged photo-carrier density, V_b is the bias voltage, μ is the mobility of the carriers, R is the reflectance of the PC substrate, $h\nu$ is the photon energy of the pump laser, P_{in} is the averaged pump laser power, and D is the PC gap. A high value of E_{THz}^{peak} is obtained if the substrate has a high mobility and a high resistivity, requirements that enable the application of high bias values V_b. These criteria are satisfied by LT-GaAs.

The experiment result is shown in Fig. 3.20. It shows that the peak value E_{THz}^{peak} is not proportional to the incoming pulse intensity and does not increase infinitely. The details will be discussed in Chapter 4.

3.5.2. Position of the Excitation

Some recent works show that optical excitation of coplanar transmission lines fabricated on compensated semiconductors (semi-insulators) can enhance electrical signal generation, and exciting near anode can make the radiation much stronger than exciting near cathode [87].

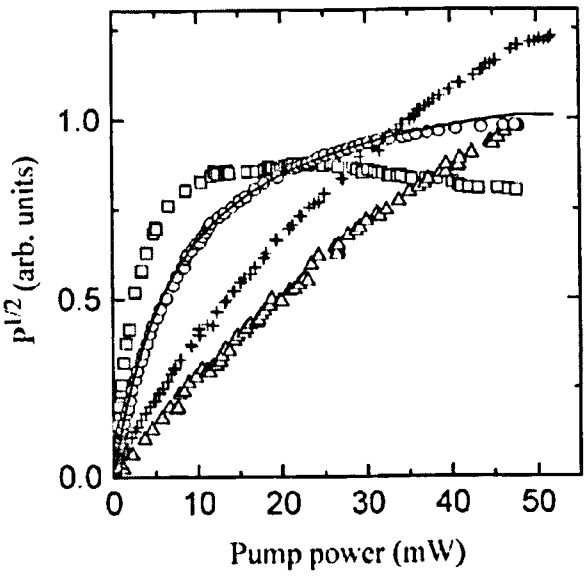

Fig. 3.20 Relationship between the laser source and the THz radiation [73]

First, exciting at the different dipole positions can change the performance of the antenna. The experiment result is shown in Fig. 3.21 [88].

It is obvious that when excitation point is near the anode, the radiated signal is larger than the signal when excitation point is near the cathode.

Second, exciting near the dipole or near the strip lines can also show different performances.

In Fig. 3.22, the upper figure is the radiated signal by exciting near the dipole and the lower figure is the radiated signal by exciting near the strip line [89]. It shows that when exciting near the dipole, the photoconductive antenna can get better performances.

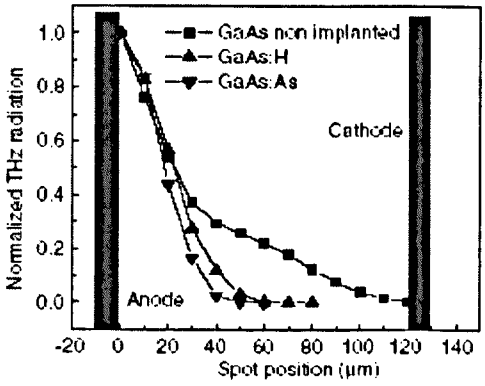

Fig. 3.21 THz radiation with different exiting positions in the gap [88]

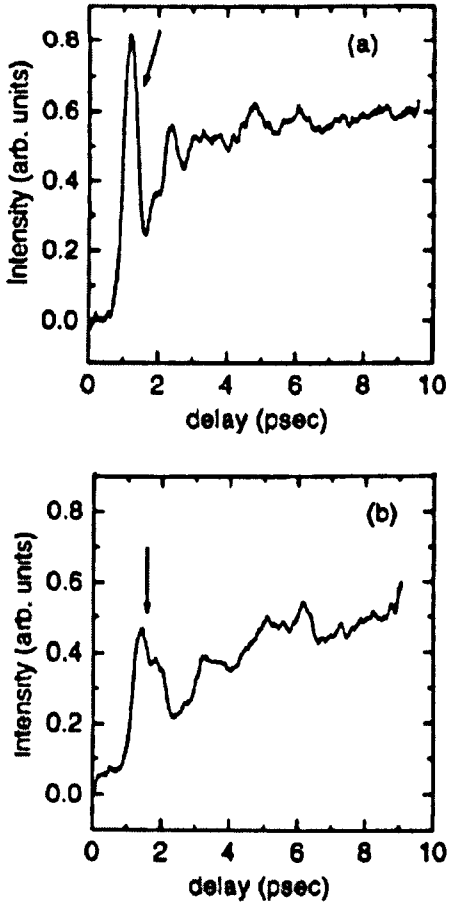

Fig. 3.22 Different THz radiation with exciting near dipole and near stripline [89]

Therefore, to obtain the best performance, the excitation position should be set near the anode.

3.5.3. Structure of the Antenna

Following experiment shows that the different structures can lead to different antenna performances [90].

In this experiment, two antennas with similar dimensions are used, one is a dipole antenna and the other is a bow-tie antenna.

The dimensions used in this experiment are L = 40 μm, g = 6 μm, W = 10 μm (dipole antenna), w = 34 μm (bow-tie antenna) and they are shown in Fig. 3.23 and Fig. 3.24 respectively.

Fig. 3.25 is the result from the experiment. ■ is the dipole antenna, and ● is the bow-tie antenna [90]. The radiation is not proportional to the incoming intensity because of the parameter I_0. It means when the incoming power intensity makes the material saturate, the radiation emitted will not be increased. In addition, the result also shows the different structures have different saturation and it leads to different performances of the similar antenna sizes.

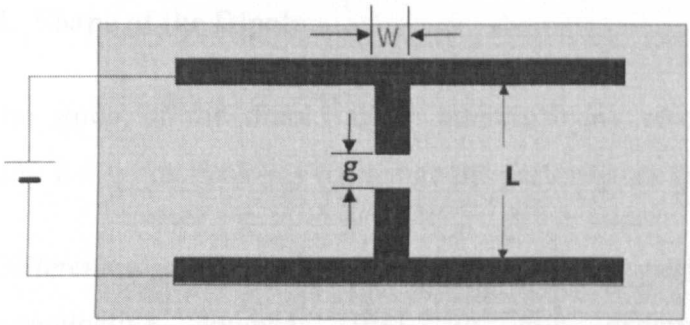

Fig. 3.23 Structure of photoconductive dipole antenna

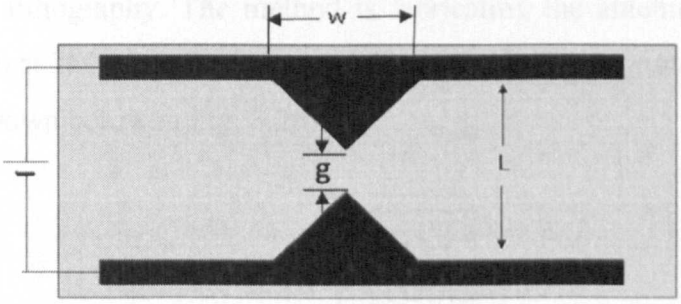

Fig. 3.24 Structure of photoconductive bow-tie antenna

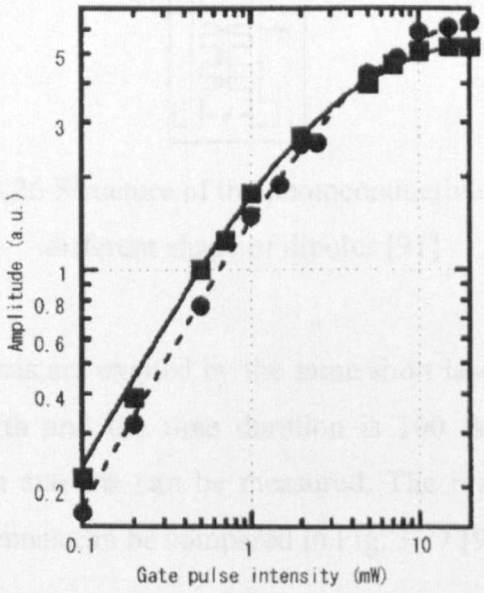

Fig. 3.25 Relationship between the radiation and the incoming intensity [90]

3.5.4. Shape of the Dipole

The study of the dipole shape attracts many researchers recently because it is a practical way to change the performance of the antennas.

Different shapes of the dipoles lead to different performances of the photoconductive antennas [91]. In this experiment, all the photoconductive antennas are fabricated on the same material by the same lithography. The method is fabricating the antennas on LT-GaAs grown at 250 °C and post-annealed at 600 °C for 1 minute. The structures are shown below in Fig. 3.26.

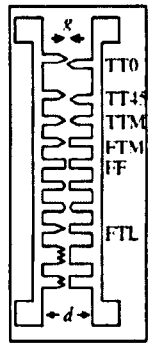

Fig. 3.26 Structure of the photoconductive antennas with different shape of dipoles [91]

All the antennas are excited by the same short laser pulse which has 780 nm wavelength and the time duration is 100 fs. Then the power emitted from each antenna can be measured. The results of the power from different antennas can be compared in Fig. 3.27 [91].

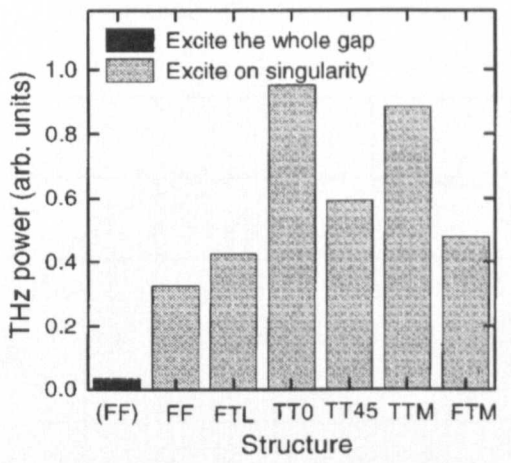

Fig. 3.27 The emitting power from the PC antenna with different dipoles [91]

According to the results, it is obvious that the performance of photoconductive antenna can be influenced by the shape of the dipole, and the TT0 structure has the best performance in this experiment. Therefore, the shape of the dipole is an important factor to change the photoconductive antenna performance.

3.5.5. Gap of the Antennas

The gap of the photoconductive antenna is a very important parameter in the photoconductive antenna. Fig. 3.28 shows the radiated signal with different gap [92].

The relationship between the gap and the radiation wave is not a simple proportional or reverse proportional because when the substrate meet the saturation conditions the antenna can get the best performance. The saturation condition is determined by the materials of the substrate. It will be discussed in Section 4.2.

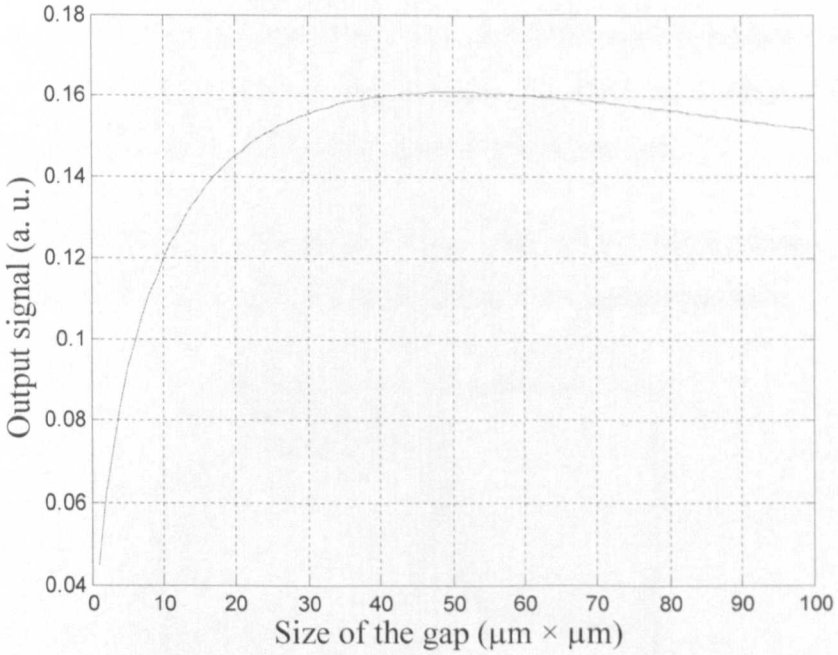

Fig. 3.28 Relationship between the THz radiation and the gap [92]

3.5.6. Material of the Antenna

The following is a comparison of the bared photoconductive antenna and the coated photoconductive antenna [93].

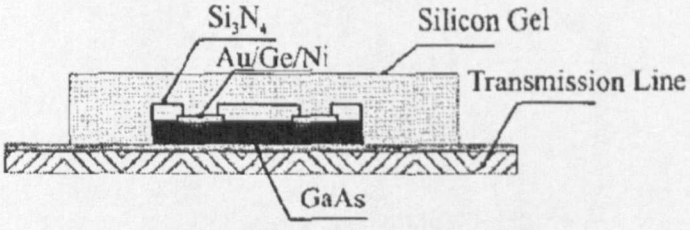

Fig. 3.29 Structure of the coated antenna [93]

The antenna is built on a semi-insulating GaAs wafer and evaporated with two Au/Ge/Ni electrodes. An 800 nm Si_3N_4 is deposited on the surface of the antenna except the electrodes and forms the coated antenna. The coated antenna will then be mounted on a plastic fibre transmission line and sealed with transparent silicone gel.

Fig. 3.30 shows the signal generated from these two antennas. The voltages are 470 V for bare antenna and 640 V for coated antenna.

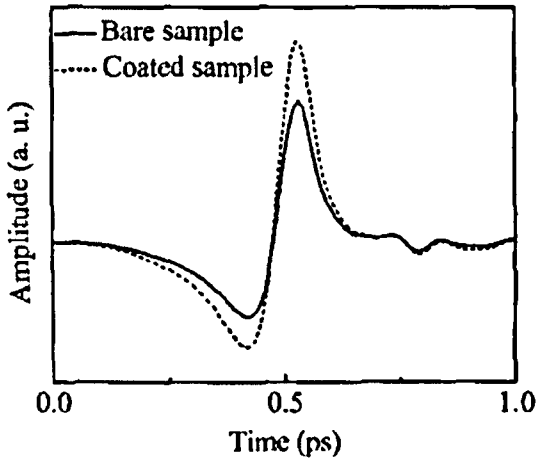

Fig. 3.30 THz signal generated from bare and coated antennas [93]

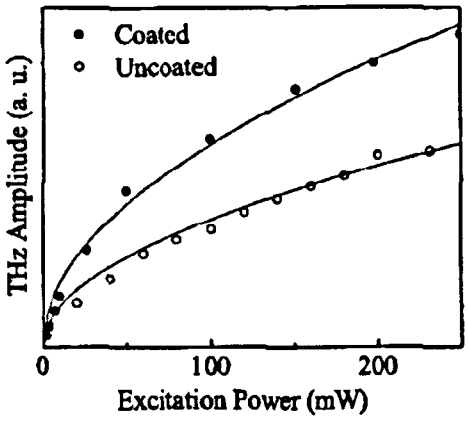

Fig. 3.31 THz amplitude with different excitation power [93]

Fig. 3.31 presents the maximum THz field generated by coated and bare antenna at various excitation powers. Coated antenna has the capability to generate stronger THz field than bare one for the same excitation power. The maximum THz field strength is proportional to the square root of the excitation power, which is due to the breakdown process [94]. Therefore, the performance is different if the antenna is made of different materials.

Low temperature GaAs is the most widely used material as the substrate of photoconductive antenna. But recently, some alternative materials have been found and the arsenic ion implanted GaAs ($GaAs:As^+$) is one of them. The following experiment can compare the performance of two materials: $GaAs:As^+$ and SI-GaAs [95].

To find out the influences of the substrate materials, the antennas are made with the same geometry and fabricated on different materials. The antenna structures are the same as Fig. 3.19, and the dimensions are L = 20 μm, W = 10 μm, g = 5 μm.

In this experiment, both antennas are excited by the same Ti:sapphire laser which can produce the pulse with 780 nm wavelength and the duration time is 80 fs [95].

The result of the experiment is shown in Fig. 3.32. The $GaAs:As^+$ antenna has a higher frequency region than the SI-GaAs antenna. It is obvious that the peak values are different because of the different substrate materials. Therefore, the materials can influence the performances of the photoconductive antenna and it is another important factor of the photoconductive antenna.

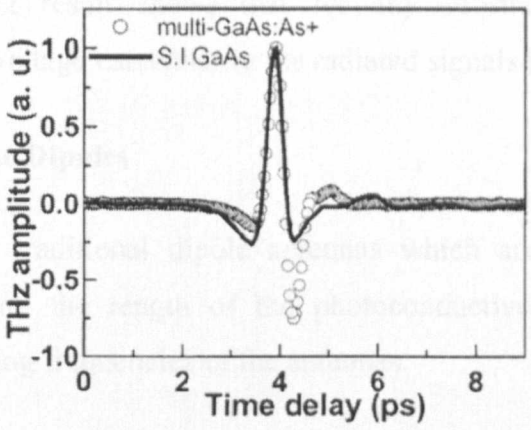

Fig. 3.32 Performances of PC antenna with different materials [95]

3.5.7. Bias Voltage

It is easy to understand that the higher the bias voltage is, the larger the signal power radiated because high voltage can make strong electric field which lead to the high speed of the electrons.

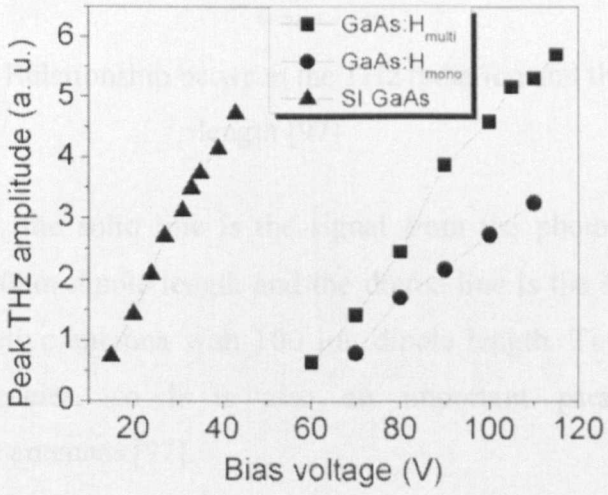

Fig. 3.33 Relationship between the THz radiation and the bias voltage [96]

The experiment result shows that for any substrate materials, increasing the bias voltage can enhance the radiated signals [96].

3.5.8. Length of the Dipoles

Similar as the traditional dipole antennas which are working in microwave spectrum, the length of the photoconductive dipoles can determine the working frequencies of the antennas.

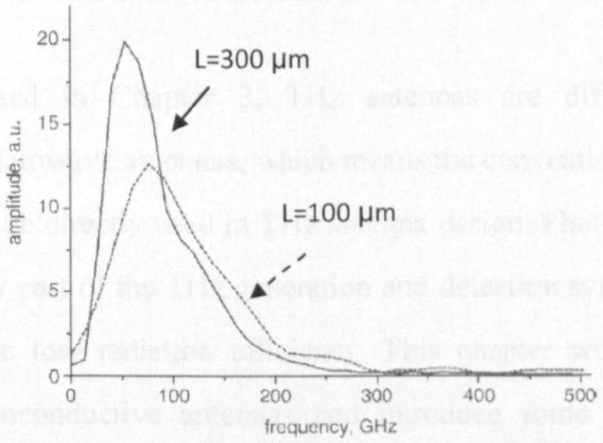

Fig. 3.34 Relationship between the THz radiation and the dipole length [97]

In Fig. 3.34, the solid line is the signal from the photoconductive antenna with 300um dipole length and the dotted line is the signal from the photoconductive antenna with 100 μm dipole length. They work at different frequencies, so it is also an important parameter for photoconductive antennas [97].

CHAPTER 4
IMPROVING PHOTOCONDUCTIVE ANTENNA RADIATION EFFICIENCY

4.1 Radiation Model and Key Parameters of THz Generation from Photoconductive Antennas

As discussed in Chapter 3, THz antennas are different from conventional microwave antennas, which means the conventional antenna theories cannot be directly used in THz antenna design. Photoconductive antenna is a key part of the THz generation and detection system but the limitation is the low radiation efficiency. This chapter will show the details of photoconductive antennas and introduce some methods to improve the antenna performance. In addition, the theories discussed in this chapter are not only for photoconductive dipole antennas but also for other types of photoconductive antennas.

To investigate the performance of the photoconductive antennas and find the methods to increase the output power of THz generation from photoconductive antenna, a radiation model should be set up.

As mentioned in Chapter 2, the Drude-Lorentz theory can explain the mechanism of photoconductive effect. To apply the theory into

photoconductive antenna, a model called drift-diffusion model was introduced. The currents in photoconductor consist of two components, one is the current produced by electrons and another is that produced by holes. These two currents can be expressed by [98]

$$J_n = q\mu_n nE + qD_n \frac{dn}{dx} \tag{4.1}$$

$$J_p = q\mu_p pE + qD_p \frac{dp}{dx} \tag{4.2}$$

where n and p is the electron and hole densities, and can be calculated by

$$\frac{dn}{dt} = G - U + \frac{1}{q} \cdot \frac{dJ_n}{dx} \tag{4.3}$$

$$\frac{dp}{dt} = G - U - \frac{1}{q} \cdot \frac{dJ_p}{dx} \tag{4.4}$$

where G is the carrier generation rate, U is the carrier recombination rate, and D, q and μ correspond to the diffusion coefficient, electronic charge, and carrier mobility, respectively. A constant electric field E is assumed across the device. The current can be found by integrating the carrier densities over the electrodes separation.

For the THz generation system, the laser should be taken into account. When the photoconductor is illuminated by a laser source [99], the generation rate G is:

$$G = \frac{\alpha A}{h\nu} \exp\left[-\frac{(x-x_0)^2}{\sigma^2} - \frac{(t-t_0)^2}{\sigma_t^2}\right] \tag{4.5}$$

where a is the absorption coefficient of the photoconductor, A is the peak optical power density, $h\nu$ is the photon energy, x_0 is the centre of the

optical beam on the photoconductor surface, and t_0 is the time at which the optical power peaks. The recombination rate U can be calculated by

$$U = \frac{np}{\tau_{p0}(n+n_1)+\tau_{n0}(p+p_1)+(C_{An}n+C_{Ap}p)np} \tag{4.6}$$

where τ_{n0} and τ_{p0} are the electron and hole lifetimes, n_1 and p_1 are electron and hole concentrations that would exist if the Fermi level were at the trap level, and C_{An} and C_{Ap} are Auger coefficients. Equation (4.6) is a simple form that assumes no carriers existing in the initial state. The diffusion coefficients D_n and D_p can be obtained by Einstein relation [99]:

$$\frac{D_n}{\mu_n} = \frac{D_p}{\mu_p} = \frac{kT}{q} \tag{4.7}$$

After dealing with the current source in photoconductive antenna, the antenna electrodes should be considered. Since the typical photoconductive antenna use short dipole as the antenna structure, it can be considered as a Herzian dipole, and the radiation field is [73]

$$E(r,t) = \frac{l_e}{4\pi\varepsilon_0 c^2 r} \cdot \frac{\partial J(t)}{\partial t} \cdot sin\theta \tag{4.8}$$

where $J(t)$ is the current in the dipole, l_e is the effective length of the dipole, ε is the dielectric constant of the radiation medium, c is the velocity of light in the vacuum, and θ is the angle from the direction of the dipole. Equation (4.8) indicates that the radiation amplitude is proportional to the time derivative of the transient photocurrent and the effective antenna length. And the resonant frequency of this antenna can be calculated as [73]

$$f_r = \frac{c}{\lambda_r} = \frac{c}{2l_e\sqrt{(1+\varepsilon)/2}} \tag{4.9}$$

where c is the velocity of the light, λ_r is the resonance wavelength, ε is the dielectric constant of the substrate. For GaAs, ε is about 12.9 in THz frequencies.

When the antenna aperture is large, the following model can be introduced. Fig. 4.1 is a side view of a photoconductive antenna. E_b is the electric field produced by bias voltage, E_{out} and E_{in} are the electric field in and out of the antenna, H_{in} and H_{out} are the magnetic field in and out of the antenna, and the directions of each parameter are also represented in this figure.

The electric field near the antenna surface can be calculated by Maxwell's equation (Faraday's law) [100]:

$$\oint_l E \bullet dl = -\frac{\partial}{\partial t}\int_s B \bullet ds \tag{4.10}$$

Because the electric field is near the surface, the m can be considered as 0, and the s is also 0. Then the formula below can be obtained

$$\lim_{m\to 0}\oint_l E \bullet dl = E_{out}l - E_{in}l = 0 \tag{4.11}$$

$$E_{out} - E_{in} = 0 \tag{4.12}$$

The magnetic field near the antenna surface can also be calculated by Maxwell's equation (Ampère's law)

$$\oint_l H \bullet dl = \int_s (J + \frac{\partial D}{\partial t}) \bullet ds \tag{4.13}$$

For the same reason as the electric field, s can be considered as 0. The formula below can be obtained

$$\lim_{m \to 0} \oint_l H \bullet dl = H_{out} l - H_{in} l = J_s \bullet l \tag{4.14}$$

$$H_{out} - H_{in} = J_s \tag{4.15}$$

where J_s is the surface current density.

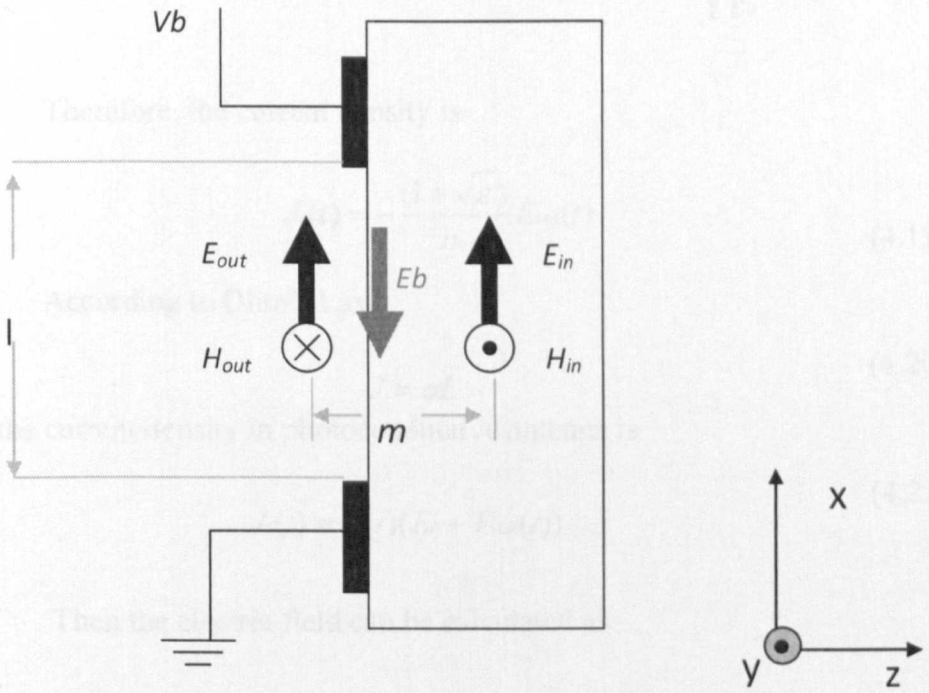

Fig. 4.1 The radiation field model of photoconductive antenna

According to [101], the relationship between H and E is

$$\frac{H}{E} = \sqrt{\frac{\varepsilon_0 \varepsilon}{\mu_0}} \tag{4.16}$$

where ε_0 is the permittivity of vacuum, ε is the relative permittivity of the substrate, and μ_0 is the permeability of vacuum.

So, in this photoconductive antenna model,

$$H_{in}(t) = \frac{\sqrt{\varepsilon}}{\eta_0} E_{in}(t) \tag{4.17}$$

$$H_{out}(t) = -\frac{1}{\eta_0} E_{out}(t) \tag{4.18}$$

where η_0 is the free space resistance, which is equal to $\sqrt{\frac{\mu_0}{\varepsilon_0}}$.

Therefore, the current density is

$$J_s(t) = -\frac{(1+\sqrt{\varepsilon})}{\eta_0} E_{out}(t) \tag{4.19}$$

According to Ohm's Law

$$J = \sigma E \tag{4.20}$$

the current density in photoconductive antenna is

$$J_s(t) = \sigma(t)(E_b + E_{out}(t)) \tag{4.21}$$

Then the electric field can be calculated as

$$E_{out}(t) = -E_b \frac{\sigma(t)\eta_0}{\sigma(t)\eta_0 + (1+\sqrt{\varepsilon})} \tag{4.22}$$

where E_b is the electric field produced by bias voltage and $\sigma(t)$ is the surface conductivity of the antenna substrate, which can be calculated by [102]

$$\sigma(t) = \frac{e(1-R)}{h\omega}\int_{-\infty}^{t} I_l(t')\mu((t,t')\exp\ -(t-t')/\tau dt' \qquad (4.23)$$

where e is the electron charge, R is the optical reflectivity of the antenna substrate, μ is the carrier mobility, $h\omega$ is the photon energy. The input laser profile is usually as the form as

$$I_l(t) = \frac{I}{\tau}\cdot \exp -\left(\frac{t}{\tau}\right)^2 \qquad (4.24)$$

And if the mobility is a constant, the surface conductivity can be expressed as

$$\sigma(t) = \frac{e(1-R)\mu}{h\omega}\cdot I \qquad (4.25)$$

where I is the laser intensity.

Therefore, Equation (4.22) is the electric field formula in near the photoconductive antenna.

Replace $\sigma(t)$ in Equation (4.22) with Equation (4.25), and I is the only variable when the antenna material and the laser source are fixed, so the relationship between the generated electric filed and the laser intensity is

$$E_{THz} \propto \left(\frac{I}{I_0 + I}\right) \qquad (4.26)$$

where I_0 is the saturation intensity and is a constant depending on the material of the photoconductive antenna.

This relationship can be shown in Fig. 4.2 and it will be used in Section 4.2 of this thesis.

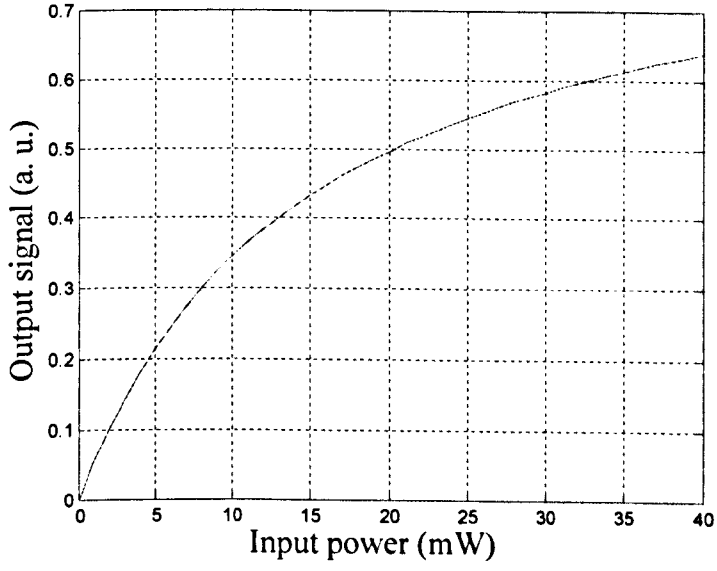

Fig. 4.2 Relationship between the generated THz signal and the laser power

Combine the Equation (4.19) and Equation (4.21), the current density should be

$$J_s(t) = \frac{\sigma(t)}{\frac{\sigma(t)\eta_0}{1+\sqrt{\varepsilon}}+1} E_b \tag{4.27}$$

From Maxwell's equations, in the Coulomb gauge,

$$E_r(r,t) = -\frac{1}{4\pi\varepsilon_0 c^2}\cdot\frac{\partial}{\partial t}\int\frac{J_s(r,t)}{r-r'}\,da' \tag{4.28}$$

where, J_s is the surface current density and E_r is the electric field in far field, so the generation field can be represented by

$$E_{THz} = -\frac{A}{4\pi\varepsilon_0 c^2 r} \cdot \frac{\mathrm{d}J_s(t)}{\mathrm{d}t} \tag{4.29}$$

Then the electric field can be presented by

$$E_{THz} = \frac{A}{4\pi \cdot \varepsilon_0 c^2 r} \cdot \frac{E_b}{[\frac{\sigma(t)\eta_0}{1+\sqrt{\varepsilon}}+1]^2} \cdot \frac{\mathrm{d}\sigma(t)}{\mathrm{d}t} \tag{4.30}$$

where E_{THZ} is the generation electric field in far-field, A is the area of the gap, E_b is the electric field produced by bias voltage, and $\sigma(t)$ is the surface conductivity which is calculated by Equation (4.25). This is the electric field in far field of the photoconductive antenna. Although this model is based on the large aperture photoconductive antenna, Equation (4.26) is also proved to be suitable for small gap photoconductive antenna [73]. Equation (4.30) indicates the reason why the methods mentioned in this paper are considered, because it contains A related to the first method, $\sigma(t)$ related to the second method and E_b related to the third and fourth methods.

4.2 Optimization of Photoconductive Antenna Gap

Fig. 4.3 is a typical structure of a photoconductive dipole antenna where g is the dipole gap, w is the width of the dipole and L is the length of the dipole.

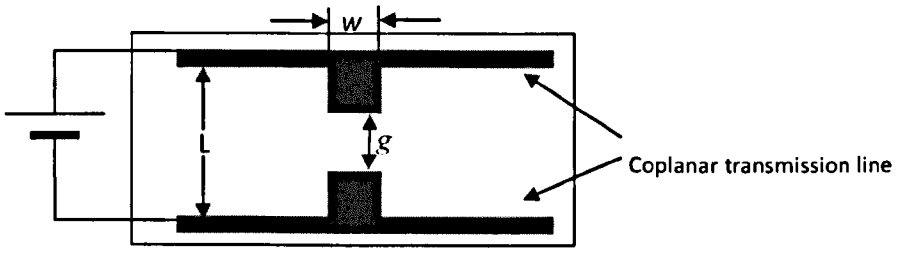

Fig. 4.3 Structure of the photoconductive antenna

Thus, the size of the antenna gap is

$$A = w \bullet g \tag{4.31}$$

This is an important parameter which can affect the output power of the photoconductive antenna. If the input power of the laser is P_{in}, its power intensity on the gap can be expressed as [103]

$$I = P_{in} / A \tag{4.32}$$

If the laser can cover all the area of the photoconductive gap and its power is large enough, all the electrons in the gap can be excited, so larger gap area A can provide more charges which will form the photo-induced current

$$\text{Charges} \propto \sqrt{A}$$

Therefore, the larger the gap size, the stronger the radiated field, because the radiated field

$$E_{THz} \propto \text{Current} \propto \text{Charges}$$

Thus,

$$E_{THz} \propto \sqrt{A} \tag{4.33}$$

where E_{THz} is the generated electric field.

The relationship between the generated electric field and the laser intensity can be shown in Equation (4.26) in last section

$$E_{THz} \propto \left(\frac{I}{I_0 + I}\right) \tag{4.34}$$

Therefore, these two results can be combined as

$$E_{THz} \propto \sqrt{A}\left(\frac{I}{I_0 + I}\right) \tag{4.35}$$

Replacing I by Equation (4.32) to give

$$E_{THz} \propto \sqrt{A}\left(\frac{P_{in}/A}{I_0 + P_{in}/A}\right) \tag{4.36}$$

This shows how the antenna gap is linked to the output signal and it can be illustrated by Fig. 4.4. The radiated signal increases rapidly as the gap opens up. Once it reaches to the maximum, the signal reduces with the gap size.

This maximum can be obtained by letting the differentiation of the field be zero, *i.e.*

$$\frac{\mathrm{d}\left[\sqrt{A}\left(\frac{P_{in}/A}{I_0 + P_{in}/A}\right)\right]}{\mathrm{d}A} = 0 \tag{4.37}$$

This means

$$P_{in}^2 - P_{in} I_0 A = 0 \tag{4.38}$$

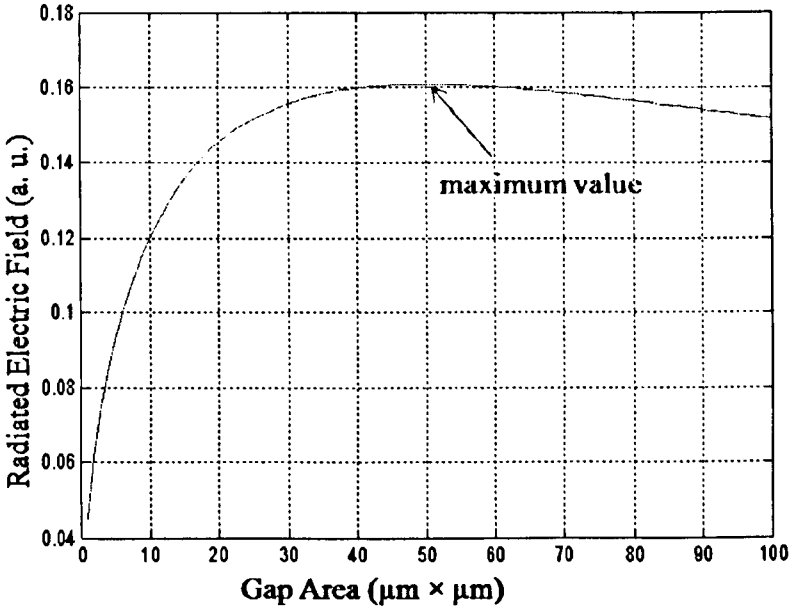

Fig. 4.4 Relationship between the generated signal and the gap of the photoconductive antenna

Therefore,

$$A = \frac{P_m}{I_0} \tag{4.39}$$

When the gap of the photoconductive antenna equals to the ratio of incident power and the saturation intensity, the photoconductive antenna can generate the maximum THz power if all other parameters are fixed.

According to the analysis above, to obtain the best performance of the photoconductive antenna by adjusting the size of the antenna gap, the value of the gap cannot be set either too large or too small [86]. The gap

size for obtaining the best performance depends on the laser power (P_{in}) and the antenna material (I_0). Therefore, once the photoconductive antenna material and the laser source are decided, the best size of the gap can be calculated using Equation (4.39).

4.3 Improvement of the Excitation Method

As mentioned in Section 3.5, excitation method is also a factor which can affect the output power of photoconductive antennas. In the conventional excitation method, the photo-induced current can be considered as a set of electrons which are evenly distributed over the whole gap as illustrated in Fig. 4.5 where g is the gap length of the photoconductive antenna and E is the electric field across the gap.

In the point excitation method, the generated electrons are focused in a small part of the gap, as shown in Fig. 4.6, and d is the length of the excitation area.

To calculate the current in the gap an observation reference plane is chosen as shown in Fig. 4.5 and Fig. 4.6. According to Larmor formula, the power radiated by one electron can be calculated as [104]

$$P = \frac{2e^2a^2}{3c^3} \tag{4.40}$$

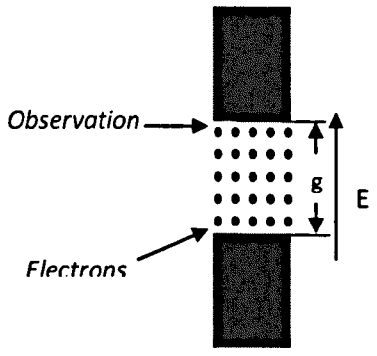

Fig. 4.5 The calculation model of the whole gap excitation method

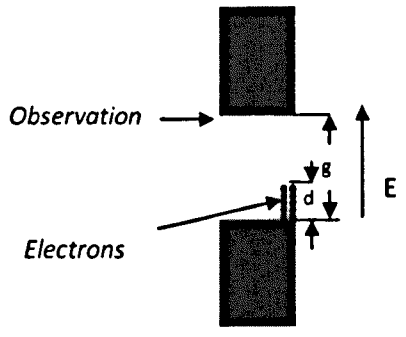

Fig. 4.6 The calculation model of the point excitation method

where e is the electron charge, a is the acceleration of carriers, c is the velocity of light. Because the mobility of holes is much smaller than that of the electrons, the radiated power contributed by the holes can be ignored. If the number of the electrons is $N(t)$, the total charge is $eN(t)$, and the acceleration should be the average acceleration of all the electrons. Therefore, the radiated power from the photoconductive antenna can be calculated by [105]

$$P_{THz}(t) = \frac{2[eN(t)\overline{a(t)}]^2}{3c^3} \tag{4.41}$$

where $\overline{a(t)}$ is the average acceleration of all the electrons, and it can be obtained by the definition of acceleration

$$\overline{a(t)} = \frac{d\overline{v(t)}}{dt} \tag{4.42}$$

where $\overline{v(t)}$ is the average velocity of all electrons at time t. the average velocity of all electrons can be calculated by

$$\overline{v(t)} = \frac{1}{n}\sum_{i=1}^{n} v_i \tag{4.43}$$

where v_i is the velocity of i^{th} electron.

Then two different excitation methods can be compared with the above model. For the conventional method, we divide the whole gap into n small parts from the top to the bottom. If eN is the total charge of all electrons in the gap, each part includes charge of eN/n and a length g/n. When the charges in the 1^{st} part (near the top) go through the observation plane, the current is

$$J_1 = \frac{eN/n}{\frac{g/n}{v_1}} \tag{4.44}$$

where v_1 is the average speed of the electrons in the 1^{st} part when they go through the observation point.

Similarly, when charges in the i^{th} part go through the observation plane, the current should be

$$J_i = \frac{eN/n}{\frac{g/n}{v_i}} \tag{4.45}$$

Due to the acceleration over the gap, the highest current appears when the charges from the last part (from the bottom) go through the observation plane, and the maximum current is

$$J\max_1 = J_n = \frac{eN/n}{\frac{g/n}{v_n}} \tag{4.46}$$

where v_n is the average speed of the electrons in the n^{th} part when they go through the observation point.

For the improved excitation method, because the excitation area is very small, it can be considered that all the electrons go through the observation point at the same time. The situation is similar as the nth part mentioned in the conventional method, so when the electrons go through the observation plane, the current is

$$J\max_2 = \frac{eN}{\frac{d}{v_n}} = \frac{eN}{\frac{g/n}{v_n}} \tag{4.47}$$

Comparing the maximum currents in the gap of these two excitation methods, it is obvious that the current of point excitation J_{max2} is larger than the current of the whole gap excitation J_{max1}. And because the generated electric filed is proportional to the current changing rate [73]

$$E(t) \propto \frac{\partial J}{\partial t} \tag{4.48}$$

the improved excitation method can generate higher THz wave power than the conventional method.

To compare these two methods clearly, a schematic current-time figure (J-t figure), Fig. 4.7, can be used to clarify the different influence of these methods. Where the dashed line is for the whole gap excitation and the solid line is for the point excitation. Therefore, the peak value of the photo-induced current by the point excitation is higher than the peak value of the whole gap excitation and the duration of point excitation is shorter than the duration of the whole gap excitation which means the current changing rate of point excitation is much larger than the current changing rate of whole gap excitation.

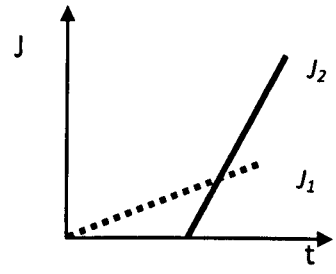

Fig. 4.7 Ideal current as a function of time: Dashed line for the whole gap excitation and solid line for the point excitation

Through this analysis presented here, it is clear that the point excitation method can generate a higher power than the whole gap excitation method, when the laser intensity is below the threshold [106]. The key is that when they are excited at a point, the coherency of the electrons in the gap leads to a stronger photo-induced current than that from the whole gap excitation. Therefore, the improved excitation method is proved to be a better method to generate higher THz power.

4.4 Increasing the Bias Voltage

The bias voltage is an important part of the photoconductive antenna and it can also change the radiated signal from the antenna. The relationship between the peak current in the photoconductive antenna and the electric field can be work out as following.

First, take one electron into account, if one electron is put in an electric field [107], the electric field should be

$$E = \frac{F}{e} = \frac{m_e a}{e} \tag{4.49}$$

where E is the electric filed, F is the electric force, e is the electron charge, m_e is the mass of the electron, and a is the acceleration. Re-arrange Equation (4.49) to get

$$a = \frac{eE}{m_e} \tag{4.50}$$

If the electron moves from the anode, which is the excited point, to the cathode, the distance should be g which is the gap length of the photoconductive antenna (see Fig.4.3), and can be calculated by

$$g = \frac{1}{2}at^2 \tag{4.51}$$

The acceleration a is replaced by Equation (4.50) to give

$$g = \frac{eE}{2m_e}t^2 \tag{4.52}$$

Therefore, the time t can be expressed as

$$t = \sqrt{\frac{2gm_e}{eE}} \tag{4.53}$$

According to the definition of the current and Equation (4.53), we can obtain the relationship between the peak photo-induced current J and the electric field E_b [108]

$$J = \frac{Q}{t} = \frac{eN}{t} = \frac{eN}{\sqrt{\frac{2gm_e}{eE}}} = \frac{eN\sqrt{e}}{\sqrt{2gm_e}} \cdot \sqrt{E_b} \tag{4.54}$$

Equation (4.54) shows that the larger the electric field, the larger the

peak current, which means the larger the radiated THz wave. Because the antenna geometry is fixed, the output power P is proportional to the square of photo-induced current J and the voltage V is proportional to the electric filed E, which is

$$P \propto J^2 \propto E \propto V \tag{4.55}$$

Thus, the output power is proportional to the bias voltage. Fig. 4.8 shows the relationship between the bias voltage and the output power of the THz wave.

The result is the same as that from experiment which was conducted by Zhang, *et al.* [109] who used traditional photoconductive dipole antenna. The experimental result shows that the voltage is proportional to the signal from the photoconductive antenna. Therefore, the bias voltage should be chosen as large as possible, but it must be smaller than the breakdown voltage of the antenna substrate to make sure that the antenna can work under normal situation.

When the antenna structure is changed to bow-tie structure, the analytical result also works. In [110], the researchers did an experiment to evaluate the performance of bow-tie photoconductive antenna, and they also observed a similar result as mentioned above. Therefore, it can be concluded that the analysis can not only be applied to traditional photoconductive dipole antennas but also to photoconductive bow-tie antennas.

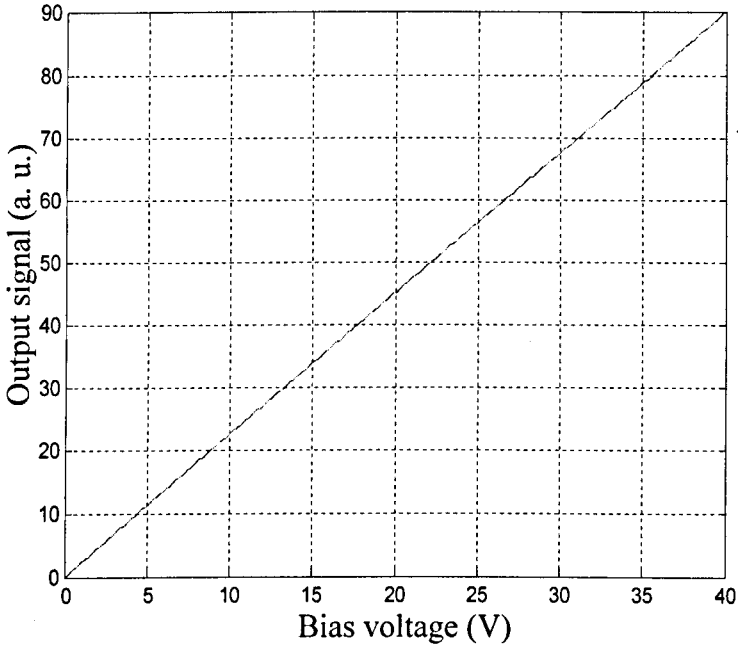

Fig. 4.8 Relationship between the voltage and the output signal

4.5 Changing the Shape of the Gap

The optimization of the antenna shape has received a great deal of attention as the best method to improve the performance of the photoconductive antenna [111], because it is not necessary to increase the energy of the laser source and bias voltage by this method.

There have been some comparison of various photoconductive antennas [91, 97, 112], but there is no quantitative explanation for the difference. To explain the reason why the shape of the dipole can affect the output power from the photoconductive antenna, two typical

photoconductive antennas are selected in this paper for performance comparison.

One type is the conventional photoconductive antenna (dipole antenna), and the other one is the dipole antenna with a sharp edge (indentation antenna). The geometries of these two antennas are shown in Fig. 4.9.

Because of the point effect the indentation antenna can form stronger electric filed than that on the dipole antenna [113]. More detailed explanation is developed below.

The electric field in the dipole antenna can be considered as the same as the electric field produced by two line charges because almost all electrons in the metal are distributed at the edge of the dipoles, which is shown in Fig. 4.10.

In addition, because two poles are connected to the same voltage source, they have the same value of charges (one has positive charges and another has negative charges). Therefore, the electric field generated by two line charges is double the electric field generated by a single line charge.

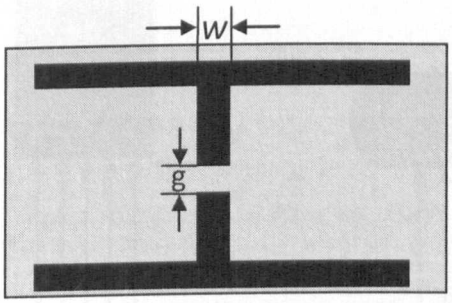

(a)

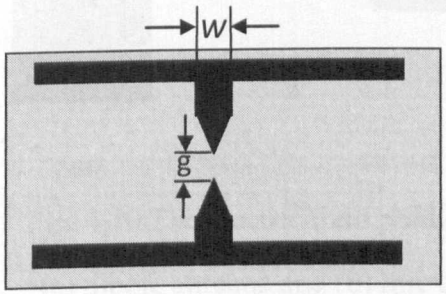

(b)

Fig. 4.9 Geometry of the photoconductive antennas
(a) dipole antenna, (b) indentation antenna

The electric field produced by line charge can be expressed as [114]

$$E_l = \frac{\rho_l}{2\pi\varepsilon_0 r\sqrt{(\frac{r}{l/2})^2 + 1}} \tag{4.56}$$

where ρ_L is the density of the line charges, r is the distance from the line charge to the observed reference, l is the length of the line charge and ε_0 is the dielectric constant.

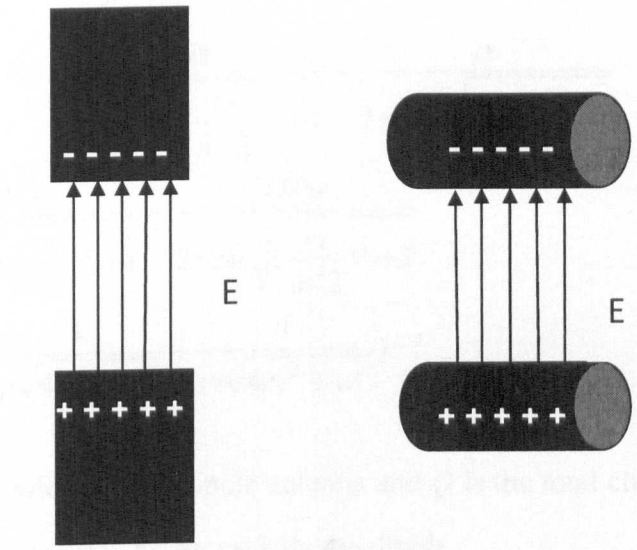

Fig. 4.10 The electric field produced by
(a) dipole antenna and (b) line charges

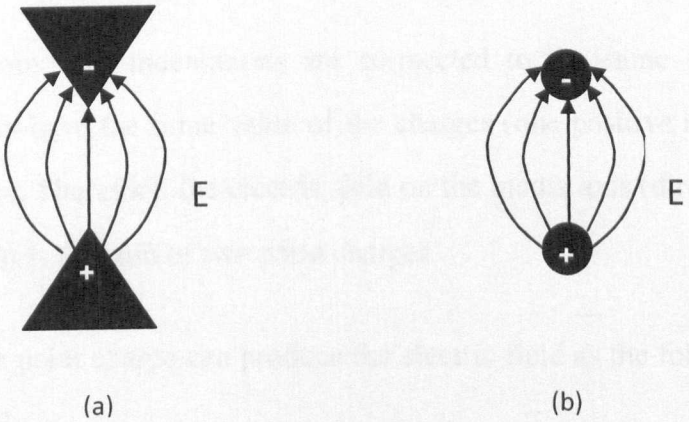

Fig. 4.11 The electric fields produced by
(a) indentation antenna and (b) point charges

The electric field in the dipole antenna is

$$E_d = E_{l1} + E_{l2} = \frac{\rho_l}{2\pi\varepsilon_0 r_1\sqrt{(\frac{r_1}{w/2})^2+1}} + \frac{\rho_l}{2\pi\varepsilon_0 r_2\sqrt{(\frac{r_2}{w/2})^2+1}}$$
$$= \frac{Q/w}{2\pi\varepsilon_0 r\sqrt{(\frac{r_1}{w/2})^2+1}} + \frac{Q/w}{2\pi\varepsilon_0 r\sqrt{(\frac{r_2}{w/2})^2+1}}$$
$$= \frac{Q}{2\pi\varepsilon_0}\cdot(\frac{1}{r_1\sqrt{4r_1^2+w^2}} + \frac{1}{r_2\sqrt{4r_2^2+w^2}}) \quad (4.57)$$

where w is the width of the dipole antenna and Q is the total charge of the dipole, r_1 and r_2 are the distances from the dipole.

The electric filed in the indentation antenna can be considered as the electric field produced by two point charges because almost all electrons are accumulated to the sharp corner of the indentations because of the point effect, which is shown in Fig. 4.10.

Furthermore, two indentations are connected to the same voltage source, so they have the same value of the charges (one positive and the other negative). Therefore, the electric field on the media axis (direct line in Fig. 4.11(b)) is the sum of two point charges.

The single point charge can produce the electric field as the following equation [114]

$$E_p = \frac{Q}{4\pi\varepsilon_0 r^2} \quad (4.58)$$

where Q is the total charge of the indentation, ε_0 is the dielectric constant, and r is the distance from the point charge to the observed point. The electric field on the medial axis of the indentation antenna is

$$E_i = E_{p1} + E_{p2} = \frac{Q}{4\pi\varepsilon_0 r_1^2} + \frac{Q}{4\pi\varepsilon_0 r_2^2} = \frac{Q}{4\pi\varepsilon_0} \cdot \left(\frac{1}{r_1^2} + \frac{1}{r_2^2}\right) \tag{4.59}$$

According to Equation (4.57) and Equation (4.59), if the same antenna substrate and same bias voltage are used, it is obvious that E_i is larger than E_d, because

$$\begin{aligned} E_d &= \frac{Q}{2\pi\varepsilon_0} \cdot \left(\frac{1}{r_1\sqrt{4r_1^2 + w^2}} + \frac{1}{r_2\sqrt{4r_2^2 + w^2}}\right) \\ &< \frac{Q}{2\pi\varepsilon_0} \cdot \left(\frac{1}{2r_1^2} + \frac{1}{2r_2^2}\right) = \frac{Q}{4\pi\varepsilon_0} \cdot \left(\frac{1}{r_1^2} + \frac{1}{r_2^2}\right) = E_i \end{aligned} \tag{4.60}$$

This relationship means that indentation antenna can produce larger electric filed than dipole antenna.

According to the relationship between the generation signal and the bias electric field which is shown by Equation (4.54), a new equation can be deduced to show the comparison of the two photoconductive antennas.

$$\frac{J_i}{J_d} = \sqrt{\frac{E_i}{E_d}} \tag{4.61}$$

Because E_i is larger than E_d, which is discussed in Equation (4.60), J_i is larger than J_d. This result means the indentation antenna can generate stronger signals than dipole antenna, so indentation antenna has better performances than dipole antenna.

The experiment which was done by Cai, *et al* [91] can be used to validate the theory discussed here. In their experiment, the power from the photoconductive dipole antenna and indentation antenna were about 0.35 and 0.85, thus the ratio of the currents of these two antennas is $(0.83/0.35)^{0.5} = 1.53$.

According to the experiment set-up (antenna width is 20 μm and gap is 5 μm), the proportion of the electric field can be calculated

$$\sqrt{\frac{E_i}{E_d}} = \sqrt{\frac{\frac{Q}{4\pi\varepsilon_0 g^2}}{\frac{Q}{2\pi\varepsilon_0 g\sqrt{4g^2+w^2}}}} = 1.50$$

It is very close to 1.53, thus it proves that the current ratio is equal to the square root of the electric field ratio, which is Equation (4.61). Also, it has proved that the indentation antenna can generate stronger signal than the traditional dipole antenna.

As mentioned in [108], the output power is proportional to the bias electric field when the antenna gap is fixed. Therefore, increasing the bias electric field can improve the output power.

Then, we are going to investigate the number of indentations and the electric field, and determine which structure can generate most power of THz wave.

First, the calculation model should be set up. The structure of the

photoconductive antenna with one pair of indentations is represented in Fig. 4.9(b). Because it can be considered as two point charges [108], the bias electric field can be calculated as [115]

$$E_1 = \frac{Q}{4\pi\varepsilon_0}(\vec{x}_0 + \vec{y}_0) \tag{4.62}$$

$$\vec{x}_0 = \frac{x}{(\sqrt{x^2 + (y - g/2)^2})^3} + \frac{-x}{(\sqrt{x^2 + (y + g/2)^2})^3} \tag{4.63}$$

$$\vec{y}_0 = \frac{y - n}{(\sqrt{x^2 + (y - g/2)^2})^3} + \frac{-y - n}{(\sqrt{x^2 + (y + g/2)^2})^3} \tag{4.64}$$

where Q is the total charge, ε_0 is the dielectric coefficient, g is the gap length and $\vec{x}_0$ and $\vec{y}_0$ are the electric field coefficient on x-axis and y-axis direction, respectively. The coordinates can be expressed as in Fig. 4.12.

The simulation result is shown in Fig. 4.13. It shows that the peak value of the electric field is near the indentations, which matches well with the theory discussed in reference [108].

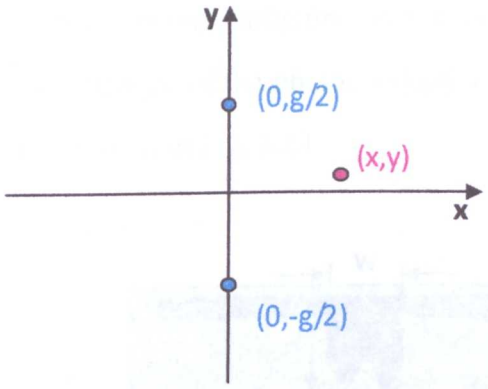

Fig. 4.12 Calculation model of one pair of indentations

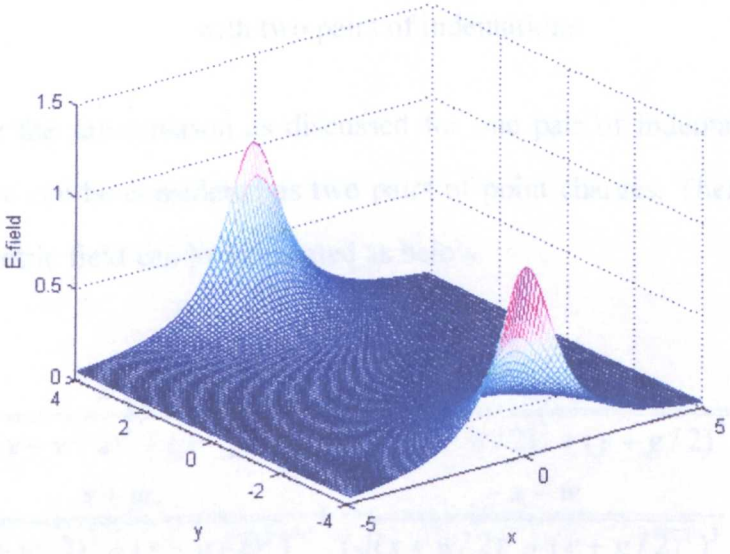

Fig. 4.13 Bias electric field of the photoconductive antenna with one pair of indentations

Then, another pair of indentations is added to the basic photoconductive antenna structure, the bias electric field should be changed. The structure of the photoconductive antenna with two pairs of indentations is shown in Fig. 4.14.

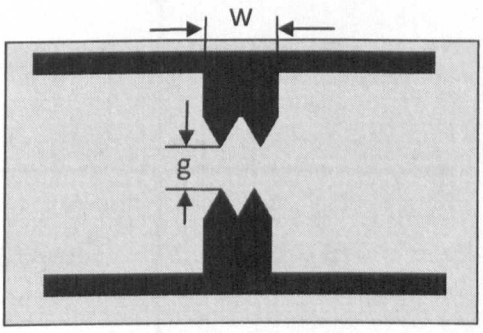

Fig. 4.14 Geometry of the photoconductive antenna with two pairs of indentations

For the same reason as discussed for one pair of indentations, this structure can be considered as two pairs of point charges. Therefore, the bias electric field can be calculated as below.

$$E_2 = \frac{Q/2}{4\pi\varepsilon_0}(\vec{x}_1 + \vec{y}_1) \tag{4.65}$$

$$\vec{x}_1 = \frac{x - w/2}{(\sqrt{(x-w/2)^2 + (y-g/2)^2})^3} + \frac{-x + w/2}{(\sqrt{(x-w/2)^2 + (y+g/2)^2})^3}$$
$$+ \frac{x + w}{(\sqrt{(x+w/2)^2 + (y-g/2)^2})^3} + \frac{-x - w}{(\sqrt{(x+w/2)^2 + (y+g/2)^2})^3} \tag{4.66}$$

$$\vec{y}_1 = \frac{y - g/2}{(\sqrt{(x-w/2)^2 + (y-g/2)^2})^3} + \frac{-y - g/2}{(\sqrt{(x-w/2)^2 + (y+g/2)^2})^3}$$
$$+ \frac{y - n}{(\sqrt{(x+w/2)^2 + (y-g/2)^2})^3} + \frac{-y - n}{(\sqrt{(x+w/2)^2 + (y+g/2)^2})^3} \tag{4.67}$$

where $\vec{x}_1$ and $\vec{y}_1$ are the electric field coefficient on the x-direction and y-direction, w is the width of the antenna, g is the length of the gap, and the coordinates can be set as in Fig. 4.15.

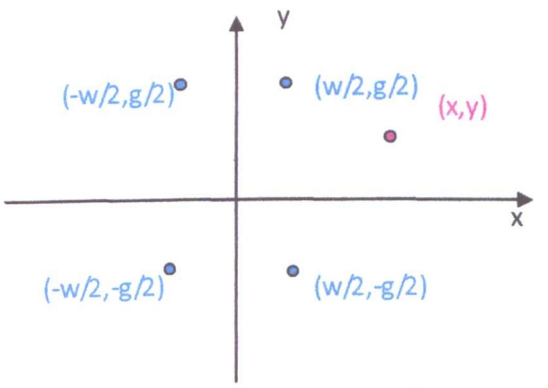

Fig. 4.15 Calculation model of two pairs of indentations

The simulation result is shown in Fig. 4.16. It shows the peak values of the bias electric field are near the indentations which is similar as the photoconductive antenna with one pair of indentations, but the peak value becomes smaller when two pairs of indentations are used instead of one pair of indentations.

When the number of indentations becomes three, the bias electric field also should be changed. The structure of the photoconductive antenna with three pairs of indentations is shown in Fig. 4.17.

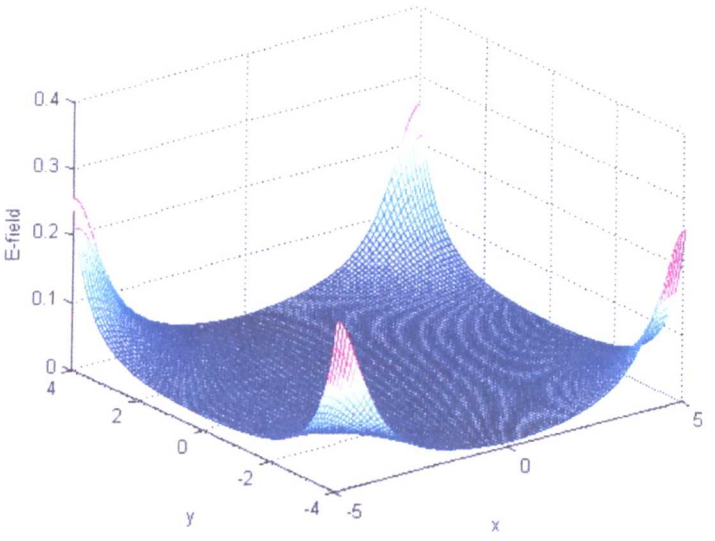

Fig. 4.16 Bias electric field of the photoconductive antenna with two pairs of indentations

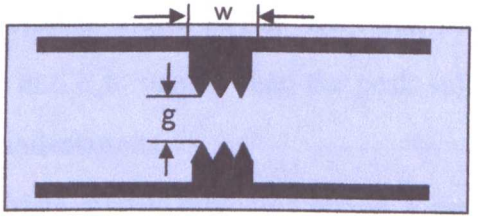

Fig. 4.17 Geometry of the photoconductive antenna with three pairs of indentations

The bias electric field can be calculated by the combination of the electric field produced by one pair of indentations and two pairs of indentations. Therefore, the bias electric field is

$$E_3 = \frac{Q/3}{4\pi\varepsilon_0}(\vec{x}_0 + \vec{x}_1 + \vec{y}_0 + \vec{y}_1) \tag{4.68}$$

where $\vec{x}_0, \vec{x}_1, \vec{y}_0, \vec{y}_1$ have the same meaning as in Equation (4.62) and Equation (4.65), and the coordinates can be schematic as in Fig. 4.18.

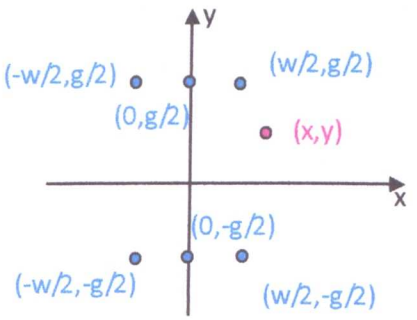

Fig. 4.18 Calculation model of three pairs of indentations

The simulation result is shown in Fig. 4.19. The peak value is also near the indentations and it is smaller than the peak values of both one pair and two pairs of indentations.

Based on three basic models discussed above, a general calculation model can be obtained. For the photoconductive antenna with multiple indentations, the general calculation model is divided into two categories: even number pairs and odd number pairs - since their expressions will be different [116]. The models are shown in Fig. 4.20 and Fig. 4.21, respectively.

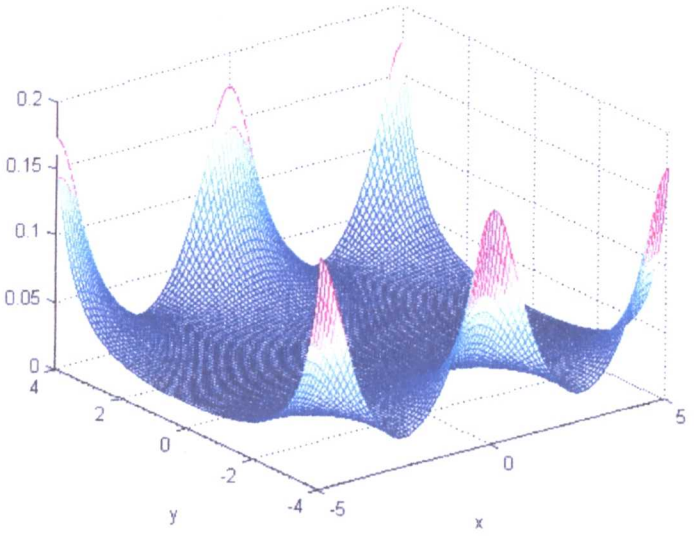

Fig. 4.19 Bias electric field of the photoconductive antenna with three pairs of indentations

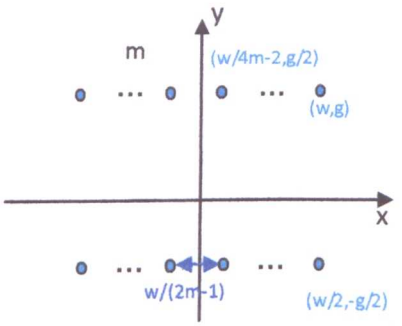

Fig. 4.20 Calculation model of even number pairs of indentations

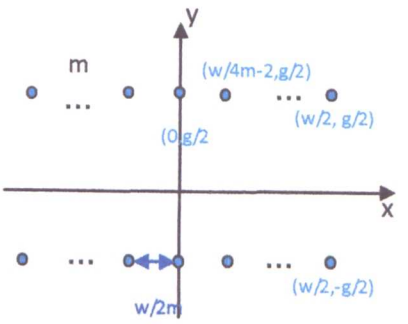

Fig. 4.21 Calculation model of odd number pairs of indentations

For the case when the pairs of indentations are even number, *2m* (*m* = *1, 2, ...*), the width of the antenna is *w* and the separation between two adjacent indentations is *w/(2m-1)*. Therefore, the bias electric field can be found as

$$E_{2m} = \frac{Q/2m}{4\pi\varepsilon}\left(\sum_{i=1}^{m} R_i^x \hat{x} + \sum_{i=1}^{m} R_i^y \hat{y}\right) \tag{4.69}$$

$$R_i^x = \frac{x-\Delta x_i}{\left(\sqrt{(x-\Delta x_i)^2+(y-g/2)^2}\right)^3} + \frac{-x+\Delta x_i}{\left(\sqrt{(x-\Delta x_i)^2+(y+g/2)^2}\right)^3} + \frac{x+\Delta x_i}{\left(\sqrt{(x+\Delta x_i)^2+(y-g/2)^2}\right)^3} + \frac{-x-\Delta x_i}{\left(\sqrt{(x+\Delta x_i)^2+(y+g/2)^2}\right)^3} \tag{4.70}$$

$$R_i^y = \frac{y-g/2}{\left(\sqrt{(x-\Delta x_i)^2+(y-g/2)^2}\right)^3} + \frac{-y-g/2}{\left(\sqrt{(x-\Delta x_i)^2+(y+g/2)^2}\right)^3} + \frac{y-g}{\left(\sqrt{(x+\Delta x_i)^2+(y-g/2)^2}\right)^3} + \frac{-y-g}{\left(\sqrt{(x+\Delta x_i)^2+(y+g/2)^2}\right)^3} \tag{4.71}$$

$$\Delta x_i = \frac{2i-1}{4m-2} w \tag{4.72}$$

where Q is the total charge, R_i^x and R_i^y are the electric field coefficients produced by i^{th} pair in x- and y-direction, respectively. The pair in the middle is set to be the 1st pair and the pair at the end is set to be the m^{th} pair.

For the odd number of indentations, the total number of the indentation pair is *2m+1*, the width of the antenna is also *w*, and the nearest distance between two indentations is *w/2m*. Therefore, the bias

electric field can be calculated as

$$E_{2m+1} = \frac{Q/(2m+1)}{4\pi\varepsilon}(R_0^x \hat{x} + \sum_{i=1}^{m} R_i^x \hat{x} + R_0^y \hat{y} + \sum_{i=1}^{m} R_i^y \hat{y}) \tag{4.73}$$

$$R_0^x = \frac{x}{(\sqrt{x^2 + (y - g/2)^2})^3} + \frac{-x}{(\sqrt{x^2 + (y + g/2)^2})^3} \tag{4.74}$$

$$R_0^y = \frac{y - g/2}{(\sqrt{x^2 + (y - g/2)^2})^3} + \frac{-y - g/2}{(\sqrt{x^2 + (y + g/2)^2})^3} \tag{4.75}$$

R_i^x and R_i^y are the same as shown in Equations (4.70) and (4.71), but Δx_i is different, where

$$\Delta x_i = \frac{i}{2m} w \tag{4.76}$$

If the number of the indentation pairs (m) is changed, the electric field of the biased photoconductive antenna will be changed. Fig. 4.22 shows the calculated electric fields in the bias photoconductive antenna with different numbers of indentations.

As shown in the simulation results, for both even and odd numbers of indentations, it is obvious that the peak value of the bias electric field is decreased when the number of indentations is increased, which means $E_{2m} > E_{2m+1} > E_{2m+2} > E_{2m+3}$. As increasing the bias electric field leads to more generated THz power [115], the output THz power from each pair of indentation will decrease when the number of indentations increases. It should be pointed out that this result is based on the assumption that the total charge Q is constant. However, the maximum bias voltage applied to

a photoconductive antenna depends mainly on the material properties thus is usually unchanged in the practical operation of a photoconductive antenna. Therefore the total charge Q will increase with the indentation number, leading to improved bias electric field of each pair of indentations of the photoconductive antenna.

Another thing must be noticed is that there are two main limiting factors on the overall THz output power of a photoconductive antenna: one is the applied electric field (the maximum bias voltage before breakdown) and the other is the photo-generated carrier density (the maximum laser pump power before saturation). The radiated electric field can be expressed as Equation (4.26)

$$E_{rad} \propto E_b \frac{I}{I + I_0} \tag{4.77}$$

where I is the input laser intensity, E_b is the bias electric field and I_0 is the saturation parameter. I_0 is set to be 4.5 in ref [90].

As shown in Fig.4.23, the THz electric field became saturated around 1 for photoconductive antenna with a single indentation. This has been increased to 2 and 5 for photoconductive antenna with two and five indentations, respectively. This trend will continue as far as the laser

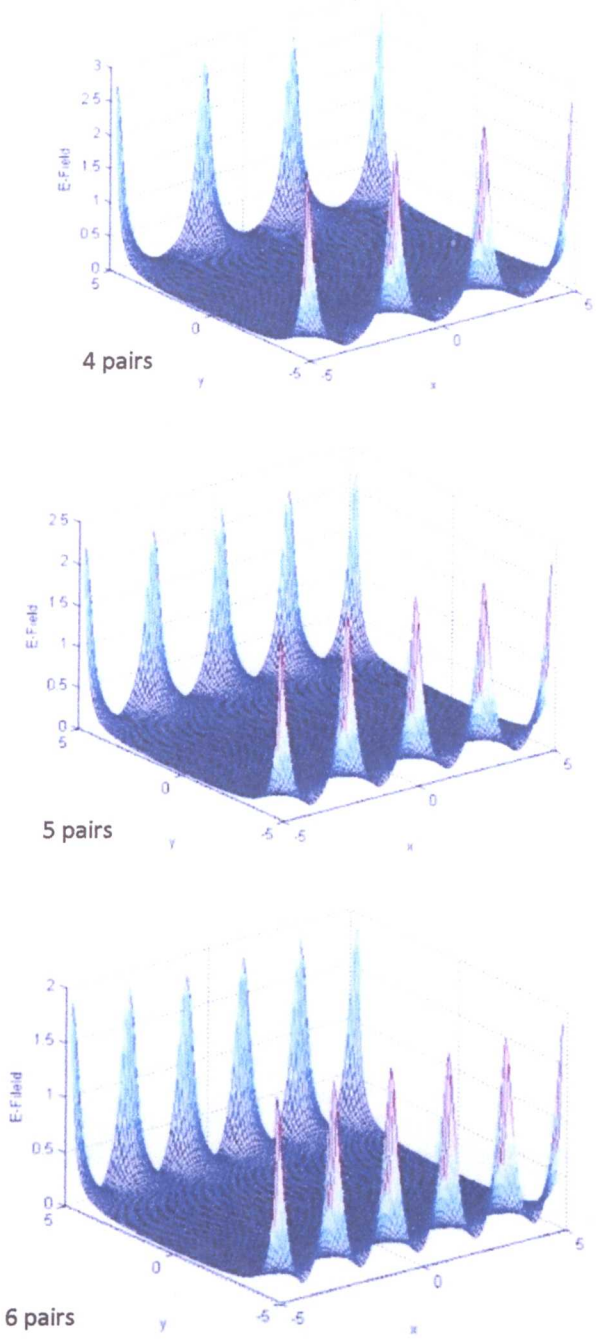

Fig. 4.22 Simulation results for the bias electric fields with different numbers of indentations

source is able to provide sufficient pumping power. Therefore, it is beneficial to increase the number of indentations.

As discussed above, increasing the number of indentations will decrease the radiated electric field of each individual indentation. However, overall the photoconductive antenna will generate more THz power as more laser pump power can be applied.

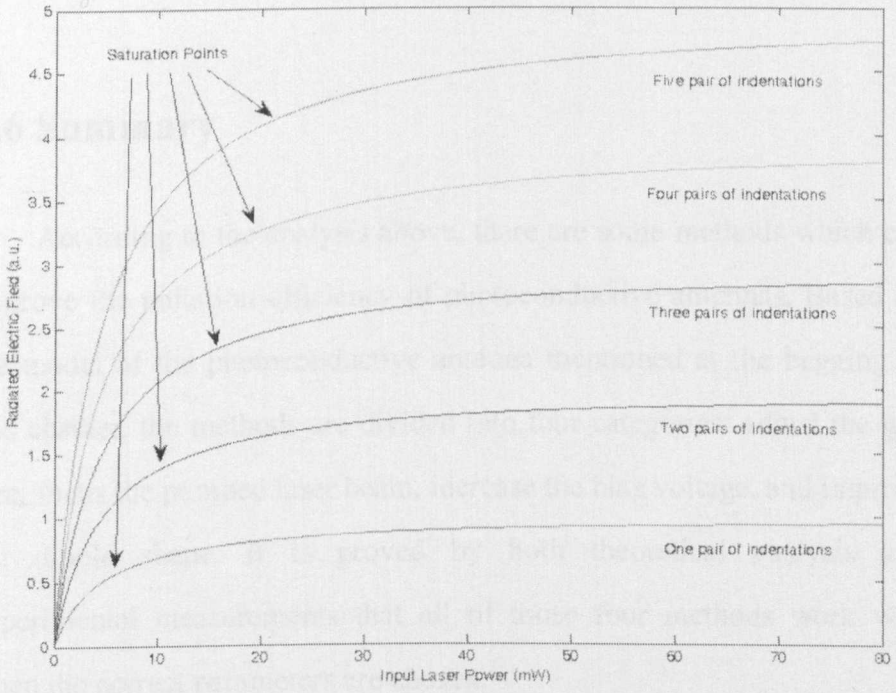

Fig. 4.23 Relationship between the input laser power and the radiated electric field

In summary, the photoconductive antenna with one pair of indentation has the best conversion efficiency as compared with those

with multiple pairs of indentations. On the other hand, the output THz power from a photoconductive antenna increases with the pump laser power but will eventually become saturated when the pump laser power exceeds a few mW. Therefore the photoconductive antenna with multiple pairs of indentation, as discussed in this work, can make full use of the laser power available (the output power of a modern femtosecond laser could well-exceed 1W), thus is a more powerful THz source.

4.6 Summary

According to the analysis above, there are some methods which can improve the radiation efficiency of photoconductive antennas. Based on the model of the photoconductive antenna mentioned at the begging of this chapter, the methods are divided into four categories: adjust the gap size, focus the pumped laser beam, increase the bias voltage, and improve the dipole shape. It is proved by both theoretical analysis and experimental measurements that all of those four methods work well when the correct parameters are chosen.

First, when the pumped laser source is larger than the threshold, the gap size cannot be too large or too small, and the optimum value of the gap size is determined by the incident laser power and the substrate material. Second, compared with excitation on the whole gap area, focusing the laser beam into a small part can increase the amplitude of the

radiated electric field. Third, increasing the bias voltage can also increase the radiated power but it must be smaller than the breakdown voltage of the antenna substrate. Fourth, the antenna shape has effect on THz generation. If indentations are added at the end of the dipole, the bias electric field is enhanced, and it leads to more radiated THz power.

CHAPTER 5
A NOVEL THZ EMITTER: A PHOTOCONDUCTIVE HORN ANTENNA

5.1 Introduction to Photoconductive Conical Horn Antennas

The antenna structure can basically determine the characteristics of the radiated THz wave. Conventional photoconductive antenna has a dipole structure and an omni-directional radiation pattern which is desirable for some applications. For example, some mobile base station antennas have an omni-directional radiation pattern to provide circular radio coverage. But for some applications, a directional radiation pattern is required (such as a satellite receiving antenna). For these applications, the omni-directional antennas are not suitable [117, 118]. Most of the conventional photoconductive antennas produce omni-directional radiation pattern and so far very few directional THz antennas have been designed and made. Therefore, this chapter will present a new type of photoconductive antenna which can radiate THz waves towards one direction, *i.e.* with a high directivity.

Among the conventional RF/microwave antennas, the conical horn antenna is identified as a suitable structure to replace the conventional

dipole structure because it may offer a good efficiency and is relatively easy to fabricate, furthermore, it can radiate the wave in a desired direction which means more power can be transmitted or received at the location of interest [119].

The new antenna structure is shown in Fig. 5.1 [120]. It consists of two parts: one is a photoconductive emitter and the other is a THz conical horn. The photoconductive emitter is a conventional dipole THz dipole antenna and placed in a circular waveguide: one end is short-circuited while the other end is connected to the second part of the antenna – the conical horn. Compared with the conventional conical horn antenna, the photoconductive conical horn antenna uses a photoconductive emitter, instead of coaxial cable, to excite the horn, and the THz wave is generated on the semiconductor substrate which is illuminated by a femto-second laser. The photoconductive emitter is employed to transfer the laser power into THz wave and the conical horn part is used to radiate THz wave. Unlike a simple dipole, this new structure will only radiate THz waves in a desired direction.

Fig. 5.2 shows the materials of the photoconductive conical horn antenna. For the photoconductive emitter part, the electrodes are made of gold and the substrate is made of LT-GaAs which is commonly used for photoconductive antennas. For the conical horn part, aluminium is chosen to make the horn and Indium Tin Oxides (ITO) is selected for the back wall of the waveguide to let the laser beam incident into the waveguide and keep THz wave transferred forward.

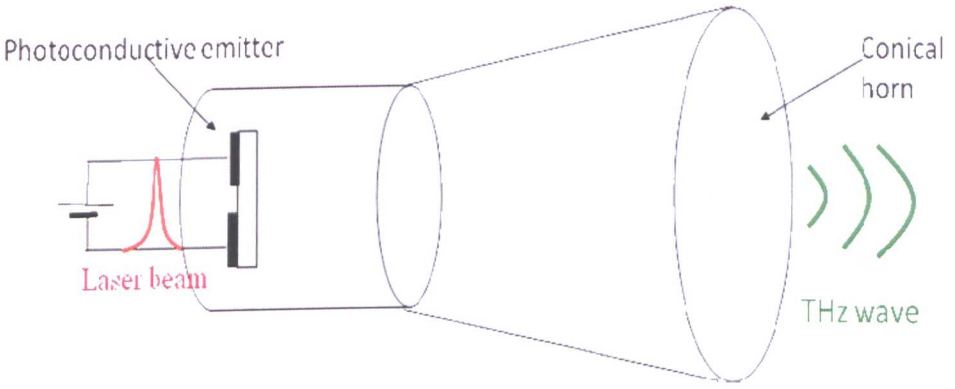

Fig. 5.1 Structure of THz conical horn antenna

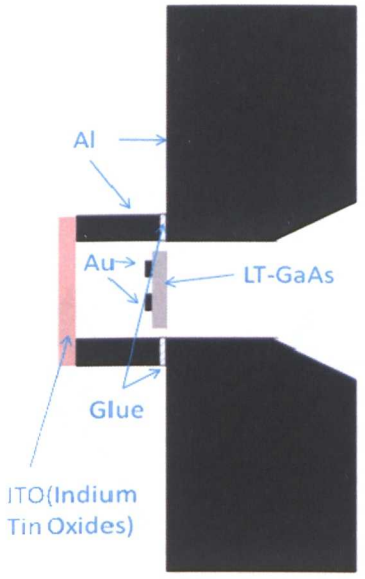

Fig. 5.2 Materials of THz conical horn antenna

The process is similar as the THz wave generation from the dipole photoconductive antenna which was discussed in Chapter 3. When a laser is input into the substrate of the photoconductive emitter, the electron-hole pairs can produce the time-variant current with the help of bias voltage source, which leads to the THz generation. Furthermore, with the integrated conical horn part, the radiated wave is more directed, which means more power can be detected in specified direction. The schematic can be briefly illustrated with Fig. 5.3.

Therefore, the designing process can be divided into two parts: first, designing an effective photoconductive emitter and second, designing a suitable conical horn structure. This chapter will discuss how to design both parts and use simulation software (CST Microwave Studio) to estimate the performance of the designed antenna.

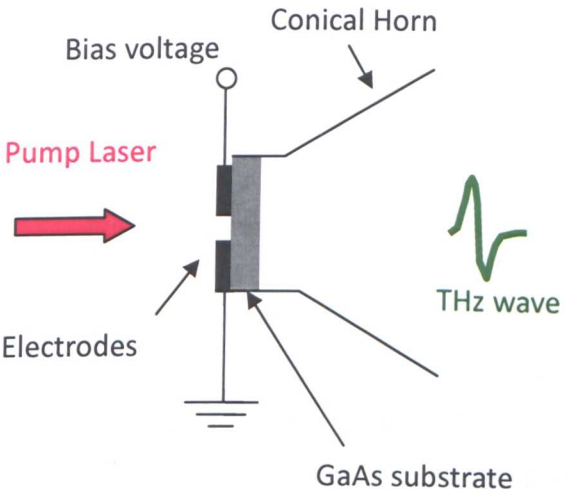

Fig. 5.3 The THz wave generation from photoconductive conical horn antenna (side view)

5.2 Design of Photoconductive Emitter

The photoconductive emitter is used to generate the THz wave and the design objective of this part is to transfer the laser power into THz power effectively.

The structure of the photoconductive emitter is shown in Fig. 5.4. It consists of a GaAs substrate, a pair of electrodes which are fabricated on the substrate, and a DC voltage source which is connected to the dipole.

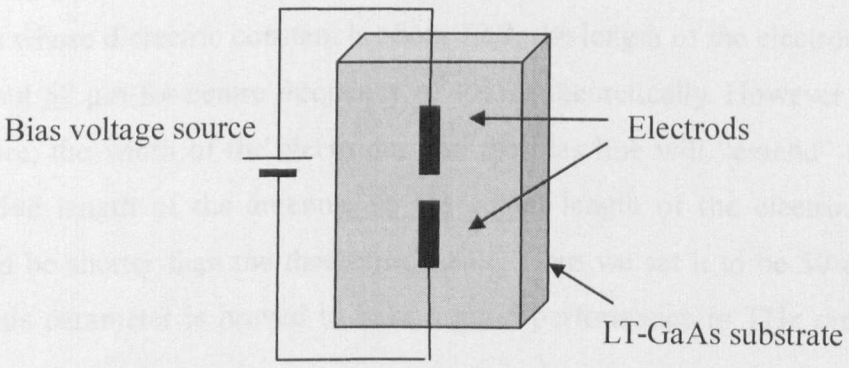

Fig. 5.4 Structure of photoconductive dipole emitter

Based on the discussion in last chapter, the optimum gap size can be determined once the incident laser power is fixed, so it will not be further analysed here. However, the length of the dipole should be considered: since the electrodes are fabricated on a semiconductor substrate, the length of the electrodes is different from the conventional dipole antenna design. If the relative dielectric constant is ε_r, the wavelength in the

substrate is [121]

$$\lambda = \frac{\lambda_0}{\sqrt{\varepsilon_r}} \tag{5.1}$$

where λ_0 is the wavelength in vacuum. The resonant length for dipole antenna fabricated on a substrate is

$$L = \frac{\lambda}{2} = \frac{\lambda_0}{2\sqrt{\frac{\varepsilon_r+1}{2}}} \tag{5.2}$$

Therefore, for the substrate made of the most popular material, LT-GaAs whose dielectric constant is about 12.9, the length of the electrodes is about 57 μm for centre frequency of 1 THz theoretically. However, in practice, the width of the electrodes and the bias line will "extend" the effective length of the antenna, so the actual length of the electrodes should be shorter than the theoretical value. Here we set it to be 50 μm and this parameter is proved to have a good performance in THz range [14].

A typical laser source usually has 20 fs pulse duration with the centre wave length of 800 nm, and the spectrum is distributed from 670 nm to 920 nm. In addition, the substrate material is chosen as the most popular material, LT-GaAs, whose carrier life-time is very short, the mobility and the dielectric constant are both very high. According to the analysis of Section 4.3, the optimised gap area should be 50 μm^2 and the width of the electrodes are usually 10 μm from manufactory point of view, the length and the width of the gap are set to be 5 μm and 10 μm, respectively.

The substrate is also a factor which affects the antenna performance. When the antenna length is fixed and the material of the substrate is determined, the radiation pattern may be various when the size of the substrate is changed.

To investigate the effect of the substrate size on the radiation pattern, the coordinates are set as shown in Fig. 5.5 and the parameters investigated here include the length, the width and the thickness. The aim of the comparison here is to find how to focus the power into one direction (in the direction of $\theta = 0^{o}$ here).

It is easy to understand that when the thickness is increased, more power will be trapped in the substrate. Fig. 5.6 to Fig. 5.9 are the radiation patterns in xoz plan of the photoconductive antenna with different thickness. In these simulations, the length and the width of the substrate are fixed (150 μm×150 μm) and the frequency is set to be 1 THz. Then the thickness is increased from 75 μm to 300 μm which correspond to from $\lambda/4$ to λ and the radiation patterns are so different from that of the thin substrate. It is obvious that when the substrate is very thin (75 μm), the value at direction of 0^{o} is the greatest.

Then the length and the width are increased to 600 μm×600 μm. Fig. 5.10 to Fig. 5.13 shows the simulation results, and the same conclusion can be drawn: thin substrate leads to more radiation power in direction of 0^{o}.

This phenomenon had been discussed by Jackson and Alexopoulos [122]. From their observations, it is found that when increasing the thickness of the substrate, the dipole antennas couple power to higher-

order substrate modes and in some cases, even more than 90% power is trapped in the substrate. Therefore, the gain of the dipole antenna fabricated on a substrate decreases when the thickness of the substrate increases.

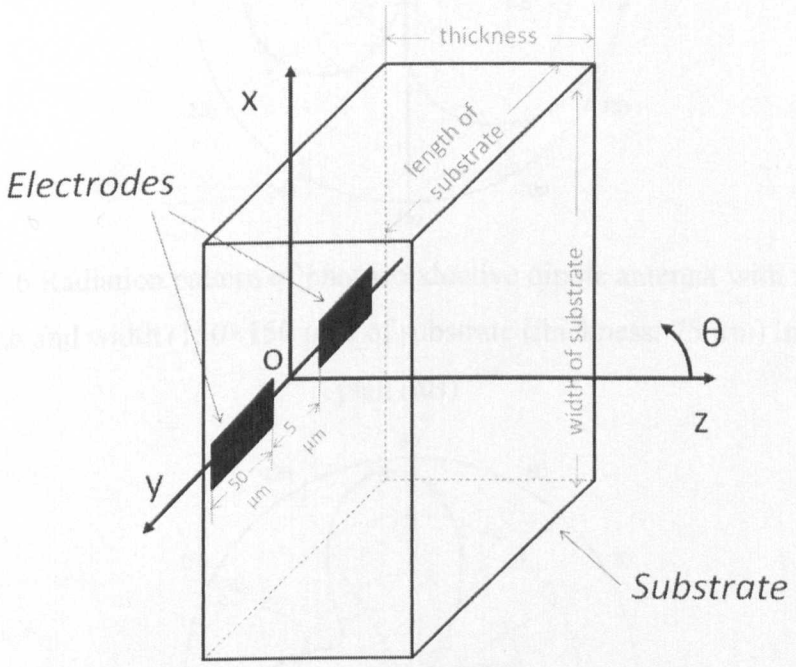

Fig. 5.5 Coordinates for photoconductive dipole antenna comparison

To examine this observation, the length and the width are increased to 1000 μm and 1000 μm, respectively, which are greater than 3 wavelengths and the width and length are set to be random numbers. Fig. 5.14 to Fig. 5.17 show that a thin substrate can work better than a thick substrate.

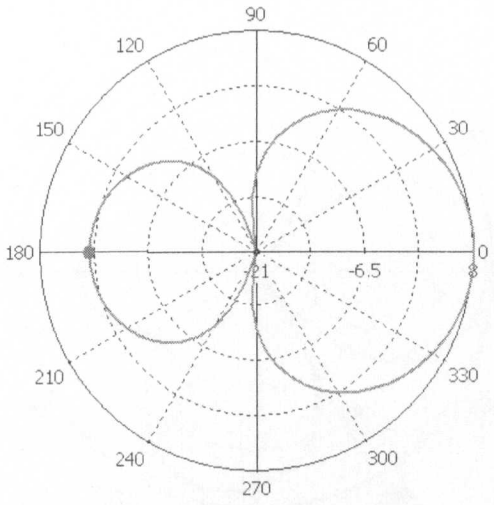

Fig.5.6 Radiation pattern of photoconductive dipole antenna with fixed length and width (150×150 μm) of substrate (thickness: 75 μm) in xoz plan (dB)

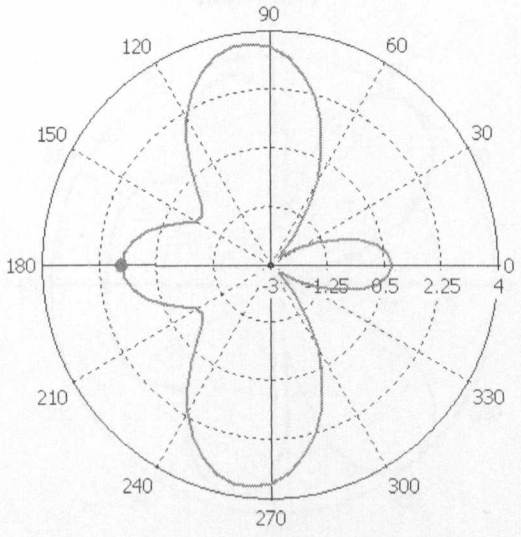

Fig.5.7 Radiation pattern of photoconductive dipole antenna with fixed length and width (150×150 μm) of substrate (thickness: 150 μm) in xoz plan (dB)

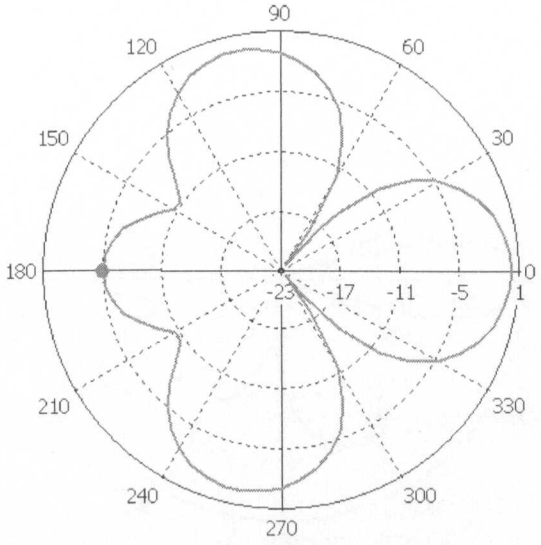

Fig.5.8 Radiation pattern of photoconductive dipole antenna with fixed length and width (150×150 μm) of substrate (thickness: 225 μm) in xoz plan (dB)

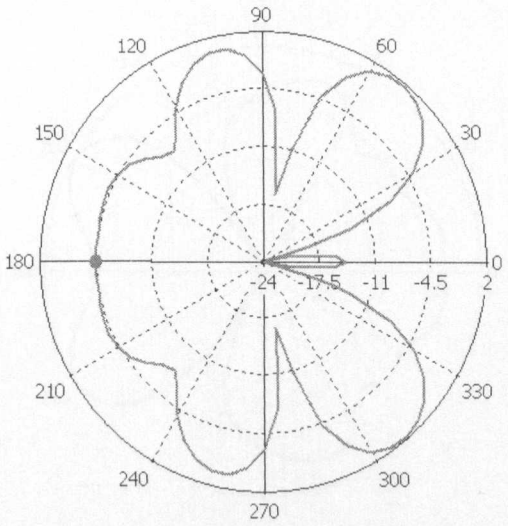

Fig.5.9 Radiation pattern of photoconductive dipole antenna with fixed length and width (150×150 μm) of substrate (thickness: 300 μm) in xoz plan (dB)

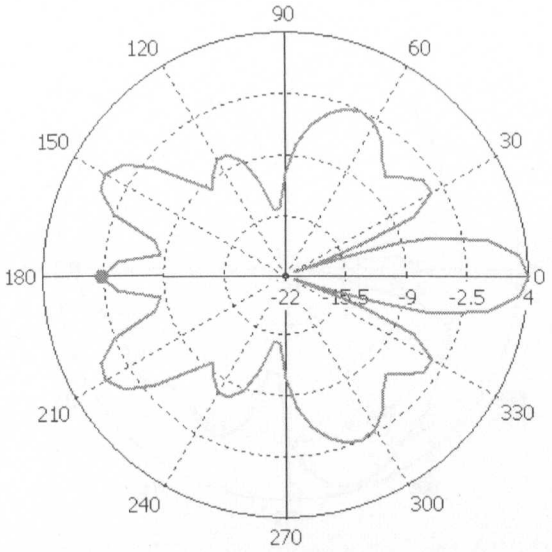

Fig.5.10 Radiation pattern of photoconductive dipole antenna with fixed length and width (600×600 μm) of substrate (thickness: 75 μm) in xoz plan (dB)

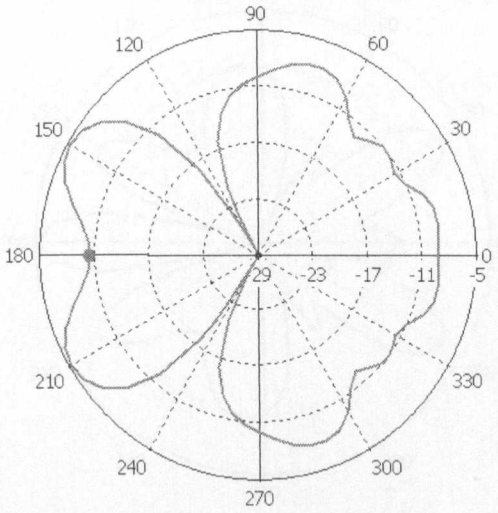

Fig.5.11 Radiation pattern of photoconductive dipole antenna with fixed length and width (600×600 μm) of substrate(thickness: 150 μm) in xoz plan (dB)

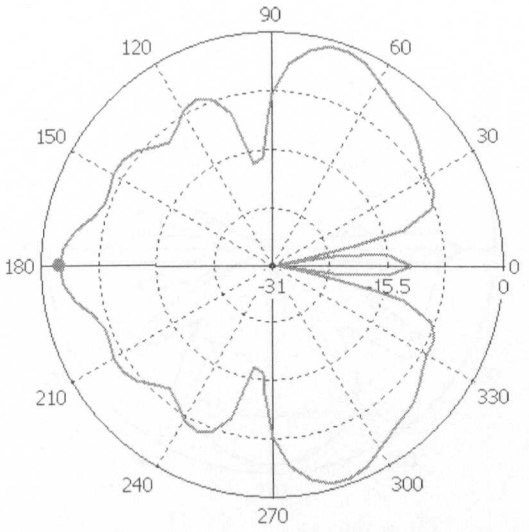

Fig.5.12 Radiation pattern of photoconductive dipole antenna with fixed length and width (600×600 μm) of substrate (thickness: 225 μm) in xoz plan (dB)

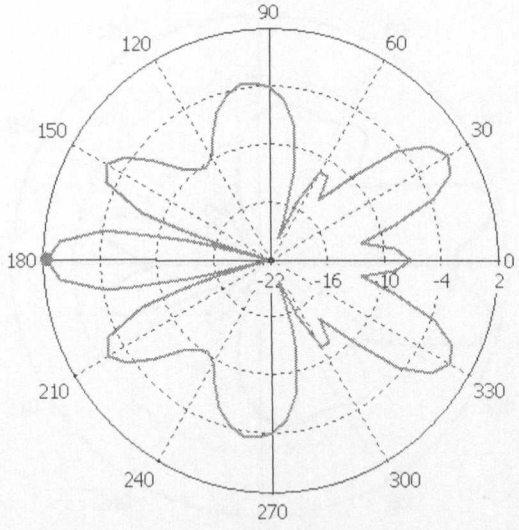

Fig.5.13 Radiation pattern of photoconductive dipole antenna with fixed length and width (600×600 μm) of substrate(thickness: 300 μm) in xoz plan (dB)

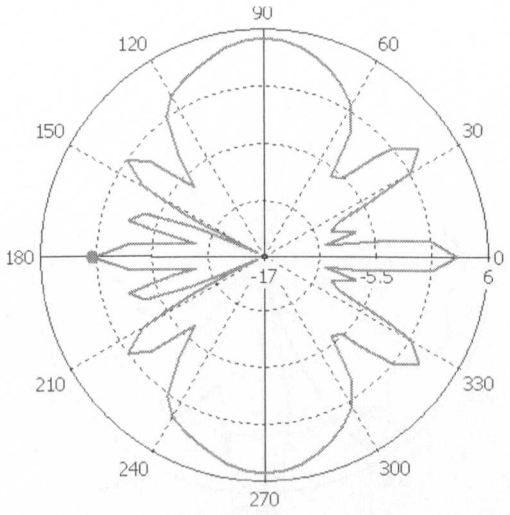

Fig.5.14 Radiation pattern of photoconductive dipole antenna with fixed length and width (1000×1000 μm) of substrate(thickness:75 μm) in xoz plan (dB)

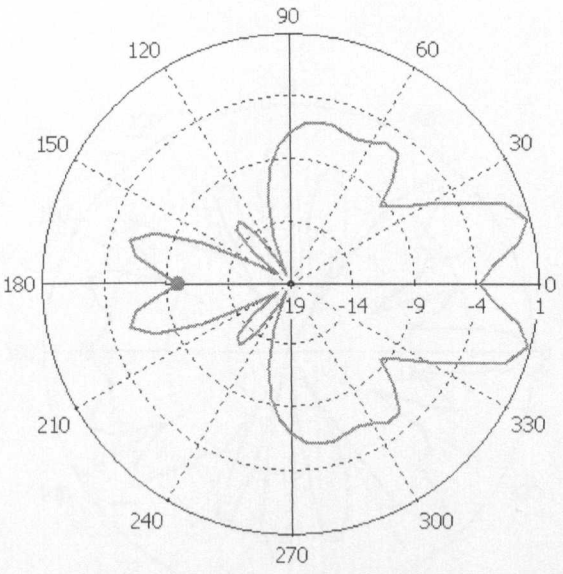

Fig. 5.15 Radiation pattern of photoconductive dipole antenna with fixed length and width (1000×1000 μm) of substrate (thickness: 112 μm) in xoz plan (dB)

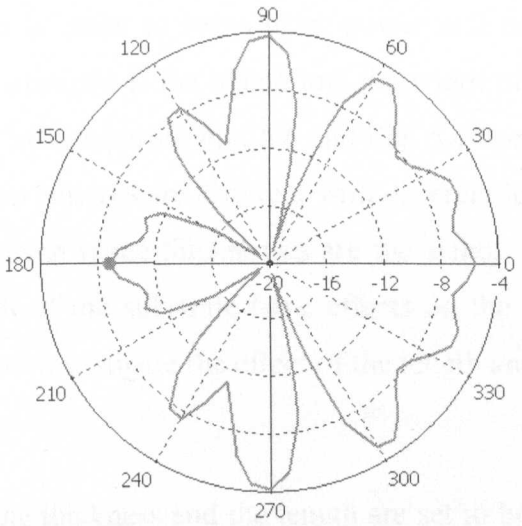

Fig.5.16 Radiation pattern of photoconductive dipole antenna with fixed length and width (1000×1000 μm) of substrate (thickness: 350 μm) in xoz plan (dB)

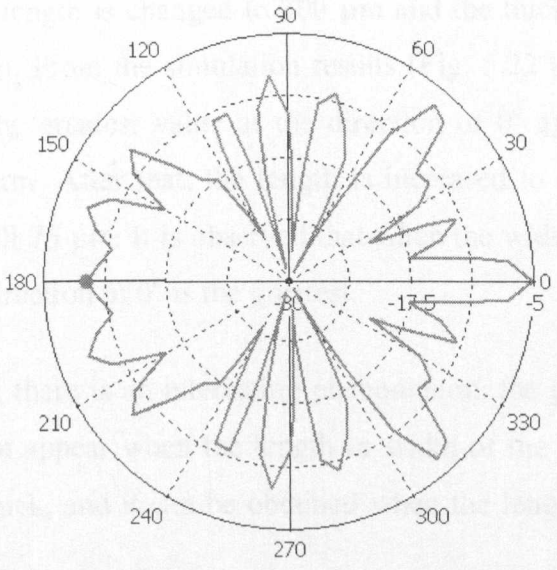

Fig.5.17 Radiation pattern of photoconductive dipole antenna with fixed length and width (1000×1000 μm) of substrate (thickness: 650 μm) in xoz plan (dB)

Therefore, it is easier to focus more power at a certain location by choosing a thin substrate if the length and the width of the substrate are fixed. However, by comparing Fig. 5.6 and Fig. 5.10 or Fig. 5.9 and Fig. 5.13, the radiation patterns are different with different lengths and widths of the substrate even if the thicknesses are the same. It means that the length and width of the substrate have effects on the radiation pattern. The next step is to investigate the effect of the length and the width of the substrate.

First, both the thickness and the length are set to be small values, 75 μm and 150 μm, respectively. When the width is changed from 150 μm to 600 μm, the simulation results are shown as from Fig. 5.18 to Fig. 5.21 When the width is 150 μm, the value on the direction of 0^{o} is the greatest.

Then, the length is changed to 300 μm and the thickness is kept the same as 75 μm. From the simulation results (Fig. 5.22 to Fig. 5.25), we can see that the greatest value at the direction of 0^{o} appears when the width is 300 μm. After that, the length is increased to 600 μm and the thickness is still 75 μm. It is observed that when the width is 600 μm, the value on the direction of 0^{o} is the greatest.

Therefore, there is an interesting phenomenon: the greatest value on z-axis does not appear when the length or width of the substrate is very thin or very thick, and it can be obtained when the length and width are the same.

To summarise the results above: if the power is expected to focus in one direction, the substrate should be square and the thickness should be very thin.

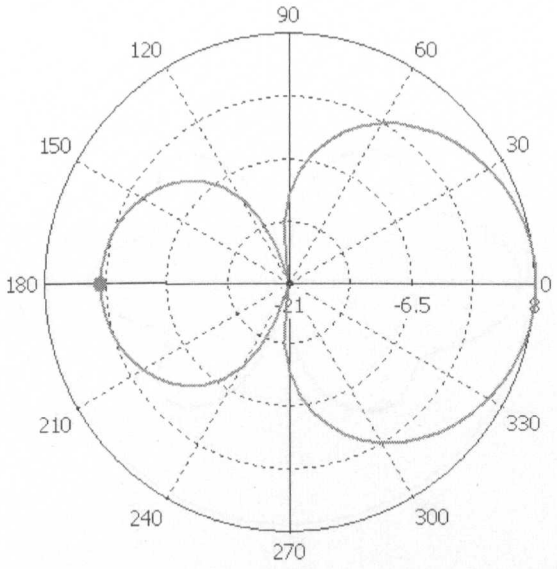

Fig.5.18 Radiation pattern of photoconductive dipole antenna with fixed length and thickness (150×75 μm) of substrate (width: 150 μm) in xoz plan (dB)

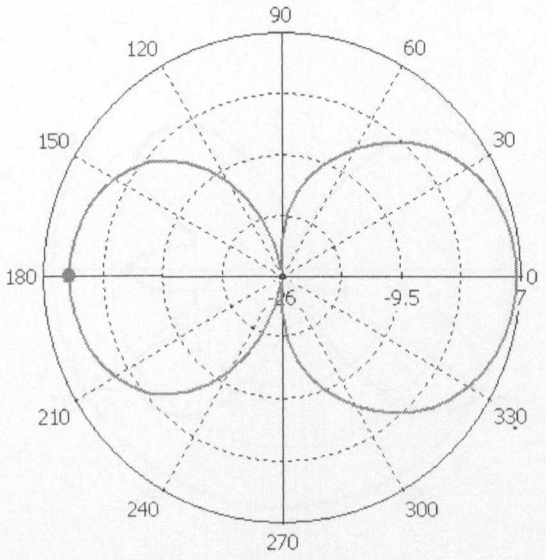

Fig.5.19 Radiation pattern of photoconductive dipole antenna with fixed length and thickness (150×75 μm) of substrate (width: 300 μm) in xoz plan (dB)

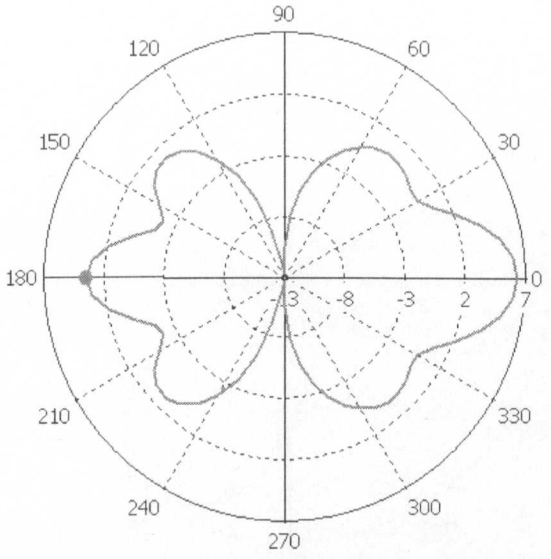

Fig.5.20 Radiation pattern of photoconductive dipole antenna with fixed length and thickness (150×75 μm) of substrate (width: 450 μm) in xoz plan (dB)

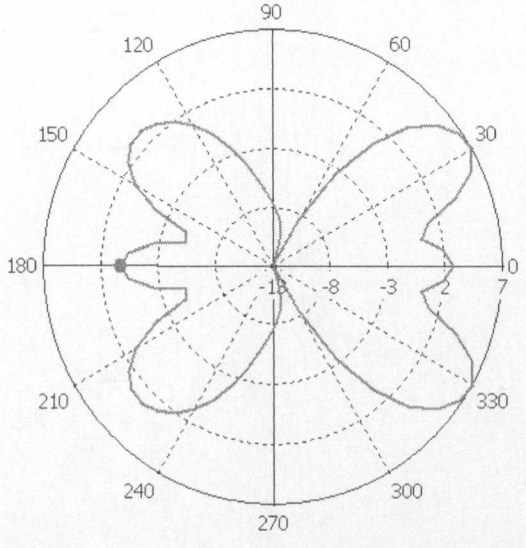

Fig.5.21 Radiation pattern of photoconductive dipole antenna with fixed length and thickness (150×75 μm) of substrate (width: 600 μm) in xoz plan (dB)

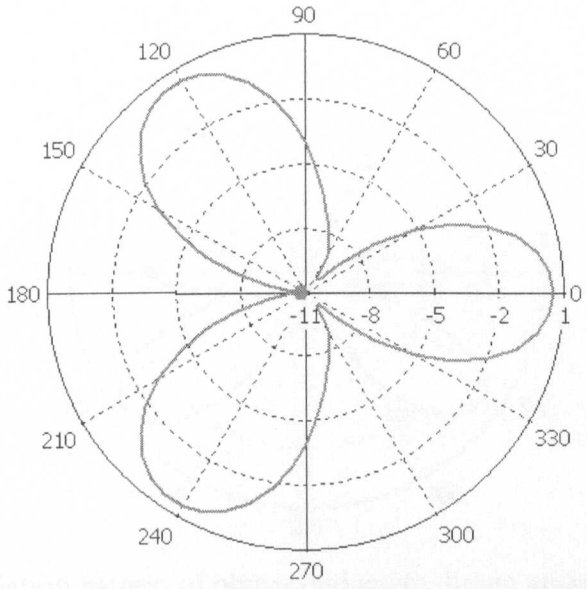

Fig.5.22 Radiation pattern of photoconductive dipole antenna with fixed length and thickness (300×75 μm) of substrate (width: 150 μm) in xoz plan (dB)

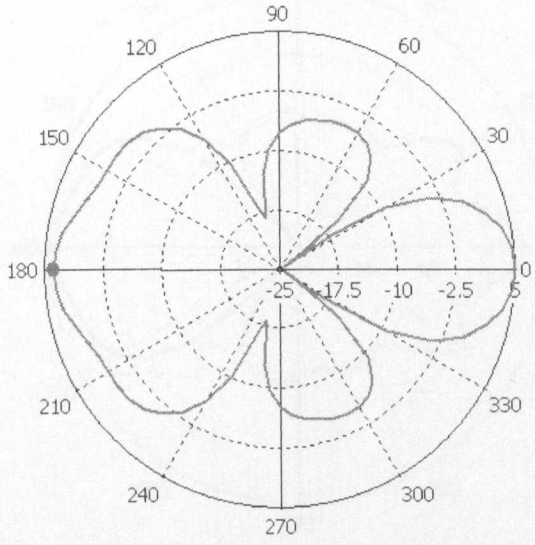

Fig.5.23 Radiation pattern of photoconductive dipole antenna with fixed length and thickness (300×75 μm) of substrate (width: 300 μm) in xoz plan (dB)

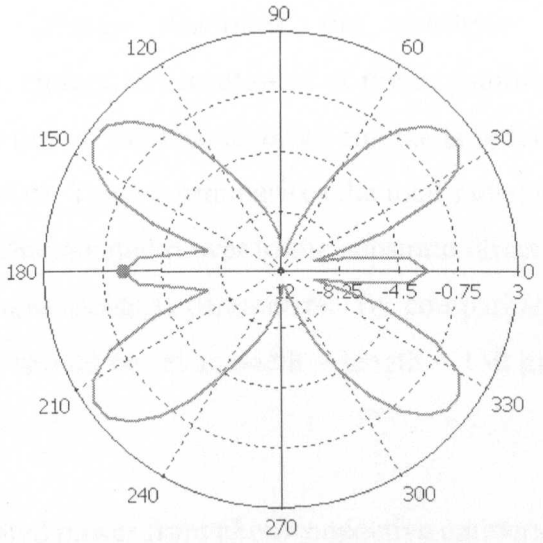

Fig.5.24 Radiation pattern of photoconductive dipole antenna with fixed length and thickness (300×75 μm) of substrate (width:450 μm) in xoz plan (dB)

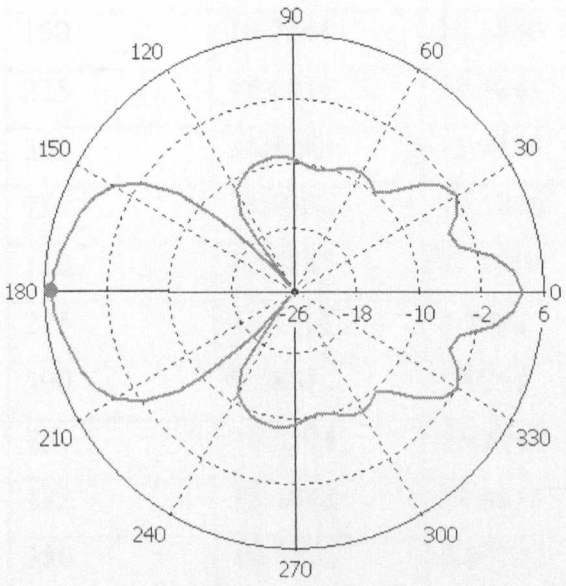

Fig.5.25 Radiation pattern of photoconductive dipole antenna with fixed length and thickness (300×75 μm) of substrate (width: 600 μm) in xoz plan (dB)

We have already discussed the substrate effect of the photoconductive emitter. As mentioned at the beginning of this section, the design objective of photoconductive emitter is radiating THz power as much as possible. Table 2 summarises the total radiated power (θ from 0° to 360°) and the radiated power to the substrate direction (θ from -90° to 90°) for different substrate parameters. By comparing all of them, the size of substrate should be set as width = length = 150 μm, and thickness = 75 μm.

Table 2. Radiated power from photoconductive emitters with different thicknesses of substrates

Length×width (μm× μm)	Thickeness (μm)	Total radiated power (dBm)	Radiated power to substrate direction (dBm)
150×150	75	20.8211	18.0087
	150	19.7164	16.1450
	225	15.6855	12.9245
	300	14.8265	11.9334
600×600	75	14.8226	12.5839
	150	13.7183	11.1119
	225	13.1511	9.7962
	300	9.1835	5.9250
1000×1000	75	19.5294	16.8344
	112	12.3648	11.4610
	350	10.5875	8.8071
	650	7.1283	4.2520

Table 3. Radiated power from the photoconductive emitter with different substrates of lengths and widths (thickness=75 μm)

Length (μm)	Width (μm)	Total radiated power (dBm)	Radiated power to substrate direction (dBm)
150	150	20.8211	18.0087
	300	19.2990	17.4054
	450	18.9662	16.7112
	600	19.7203	17.6291
300	150	15.6054	11.4472
	300	17.6079	13.9170
	450	16.4639	12.9825
	600	16.9306	11.6349

As discussed in last chapter, the antenna shape can affect the antenna performance. Among microwave antennas, a bow-tie is normally having a broader bandwidth than a dipole structure, and according to [117], the saturated power of bow-tie is larger than that of a dipole, which means the bow-tie shape can radiate more power than the dipole when the pumped laser is large enough.

For this design, we choose the same length of bow-tie as that of the dipole discussed above, and Fig. 5.26 shows the structure of the bow-tie photoconductive emitter.

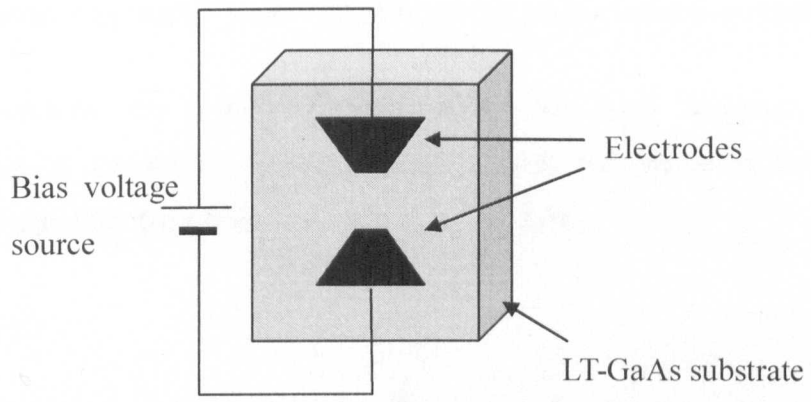

Fig. 5.26 Structure of bow-tie photoconductive emitter

The resonant frequency can be estimated as following. The resonant frequency of dipole antenna can be calculated by Equation (4.9) introduced in Chapter 4, and the bow-tie antenna is composed of dipole antennas whose directions change continuously from 0° to 45° rotation. The lower limit of the resonant frequency is happened when it is on 45° rotation and the equivalent effective length is about $50\sqrt{2} \approx 70\ \mu m$. Then the resonant frequency for 76 μm can be calculated by Equation (4.9), and the value is about 0.8 THz. Therefore, the resonant frequency of this bow-tie antenna should between 0.8 THz and 1 THz.

Some simulation results for bow-tie photoconductive emitter with different frequencies are shown from Fig. 5.27 to Fig. 5.31. Compared the value at 0^0 direction in each figure, it is obvious that they are much larger when the frequencies are 0.8 THz, 0.9 THz and 1.0 THz than those when the frequencies are 0.7 THz and 1.1 THz. It proves that the estimation of the resonant frequency is correct. Because the peak value

of the gain of the bow-tie antenna is comparable with that of dipole and it has broader bandwidth, it can be chosen as the photoconductive emitter.

Therefore, the photoconductive emitter has been designed. The substrate is chosen as 150μm×150μm×75μm, the shape is bow-tie structure and the parameters are shown in Fig. 5.36.

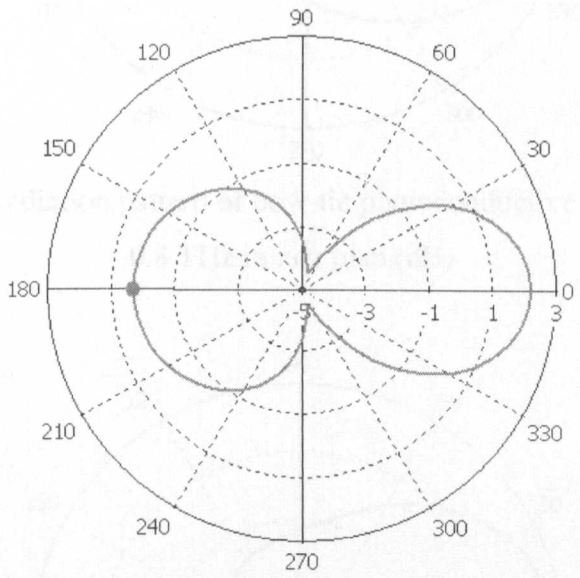

Fig.5.27 Radiation pattern of bow-tie photoconductive antenna at 0.7 THz in xoz plan (dB)

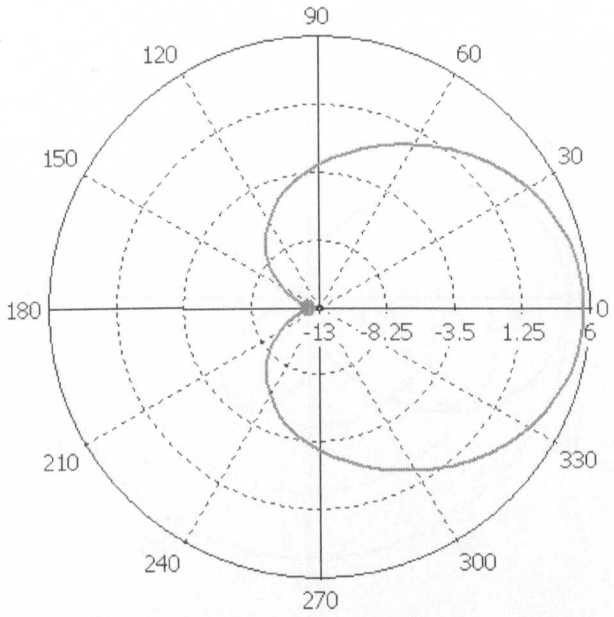

Fig.5.28 Radiation pattern of bow-tie photoconductive antenna at 0.8 THz in xoz plan (dB)

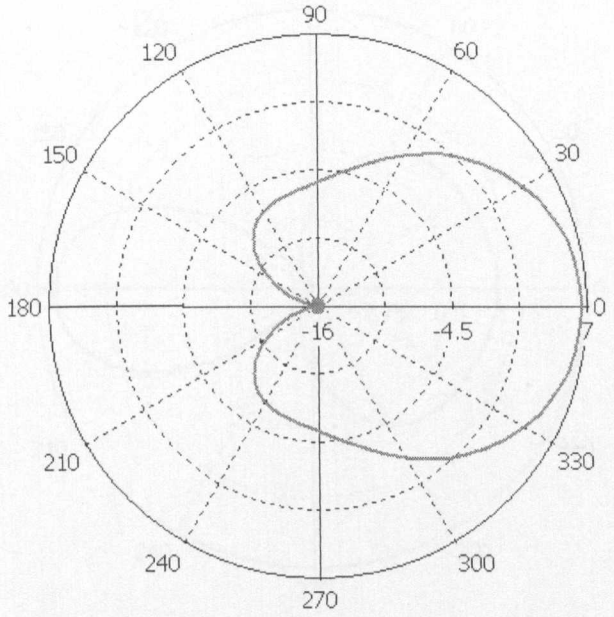

Fig.5.29 Radiation pattern of bow-tie photoconductive antenna at 0.9 THz in xoz plan (dB)

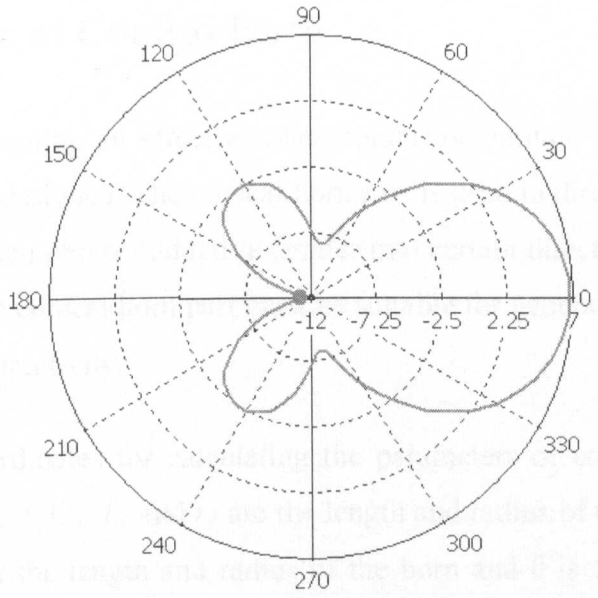

Fig.5.30 Radiation pattern of bow-tie photoconductive antenna at 1.0 THz in xoz plan (dB)

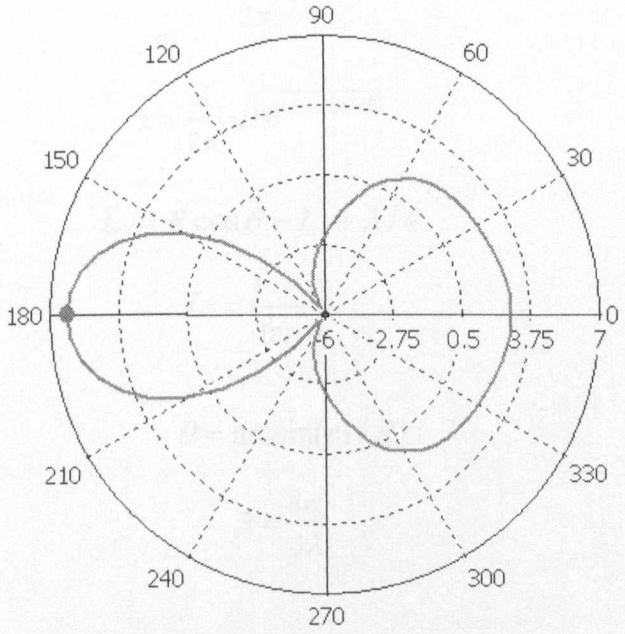

Fig.5.31 Radiation pattern of bow-tie photoconductive antenna at 1.1 THz in xoz plan (dB)

5.3 Design of Conical Horn

After designing an effective photoconductor emitter, a conical horn part must be designed. The conical horn part is used to direct the radiated THz wave from photoconductive emitter into certain directions, so all the parameters of conical horn part must be suitable for generating THz wave with a high directivity.

The co-ordinates for calculating the parameters of conical horn are shown in Fig. 5.32. L_1 and r_1 are the length and radius of the waveguide, L_2 and r_2 are the length and radius of the horn and θ is the flare angle. According to antenna theory, to design a conical horn antenna with high gain, the parameters can be estimated by the following equations [123].

$$r_1 = \frac{3\lambda}{2\pi} \tag{5.3}$$

$$r_2 = \frac{\lambda}{2\pi}\sqrt{10^{(D+2.91)/10}} \tag{5.4}$$

$$L_1 = R\cos\theta - L_2 + \lambda/4 \tag{5.5}$$

$$L_2 = \frac{r_2 - r_1}{\tan\theta} \tag{5.6}$$

$$\theta = \arcsin(r_2/R) \tag{5.7}$$

$$R = \frac{4r_2^2}{3\lambda} \tag{5.8}$$

With the help of the simulation software, the values for them can be obtained and all the key parameters will be shown later.

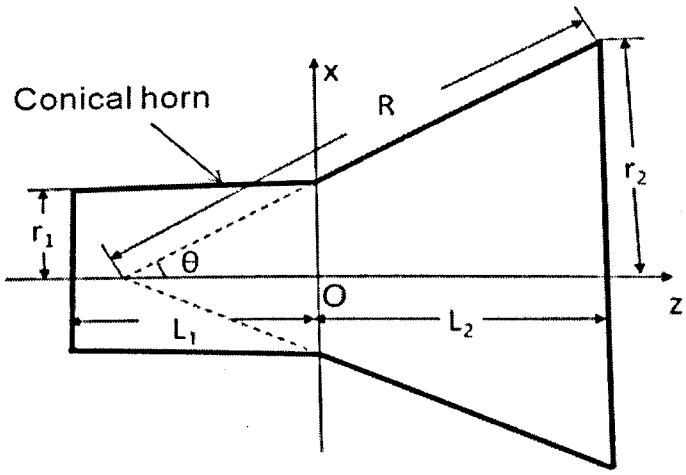

Fig. 5.32 Coordinate of horn part calculation

Then, the photoconductive emitter is added into this horn. The radiated electric fields of both photoconductive emitter and conical horn should be taken into account.

The radiated electric field from photoconductive emitter is similar as discussed in Chapter 4. It can be calculated by

$$E(r,t) = \frac{l_e}{4\pi\varepsilon_0 c^2 r} \cdot \frac{\partial J(t)}{\partial t} \cdot sin\theta \qquad (5.9)$$

which is the same as Equation (4.8).

To simplify the calculation model, the coordinates for conical horn antenna can be set as shown in Fig.5.33. *P* is the observation point which is far from the antenna. The electric field on *P* can be calculated by the following formulas [124].

$$E_p = f(R)\hat{R} \times \oint_s \{[\sqrt{\frac{\mu}{\varepsilon}}\hat{R} \times (\hat{n} \times H_{ts}) - \hat{n} \times E_{ts}]\exp(jkr'\hat{R})\}ds \tag{5.10}$$

$$f(R) = jk/4\pi \exp(-jkR)/R \tag{5.11}$$

where μ and ε is the permittivity and permeability, respectively. To transfer the generated THz wave from the photoconductive emitter effectively into conical horn part, the length of the conical horn antenna is set to 3λ, where λ is the wavelength of the operation frequency. In THz range, the wavelength of 300 μm is selected, so the total length of the conical horn antenna L is 900μm. According to the waveguide theory and the conventional horn antenna design theory [123, 125, and 126], the diameter of the waveguide and the aperture of the horn can be approximated. Then, with the help of the simulation software, the diameter of the waveguide is set to be 980.4 μm and the aperture of the horn is set to be 1800 μm.

After calculating the parameters of the photoconductive emitter part and the conical horn part, the whole THz photoconductive conical horn antenna is designed. To test the theory, some simulations have been carried out for this design.

First, only the horn part is considered (no back wall was added to the waveguide). The simulation result is shown in Fig. 5.34. It proves the horn can radiate THz wave with high directivity. The peak directivity is 14.9 dBi in the 0^o direction.

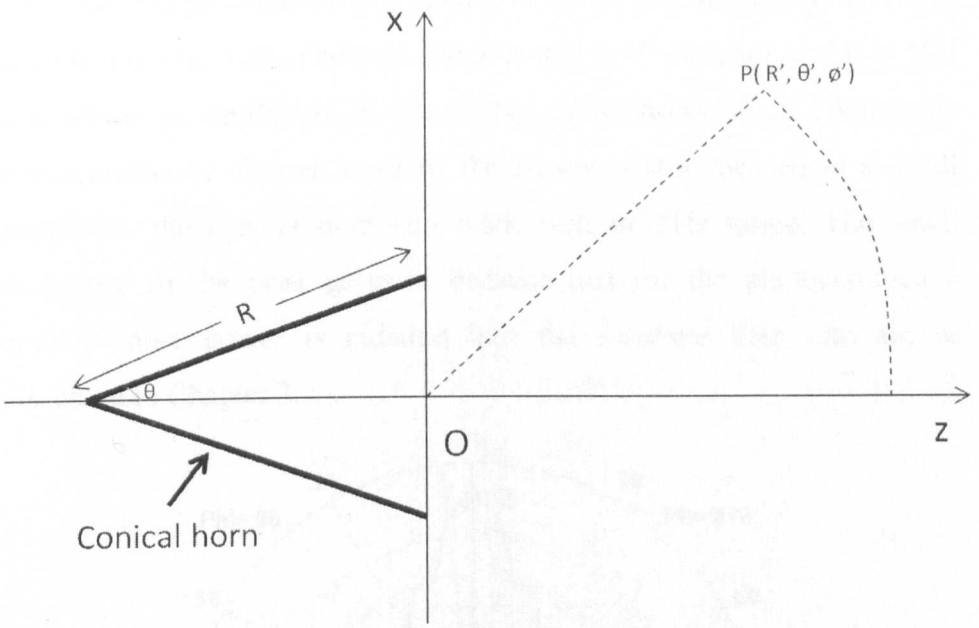

Fig.5.33 The radiated electric field calculation coordinates of conical horn antenna

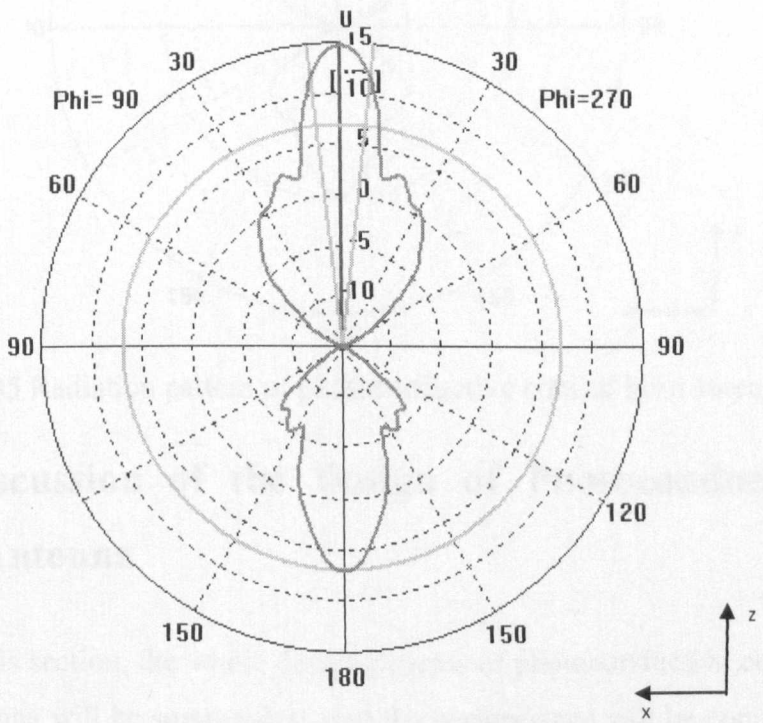

Fig.5.34. Radiation pattern of conical horn part

Then the photoconductive emitter is added and the simulation result is shown in Fig. 5.35. The peak value is still at 0^{o} direction and it is 15.1 dBi which is similar as in Fig. 5.34, so it shows when adding the photoconductive emitter, most of the power is still focused in a small angle, *i.e.* the conical horn can work well in THz range. The small difference of the peak gains is because that for the photoconductive emitter, more power is radiated into the substrate than into air, as discussed in Chapter 3.

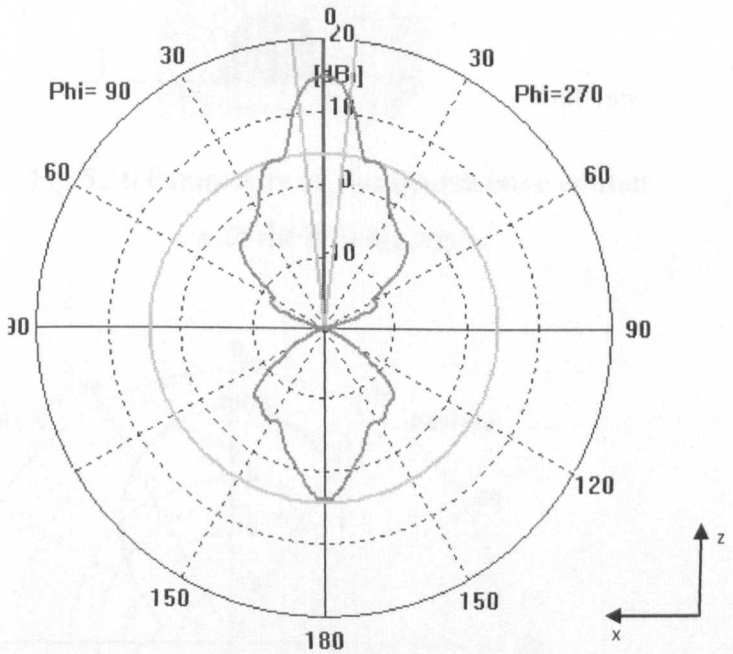

Fig. 5.35 Radiation pattern of photoconductive conical horn antenna

5.4 Discussion of the Design of Photoconductive Horn Antenna

In this section, the whole design process of photoconductive conical horn antenna will be summarised, and the performance will be compared with the conventional photoconductive antenna.

First, the parameters of the photoconductive emitter and the radiation pattern in xoz plan in dB scale are shown in Fig. 5.36 and Fig. 5.37. The result indicates that the peak directivity of the conventional photoconductive antenna structure is about 6.7 dBi.

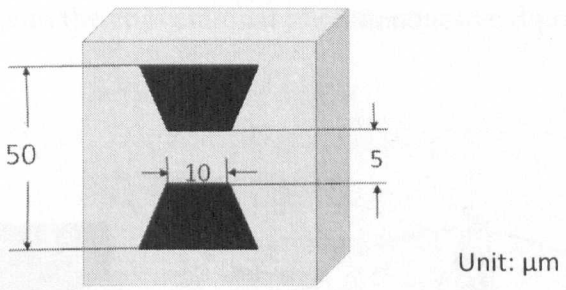

Fig.5.36 Parameters of photoconductive emitter with the bow-tie shape

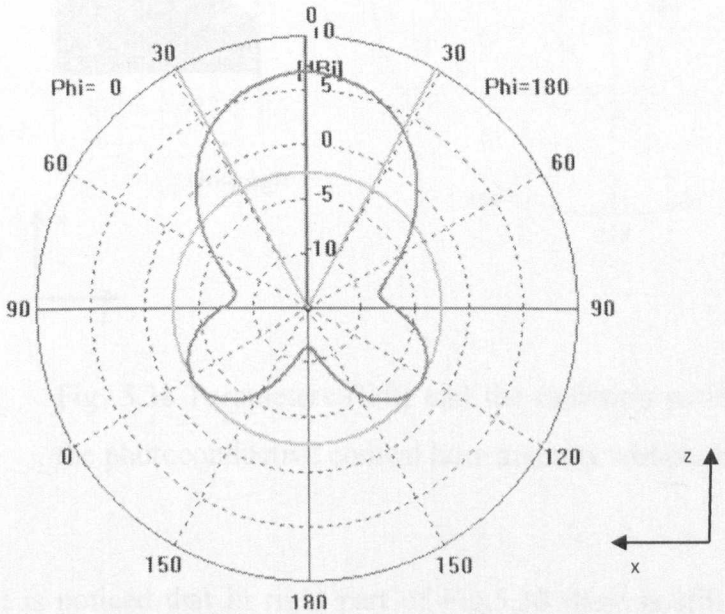

Fig.5.37 Radiation pattern of photoconductive emitter with the bow-tie shape

Then, a conical horn part is added into this design. The parameters are the same as discussed in last section (left part of Fig. 5.38). The simulation result, shown in right part of Fig. 5.38, illustrates the peak directivity of the conical horn is about 15.1 dBi. It proves the design of the conical horn indeed increases the directivity of the radiated wave much compared with the conventional photoconductive dipole antenna.

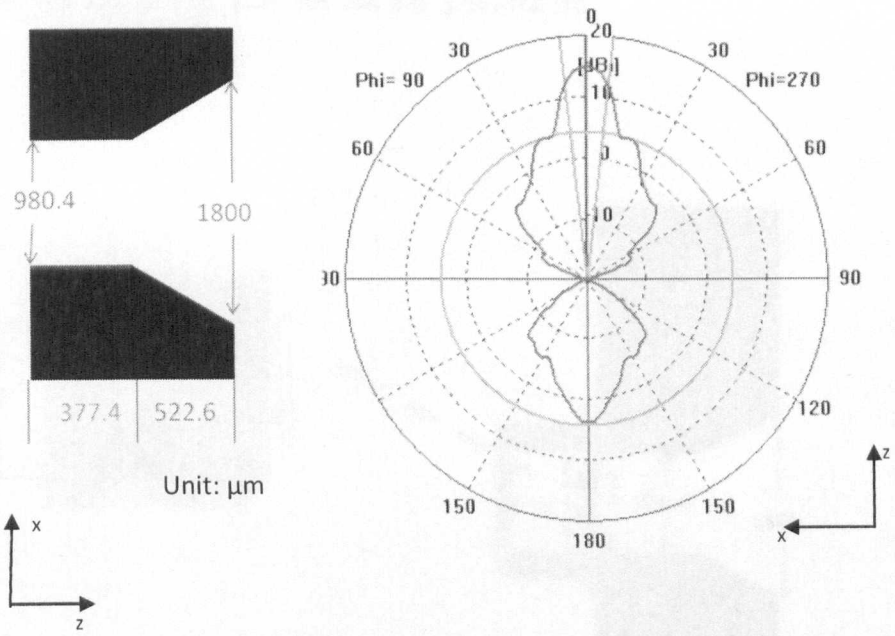

Fig. 5.38 Parameters (left) and the radiation pattern (right) of the photoconductive conical horn antenna without back wall

It is noticed that in right part of Fig.5.38 there is still some power radiated into the opposite direction of the expected direction (0^{o}-direction). Then, a back wall made of ITO is added to reflect this part of

the power to the expected direction. ITO is a material which can reflect THz power and let laser power go through. Here introduced another parameter: the distance between the back wall and the photoconductive emitter. From the conventional horn antenna design theories, the distance should be a quarter of a wavelength. With the help of the simulation software, it is found that it is still suitable for the THz range. Thus, the distance is set to be 75 μm for 1 THz. Therefore, the completed design of the photoconductive conical horn antenna is presented as in Fig. 5.2 for the materials and in Fig. 5.39 for the key parameters.

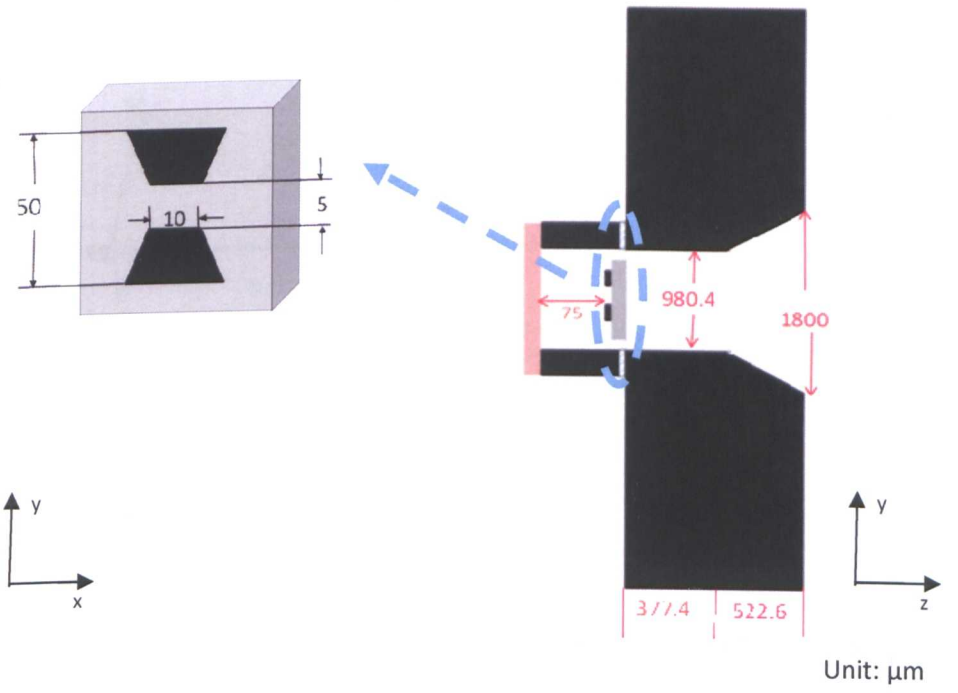

Fig.5.39 Parameters of photoconductive conical horn antenna

Due to the limitation of the software, we cannot choose ITO as the material for simulation, but since it has similar properties as metal in THz range, we also use metal as the back wall in the simulation. Fig. 5.40 is the simulation result about this completed design of photoconductive conical horn antenna. The peak value of the directivity is about 18.7 dBi which is greater than the design without the back wall. It means the back wall makes the further improvement for the directivity of the radiated wave. The HPBW of this design is only about 16°, which means most of the power is focused in a small area.

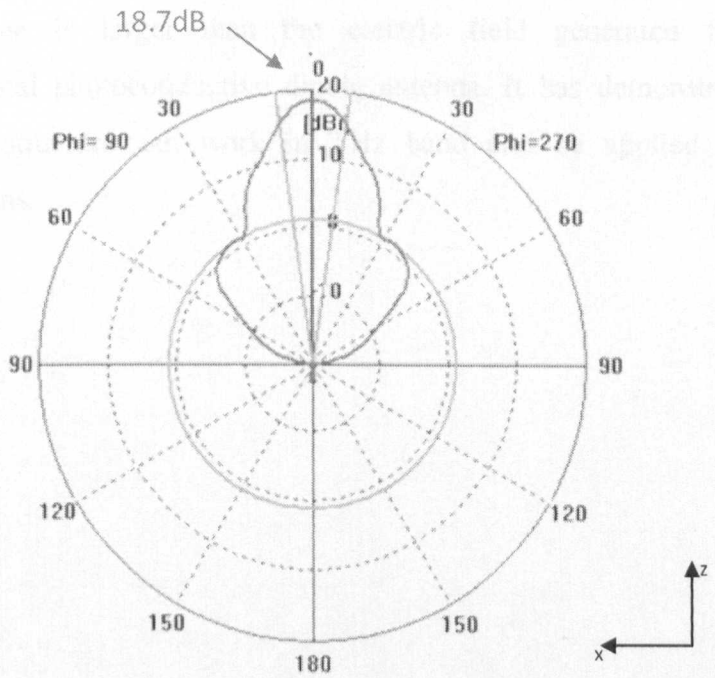

Fig.5.40 Radiation pattern of photoconductive conical horn antenna

5.5 Summary

In this Chapter, a THz conical horn antenna which can generate the THz wave more effectively has been presented. This new type of antenna consists of a conical horn structure and a photoconductive emitter which are nicely integrated, and this structure leads to directional emission of THz wave which can increase the radiated power in certain directions. Although not all THz application cares about the radiation pattern, this kind of analysis is also useful to predict the total radiated power. According to the analysis, the radiated electric field is simulated and the peak value is larger than the electric field generated from the conventional photoconductive dipole antenna. It has demonstrated that the new structure can work in THz band and be applied to many applications.

CHAPTER 6
CONCLUSIONS
AND FUTURE WORK

6.1 Conclusions

THz technology is a relatively new area for researchers. Although it has a lot of benefits as mentioned in Chapter 1, there are at the moment limited applications due to the lack of high power THz source with low cost. The focus of this research has been on how to design an efficient photoconductive antenna which is currently the most popular device used to generate and detect THz wave in practice.

Photoconductive antenna consists of an antenna structure fabricated on a semiconductor substrate which has a short carrier lifetime and high mobility. The theory behind it is the photoconductive effect which was introduced in Chapter 2. It utilises the photo-induced current to generate THz waves. This mechanism makes the photoconductive antenna different from the conventional RF/microwave antennas. The whole THz generation and detection system was presented in Chapter 3, and key parameters of the photoconductive antenna were also introduced.

In Chapter 4, the calculation model was developed and four methods which can improve the radiation efficiency were discussed. According to the analysis of this thesis, a theoretical calculation model was presented

and the radiation properties of photoconductive antennas can be obtained from this model. It revealed that the gap size of the antenna, the laser source and the electric field produced by the bias voltage can affect the performance of the photoconductive antennas. Therefore, to improve the efficiency of the photoconductive antennas, some methods can be considered.

The first method is about how to optimise the gap size within the antenna. It is easy to understand that increasing the gap size can produce more electron-hole pairs which may lead to more radiated THz power, but if the input laser power is a constant, increasing gap size will reduce the laser intensity which will decrease the radiated THz power. Therefore, the best value of the gap size should not be too large or too small. It has been found that this parameter should be determined by the ratio of the incident laser power and the substrate material.

The second method is how to use the laser beam to optimise the radiation efficiency. The conventional method is using the laser beam to cover the whole gap of the antenna, and if the incident laser beam is focused on a small part of the gap, the amplitude of the radiated electric field can be increased because it leads to a stronger photo-induced current. Therefore, compared with excitation on the whole gap area, the laser beam should be focused on a small part of the antenna gap, which can increase the generated THz power.

The third method is choosing the suitable bias voltage. It is obvious that increasing the bias voltage is a simple way to enhance the bias electric field which leads to stronger THz radiation but if it is beyond the

breakdown voltage of the substrate, the antenna will be damaged. Therefore, the bias voltage should be set as large as possible but smaller than the breakdown voltage to produce the highest possible radiated THz power.

The fourth approach is about how to design the ends of the dipole, and it is also a method to enhance the bias electric field. It was found that the electric field from the indentation shape of the dipole is greater than that from the conventional dipole shape. Therefore, when the indentations are added at the end of the dipole, the bias electric field is enhanced, and it leads to more radiated THz power.

All these four methods are proved by both theoretical analysis and simulation results and they are useful for designing effective photoconductive antennas.

Conventional photoconductive antennas are omni-directional antennas, which are not suitable for all applications. The current approach to make the radiated wave directional is by adding a Si hemispherical lens on the substrate of photoconductive antennas, but this method has some disadvantages, for example, it is very difficult to adjust the focal point of the lens on the centre of the dipole antenna, and some power will be reflected back to the substrate on the interface of the Si lens and air. The details were discussed in Chapter 3.

To avoid the problems of the lens coupled photoconductive antenna, a novel photoconductive conical horn antenna was introduced and simulated in Chapter 5. This new antenna consists of a photoconductive emitter and a conical horn. It has been shown that, to obtain more power

in the expected direction, the thickness of the substrate should be very thin, and the length and the width should be equal. It has also been demonstrated that the bow-tie shape can provide broader bandwidth than the dipole shape for electrode. The carefully designed horn antenna was simulated and the results show that the photoconductive conical horn has a much higher directivity than the conventional photoconductive dipole antenna.

6.2 Future Work

THz technologies include many areas such as electronics, optics and materials, so there are a lot of interesting topics needed to be investigated. Even if only about the technology of photoconductive antennas there are a lot of topics, which I have not had time to study properly, can be further investigated.

First, although some methods of improving the radiated power from photoconductive antennas have been provided in this thesis, the efficiency of photoconductive antenna is still very low compare with the microwave antennas. Therefore, more factors should be taken into account and the efficiency can be further increased. As mentioned in Chapter 3, the impedance of antenna structure and the impedance of the source are mismatched, and it makes the low efficiency of the photoconductive antenna from antenna point of view. Thus, there are two possible further investigations: one is working out the impedance of the source and another is design a new type of antenna structure to match this source impedance.

Another research subject is, once the complete photoconductive conical horn antenna is made, measurements should be conducted to validate the theory discussed in this thesis. We have already obtained the conical horn part, as shown in Fig. 6.1, and once the photoconductive emitter is produced, the experiment can be done and a new type of photoconductive antenna is produced. Then this antenna will be installed in a THz experiment system as shown in Fig. 3.5 and test if it has the same performance as the prediction in this thesis. Further step is looking for some other antenna designs which have better performances.

In conclusion, THz technology is of great potential for many applications but is still in its early stage. A lot of work is to be undertaken, especially the development of high power THz sources, before its application becomes a common place.

Fig.6.1 Product of conical horn (left) and size comparison (right)

References

[1] R. Miles, P. Harrison and D. Lippens, "Terahertz sources and systems", Kluwer Academic Pub, 2001.

[2] D. Mittleman, "Sensing with terahertz radiation", Springer Pub, 2003.

[3] J. Dickinson, T. Goyette, A. Gatesman, C. Joseph, Z. Root, R. Giles, J. Waldman, and W. Nixon, "Terahertz imaging of subjects with concealed weapons", Terahertz for Military and Security Applications IV, Proceedings of the SPIE, Vol. 6212, 2006.

[4] M. Nagel, H. Brucherseifer, and M. Kurz, "Integrated THz technology for label-free genetic diagnostics", Appl. Phy. Lett., vol. 80, 2002.

[5] Z. Jiang and X. Zhang, "Terahertz imaging via electrooptic effect", IEEE Transactions on Microwave Theory and Techniques no. 12, pp. 2644, Dec. 2002.

[6] N. Kukutsu and Y. Kado, "Overview of millimeter and terahertz wave application research", NTT technical Review, vol. 7, Mar. 2009.

[7] K. Huang and D. Edwards, "Millimeter wave antennas for gigabit wireless communications", Wiley, 2008.

[8] D. Auston, "Picosecond optoelectronic switching and gating in silicon", Appl. Phy. Lett., vol.26, 1975.

[9] D. Auston, A. Johnson, P. Smith and J. Bean, "Picosecond optoelectronic detection, sampling, and correlation measurements in amorphous semiconductors", Appl. Phy. Lett., vol 37, 1980.

[10] P. Smith, D. Auston, A. Johnson and W. Augustyniak, "Picosecond photoconductivity in radiation-damaged silicon-on-sapphire films", Appl. Phys. Lett., vol. 38, pp. 47, 1981.

[11] G. Mourou, C. V. Stancampiano, A. Antonetti, and A. Orszag, "Picosecond microwave pulses generated with a subpicosecond laser-driven semiconductor switch", Appl. Phys. Lett., vol. 39, pp. 295, 1981.

[12] R. Heidemann, T. Pfeiffer and D. Jager "Optoelectronically pulsed slot-line antennas", Electron. Lett., vol. 19, pp. 316, 1983.

[13] D. Auston, K. Cheung and P. Smith, "Picosecond photoconducting Hertzian dipoles", Appl. Phys. Lett., vol. 45, pp. 284, 1984.

[14] P. Smith, D. Auston and M. Nuss, "Subpicosecond photoconducting dipole antennas", IEEE J. Quantum Electron, vol. 24, pp. 255, 1988.

[15] M. van Exter, Ch. Fattinger and D. Grischkowsky, "High-brightness terahertz beams characterized with an ultrafast detector", Appl. Phys. Lett., vol 55, pp. 337, 1989.

[16] F. Smith, A. Calawa, C.-L. Chen, M. Manfra and L. Mahoney, "New MBE buffer used to eliminate backgating in GaAs MESFETs", IEEE Electron Device Lett., vol. 9, pp. 77, 1988.

[17] D. Spence, P. Kean and W. Sibbett, "60-fsec pulse generation from a self-mode-locked Ti:sapphire laser", Opt. Lett., vol. 16, pp. 42, 1991.

[18] T. Kamiya and M. Tsuchiya, "Progress in ultrafast photonics", Japanese Journal of Applied Physics, vol. 44, no. 8, pp. 5875, 2005.

[19] X.-C. Zhang, B. Hu, J. Darrow and D. Auston, "Generation of femtosecond electromagnetic pulses from semiconductor surfaces", Appl. Phys. Lett., vol. 56, pp. 1011, 1990.

[20] X.-C. Zhang and D. Auston, "Optoelectronic measurement of semiconductor surfaces and interfaces with femtosecond optics", J. Appl. Phys., vol. 71, pp. 326, 1992.

[21] B. Hu, X. Zhang, and D. Auston, "Temperature dependence of femtosecond electromagnetic radiation from semiconductor surfaces", Appl. Phys. Lett., vol. 57, pp. 2629, 1990.

[22] K. Leo, J. Shah, E. Gobel, T. Damen, S. Schmitt-Rink and W. Schafer, "Coherent oscillations of a wave packet in a semiconductor double-quantum-well structure" , Phys. Rev. Lett., vol. 66, pp. 201, 1991.

[23] P. Planken, M. Nuss, I. Brener, K. Goossen, M. Luo, S. Chuang and L. Pfeiffer, "Terahertz emission in single quantum wells after coherent

optical excitation of light hole and heavy hole excitons", Phys. Rev. Lett., vol. 69, pp. 3800, 1992.

[24] C.Waschke, H. Roskos, R. Schwedler, K. Leo, H. Kurz and K. K¨ohler, "Coherent submillimeter-wave emission from Bloch oscillations in a semiconductor superlattice", Phys. Rev. Lett., vol. 70, pp. 3319, 1993.

[25] M. Hangyo, S. Tomozawa, Y. Murakami, M. Tonouchi, M. Tani, Z. Wang, K. Sakai and S. Nakashima, "Terahertz radiation from superconducting $YBa_2Cu_3O_{7-\delta}$ thin films excited by femtosecond optical pulses", Appl. Phys. Lett., vol. 69, pp. 2122, 1996.

[26] M. Tonouchi, M. Tani, Z. Wang, K. Sakai, N. Wada and M. Hangyo, "Novel terahertz radiation from Flux-Trapped $YBa_2Cu_3O_{7-\delta}$ thin films excited by femtosecond laser pulses", Jpn. J. Appl. Phys., vol. 36, Pt.2, 1997.

[27] S. Gearhart, C. Ling, G. Rebeiz, H. Davee and G. Chin, "Integrated 119-μm linear corner-cube array", IEEE Microwave and Guided Wave Letters, vol. 1, pp. 155, 1991.

[28] G. Rebeiz, L. Katehi, W. Ali-Ahmad, G. Eleftheriadws and C. Ling, "Integrated horn antennas for millimeter-wave applications", IEEE Antenna and Propagation Magazine, vol. 34, pp. 7, 1992.

[29] J. Pedersen, V. Lyssenko, J. Hvam, P. Jepsen, S. Keiding, C. Sorensen and P. Lindelof, "Ultrafast local field dynamics in photoconductive THz antennas", Appl. Phys. Lett., vol. 62, pp. 1265, 1993.

[30] P. Jepsen and S. Keiding, "Radiation patterns from lens-coupled terahertz antennas", Opt. Lett., vol. 20, pp. 807, 1995.

[31] C. Ludwig and J. Kuhl, "Studies of the temporal and spectral shape of terahertz pulses generated from photoconducting switches", Appl. Phys. Lett., vol. 69, pp. 1194, 1996.

[32] Y. Cai, I. Brener, J. Lopata, J. Wynn, L. Pfeiffer and J. Federici, "Design and performance of singular electric field terahertz photoconducting antennas", Appl. Phys. Lett., vol. 71, pp. 2076, 1997.

[33] P. Goldsmith, "Quasioptical systems", IEEE Press, 1998.

[34] J. Rudd, J. Johnson and D. Mittleman, "Quadrupole radiation from terahertz dipole antennas", Opt. Lett., vol. 25, pp. 1556, 2000.

[35] R. Dean, P. Nordin and C. Christodoulou, "3-D helical thz antennas", Microwave and Optical technology Letters, vol.24, no. 2, Jan, 2000.

[36] P. Burke, "Carbon nanotube devices for Ghz to Thz applications", Proceedings of SPIE 5593, pp.52, 2004.

[37] R. Mendis, C. Sydlo, J. Sigmund, M. Foeignov and H. L. Hartnagel, "Spectral characterisation of broadband THz antennas by photoconductive mixting: toward optimal antenna design", IEEE Antennas and Propagation Letters, vol. 4, pp. 85, 2005.

[38] J. Deibel, M. Escarra and D. Mittleman, "Photoconductive terahertz antenna with radial symmetry", Quantum Electronics and Laser Science Conference (QELS), pp. 1239, 2005.

[39] M. Tani, Y. Hirota, C. Que, S. Tanaka, R. Hattori, M. Yamaguchi, S. Nishizawa and M. Hangyo, "Novel THz photoconductive antennas ," International Journal of Infrared and Millimeter Waves, vol 27, no 4, pp. 531, Apr. 2006.

[40] K. Moon, H. Han and I. Park, "THz folded half-wavelength dipole antenna for high output power", Infrared Millimeter Waves and 14th Conf. on THz electronics, IRMMW-THz, 2006.

[41] E. Peytavit, J-F. Lampin, T. Akalin and L. Desplanque, "Integrated terahertz TEM horn antenna", Electronics Letters, vol. 43, No. 2, Jan. 2007.

[42] M. Rodwell, D. Bloom and B. Auld, "Nonlinear transmission line for picosecond pulse compression and broadband phase modulation", Electron. Lett., vol. 23, no. 109, 1987.

[43] P. Siegel, "Terahertz technology", IEEE Transactions on Microwave Theory and Techniques, no. 3, pp. 910, Mar. 2002.

[44] Y. Lan, B. Zeng, H. Zhang, B. Chen and Z. Yang, "Simulation of

carbon nanotube Thz antenna array", International Journal of Infrared and Millimeter Waves, 27(6), pp. 871–877, 2006.

[45] K. Ezdi, "Terahertz sources and systems: a brief overview", International Students and Young Scientists Workshop, 2004.

[46] Y. Huang and D. Li, "Invited paper on THz antennas", China-UK/Europe Workshop on Millimetre Waves and Terahertz Technologies,China, Chengdu:IET, pp. 5, 2008.

[47] Chau, R. Doyle, B. Kavalieros, J. Barlage, D. Murthy, A. Doczy, M. Arghavani and R. Datta, "Advanced depleted-substrate transistors: Single-gate, double-gate and tri-gate", International Conference on Solid State Devices and Materials, pp. 68–69, Nagoya, Japan, 2002,.

[48] TeraView Ltd., http://www.teraview.com, 2009.

[49] Picometrix Inc., http://picometrix.com, 2009.

[50] J. Chamberlain, R. Miles, C. Collins and D. Steenson, "New directions in terahertz technology", ed. J M Chamberlain and R E Miles (NATO ASI Series, Kluwer), 1997.

[51] D. Li and Y. Huang, "A quantitative comparison of terahertz antennas", The 12th Annual Conference of Chinese Automation and Computing Society in the UK, Sep. 2006.

[52] K. Sakai, "Terahertz optoelectronics", Springer Pub, 2005.

[53] G. Mourou, C. Stancampiano, A. Antonetti and A. Orszag, "Picosecond microwave pulses generated with a subpicosecond laser-driven semiconductor switch", Appl. Phy. Lett., vol. 39, 1981.

[54] K. Tsen, "Ultrafast dynamical processes in semiconductors", Springer Pub, 2004.

[55] Q. Chang, D. Yang and L. Wang, "Broadband THz generation from photoconductive antenna", Progress In Electromagnetic Research Symposium, 2005.

[56] Z. Piao, T. Masahiko and S. Kiyomi, "Carrier dynamics and terahertz

radiation in photoconductive antennas", J. Applied Physics, vol. 39, pp. 96, 2000.

[57] C. Sydlo, J. Sigmund, H. Hartnagel, R. Mendis, M. Feiginov and P. Meissner, "Planar THz antenna optimisation", IEEE/ACES Conf. on Wireless Comm. and Applied Comp. EM, 2005.

[58] R. Heidemann, T. H. Pfeiffer and D. Jager, "Optoelectronically pulsed slot-line antennas," Electron. Lett.,vol. 19, pp. 316, Apr. 28, 1983.

[59] R. Mendis, C. Sydlo, J. Sigmund, M. Foeignov and H. L. Hartnagel, "Spectral characterisation of broadband THz antennas by photoconductive mixting: toward optimal antenna design", IEEE Antennas and Propagation Letters, vol. 4, pp. 85, 2005.

[60] G. Rebeiz, "Millimeter-wave and terahertz integrated circuit antennas", Proceedings of IEEE, vol. 80, pp. 1748, Nov. 1992.

[61] P. Jepsen and S. Keiding, "Radiation patterns from lens-coupled terahertz antennas", Optics Letters, vol. 20, no. 8, Apr. 1995.

[62] S. Park, M. Melloch and A. Weiner, "Comparison of terahertz waveforms measured by electro-optic and photoconductive sampling", Appl. Phy. Lett., vol. 73, pp. 3184, Nov. 1998.

[63] C. Winnewisser, P. Jepsen, M. Schall, V. Schyja and H. Helm, "Electro-optic detection of THz radiation in $LiTaO_3$, $LiNbO_3$ and ZnTe", Appl. Phy.Lett., vol. 70, pp. 3059, 1997.

[64] P. Han and X. Zhang, "Coherent, broadband midinfrared terahertz beam sensors", App. Phy. Lett., vol. 73, pp. 3049, 1998.

[65] M. Dragoman and D. Dragoman, "An overview of nonlinear microwave and millimeter wave generation in magnetic, acoustic and electromagnetic distributed nonlinear physical systems", Nonlinear Microwave Signal Processing: Towards a New range of Devices, R. Marcelli, S. Nikitov (Eds.), NATO ASI Series, Vol. 20, pp. 13, 1996.

[66] Y. Lan, B. Zeng, H. Zhang, B. Chen and Z. Yang, "Simulation of carbon nanotube Thz antenna array", International Journal of Infrared and Millimeter Waves, vol. 27(6), pp. 871, 2006.

[67] G. Hanson, "Fundamental transmitting properties of carbon nanotube antennas", IEEE Transactions on Antennas and Propagation, vol. 53, pp. 3426, 2005.

[68] P. J. Burke, S. Li and Z. Yu, "Quantitative theory of nanowire and nanotube antenna performance", IEEE Transactions on Nanotechnology, vol. 5, pp. 314, 2006.

[69] C. Ling, J. Landdry, H. Davee, G. Chin and G. Rebeiz, "Large area bolometers for THz power measurements", IEEE transactions on microwave theory and techniques, vol. 42, pp. 758, 1994.

[70] D. Dragoman and M. Dragoman, "Terahertz field characterization using Fabry–Perot-like cantilevers", Appl. Phy. Lett., vol. 79, pp. 581, 2001.

[71] M. Tani, K. Sakai, H. Abe, S. Nakada, H. Harima, M. Hangyo, Y. Tokuda, K. Kanamoto, Y. Abe and N. Tsukada, "Spectroscopic characterization of low-temperature grown GaAs epitaxial films", Jpn, J. Appl.Phy., vol. 33, pp. 4807, 1994.

[72] H. Abe, M. Tani, K. Sakai and S. Nakashima "Spectral response of THz detectors made on LT-GaAs grown at different temperatures", Conference on Lasers and Electro-Optics, 1998.

[73] M. Tani, S. Matsuura, K. Sakai and S. Nakashima, "Emission characteristics of photoconductive antennas based on low-temperature-grown GaAs and semi-insulating GaAs", Applied Optics, vol. 36, 1997.

[74] G. Rodrigrez and A. Taylor, "Screening of the Bias Field in Terahertz Generation from Photoconductors", Optics Letters, vol. 21, no. 14, Jul. 1996.

[75] R. Keyes, "Optical and infrared detectors", Springer Pub., 1977.

[76] L. Duvillaret, F.-F. Garet, J.-F. Roux and J.-L. Coutaz: IEEE J. Sel. Top. Quantum Electron., vol. 7, no. 615, 2001.

[77] D. Rutledge, D. Neikirk and D. Kasilingam, "Integrated circuit antennas", Infrared and MillimeterWaves, vol. 10, Academic Press, New York, 1983.

[78] B. Hu, J. Darrow, X.-C. Zhang, D. Auston and P. Smith, "Optically steerable photoconducting antennas", Appl. Phys. Lett., vol. 56, no. 886, 1990.

[79] C. Balanis, "Modern antenna handbook", Wiley, 2008.

[80] L. Xu, X.-C. Zhang and D. Auston, "Terahertz radiation from large aperture Si p-i-n diodes", Appl. Phys. Lett., vol. 59, pp. 3357, 1991.

[81] S. Ralph, S. Perkowotz, N. Katzenllenbogen and D. Grischkowsky, "Terahertz spectroscopy of optically thick multilayered semiconductor structures", J. Opt. Soc.Am. B, vol. 11, pp. 2528, 1994.

[82] D. Pozar, "considerations for millimeter wave printed antennas", IEEE transactions on antennas and propagation, vol. 31, no. 5, Sep., 1983.

[83] Y. Shen, P. Upadhya, E. Linfield, H. Beere and A. Davies, "Ultrabroadband terahertz radiation from low-temperature-grown GaAs photoconductive emitters". Appl. Phy. Lett., vol. 83, pp. 3117, 2003.

[84] T. Liu, M. Tani, M. Nakajima, M. Hangyo and C. Pan, "Ultrabroadband terahertz field detection by photoconductive antennas based on multi-energy arsenic-ion-implanted GaAs and semi-insulating GaAs", Appl. Phy. Lett., vol. 83, no. 7, Aug. 2003.

[85] N. Chimot, J. Mangeney, R Crozat, K. Blary and J. Lampin, "TeraHertz emission and detection from ionirradiated $In_{0,53}Ga_{0,47}$ As gated at 1.55 μm", 17th International Symposium on Space Terahertz Technology, 2006.

[86] P. Gu, M. Tani, K. Saika and T. Yang, "Detection of terahertz radiation from longitudinal optical phonon–plasmon coupling modes in InSb film using an ultrabroadband photoconductive antenna", Appl. Phy. Lett., vol. 77, pp. 1798, 2000.

[87] S. Ralph and D. Grischkowsky, "Trap-enhanced electric fields in semi-insulators: The role of electrical and optical carrier injection", Appl. Phy. Lett., vol. 59, Oct. 1991.

[88] B. Salem, D. Morris, V. Aimez, J. Beerens, J. Beauvais and D. Houde, "Pulsed photoconductive antenna terahertz sources made on ion-

implanted GaAs substrates", Journal of Physics Condensed Matter, vol. 17, no. 46, pp. 7327, Nov 23, 2005.

[89] Q. Wu and X. Zhang, "Design and characterization of treahertz-wave electrooptic terahertz sensors", IEEE J. of Selected Topics in Quantum Electronics, vol. 2, Sep. 1996.

[90] R. Yano and H. Gotoh, "Terahertz wave detection performance of photoconductive antennas: Role of antenna structure and gate pulse intensity", J. Appl. Phy., vol. 97, 2005.

[91] Y. Cai and I. Brener, "Design and performance of singular electric field terahertz photoconducting antennas", Appl. Phy. Lett., vol. 71 (15), 13 October, 1997.

[92] D. Li, Y. Huang, C. Yang and X. Tian, "Optimization of photoconductive antenna gap", European Conference on Antennas and Propagation, 2007.

[93] J. Xu, W. Shi, L. Hou, W. Jia, K. Liu, X. Xie and X. Zhang, "Terahertz generation from multiple transparent dielectric coated GaAs antenna", Conference Digest of the 2004 Joint 29th International Conference on Infrared and Millimeter Waves and 12th International Conference on Terahertz Electronics, 2004.

[94] J. Sigmund, C. Sydlo, H. Hartnagel, N. Benker, H. Fuess, F. Rutz, T. Kleine-Ostmann and M. Koch, "Structure investigation of low-temperature-grown GaAsSb, a material for photoconductive terahertz antennas", Appl. Phy. Lett., vol. 87, 2005.

[95] T. Liu, M. Tani and C. Pan, "THz radiation emission properties of multienergy arsenic-ion-implanted GaAs and semi-insulating GaAs based photoconductive antennas", J. Appl. Phy., vol. 93, no. 51, Mar., 2003.

[96] B. Salem, D. Morris, V. Aimez, J. Beauvais and D. Houde, "Improved characteristics of a terahertz set-up built with an emitter and a detector made on proton-bombarded GaAs photoconductive materials", Semiconductor Science and Technology, vol. 21, no. 3, Mar. 2006.

[97] J. Zhang, Y. Hong, S. Braunstein and K. Shore, "Terahertz pulse generation and detection with LT-GaAs photoconductive antenna", IEE

Proceedings: Optoelectronics, vol. 151, no. 2, Apr. 2004.

[98] A. Reineix, M. Ariaudo, C. Chatenet and B. Jecko, "Theoritecal analysis of photoconducting dipole antennas", Microwave and Optical Technology Letters, vol.15, no. 2, Jun. 1997.

[99] J. Zhang, Z. Chen and X. Chen, "FDTD analysis of photoconducting antennas for millimeter-wave generation", International Journal of Microwave and Millimeter-Wave, vol. 10, Issue 4, pp. 213, 2000.

[100] J. Vanderlinde, "Classical electromagnetic theory", Wiley, New York, 1993.

[101] D. Kraus, "Antennas", 2nd edition, New York: McGraw-Hill, 1988.

[102] D. Grischkowsky and N. Katzenellenbogen, "Femtosecond pulses of terahertz radiation: physics and applications", Picosecond Electronics and Optoelectronics, Springer, Berlin, 1985.

[103] R. Keyes, "Optical and infrared detectors", Springer-Verlag, 1977.

[104] G. Carr, C. Michael, R. Wayne, K. Jordan, R. George and G. Williams, "Very high power THz radiation at Jefferson Lab", Phys. Med. Biol., vol. 47, pp. 3761, 2002.

[105] K. McIntosh, E. Brown, K. Nichols, O. McMahon, W. DiNatale and T. Lyszczarz, "Terahertz measurements of resonant planar antennas coupled to low-temperature-grown GaAs photomixers", Appl. Phy. Lett., vol. 69, pp. 3632, 1996.

[106] D. Li and Y. Huang, "A theory of how to improve the excitation of the photoconductive antenna", International Workshop on Antenna Technology, 2007.

[107] J. Kraus and D. Fleisch, "Electromagnetics with applications", 5th edition, McGraw-Hill companies, Singapore, 1999.

[108] D. Li, and Y. Huang, "Comparison of terahertz antennas", European Conference on Antennas and Propagation, 2006.

[109] J. Zhang, Y. Hong, S. Braunstein and K. Shore, "Terahertz pulse

generation and detection with LT-GaAs photoconductive antenna", IEE Proceedings: Optoelectronics, vol. 151, pp. 98, 2004.

[110] Z. Huang, B. Yu, G. Zhao, C. Zhang, L. Cui and Y. Li, " Study on terahertz emission properties of bow-tie photoconductive antenna", 2008 International Conference on Optical Instruments and Technology: Microelectronic and Optoelectronic Devices and Integration, 2009.

[111] A. Rice, Y. Jin, X. Ma and X. Zhang, "Terahertz optical rectification from 110 zinc-blende crystals", Appl. Phy. Lett., vol. 64, pp. 1324, 1994.

[112] I. Brener, D. Dykaar, A. Frommer, L. Pfeiffer, J. Lopata, J. Wynn, K. West and M. Nuss, "Terahertz emission from electric field singularities in biased semiconductors", Opt. Lett., vol. 21, Dec. 1996.

[113] J. Manners, "Quantum physics: an introduction", The open university, Milton Keynes, UK, 2000.

[114] C. Balanis, "Antenna theory", 2nd edition, John Wiley & Sons Inc, 1997.

[115] D. Li, Y. Huang and Y. Shen, "Investigation on bias electric fields produced by improved photoconductive antenna structures", International Workshop on Antenna Technology, 2008.

[116] D. Li, Y. Huang and Y. Shen, "Analytical modelling of electric field in biased photoconductive antennas with advanced structure", Loughborough Antennas and Propagation Conference, 2008.

[117] Y. Lo and S. Lee, "Antenna handbook: antenna applications", Chapman and Hall Pub., 1993.

[118] Y. Huang and K. Boyle, "Antennas from theory to practice", Wiley, 2008.

[119] Y. Lo and S. Lee, "Antenna handbook", Van Nostrand Reinhold, 1993.

[120] D. Li, Y. Huang and Y. Shen, "A terahertz conical horn antenna", European Conference on Antennas and Propagation, 2009.

[121] R. Waterhouse, "Printed antennas for wireless communications", John Wiley & Sons, 2007.

[122] D. R. Jackson and N. G. Alexopoulos, "Gain enhancement methods for printed circuit antennas," IEEE Trans. Antennas Propagation, vol. 33, pp. 976, Sept. 1985.

[123] W. Stutzman and G. Thiele, "Antenna theory and design", 2nd edition, John Wiley & Sons, 1998.

[124] M. Schorr and F. Beck, "Electromagnetic field of the conical horn", Appl. Phys., vol. 21, pp. 795, 1950.

[125] N. Marcuvitz, "Waveguide handbook", 1st edition, McGraw-Hill Book Company, 1951.

[126] J. Kraus, "Antennas", 2nd edition, McGraw-Hill Book Company, 1988.